Stony Brook University

Low Temperature Thermal Conductivity and Competing Orders in d-wave Superconductors

A Dissertation Presented

by

Philip Ross Schiff

to

The Graduate School

in Partial Fulfillment of the Requirements

for the Degree of

Doctor of Philosophy

in

Physics

Stony Brook University

August 2009

Stony Brook University

The Graduate School

Philip Ross Schiff

We, the dissertation committee for the above candidate for the Doctor of Philosophy degree, hereby recommend acceptance of this dissertation.

Adam Craig Durst – Dissertation Advisor
Assistant Professor, Department of Physics and Astronomy

Alfred Scharff Goldhaber – Chairperson of Defense
Professor, Department of Physics and Astronomy

Matthew Dawber
Assistant Professor, Department of Physics and Astronomy

Dimitri V Donetski
Assistant Professor, Department of Electrical and Computer Engineering
Stony Brook University

This dissertation is accepted by the Graduate School.

Lawrence Martin
Dean of the Graduate School

Abstract of the Dissertation

Low Temperature Thermal Conductivity and Competing Orders in d-wave Superconductors

by

Philip Ross Schiff

Doctor of Philosophy

in

Physics

Stony Brook University

2009

The low energy excitations of cuprate superconductors are Dirac fermions which arise due to the d-wave nature of the superconducting order parameter. At low temperatures, these quasiparticles lead to a striking prediction of a universal thermal conductivity, κ_{00}, which is independent of disorder.The universality of the low temperature thermal conductivity is not always observed, however, in the underdoped region of the phase diagram for several materials. In this region, the situation is complicated by evidence of coexisting order parameters, such as charge and spin density waves. These competing orders may be responsible for suppressing the universal limit thermal conductivity via their effect on the quasiparticle spectrum.

In this thesis we present the two following results. First, we suppose the addition of a $\mathbf{Q} = (\pi, 0)$ charge density wave to a d-wave BCS-like superconductor. At low temperatures, where impurities are the dominant scattering mechanism, we calculate the thermal

conductivity, including the effects of vertex corrections within the self-consistent Born approximation.

Using the results of the previous calculation, which indicates that simpler bare-bubble results are adequate to describe the thermal conductance, we proceed to write a mean-field description of a d-wave superconductor in the presence of a variety of density waves. By calculating the effect of these competing orders on the quasiparticle spectrum and comparing it to the low-temperature thermal conductivity, we examine the way in which the universal limit thermal conductivity is affected by the incipient density waves. In general, the presence of competing orders induces disorder dependence in κ_{00}, and can suppress it entirely given sufficient amplitude of density wave.

Contents

List of Figures

Preface

In the near century since its first discovery by man, the phenomenon of superconductivity has revealed itself to be one of the most intriguing subjects under study in the natural sciences. While the first superconductors discovered were elemental metals, in subsequent years superconductivity was observed in compounds with magnetic impurities, a wide variety of alloys and thin films, in organic compounds, as well as layered ceramic, and recently, iron-based materials. We now know that the origins of this unusual phase of matter lie deep in the foundations of quantum many body theory, as an example of macroscopic phase coherence in a quantum system. Conventional superconductors, described by the Bardeen-Cooper-Schrieffer (BCS) theory, bear a deep theoretical correspondence with Bose-Einstein condensates, another intriguing phenomenon which requires global coherence of its constituent particles.

The discovery of superconductivity in layered ceramics referred to as cuprates launched an explosion of theoretical and experimental work in 1986 as well as a Nobel prize in 1987. The precise nature of these cuprates' superconducting state is similar, in some aspects, but very different in others, to that of the conventional BCS superconductors. The cuprates display superconductivity at much higher temperatures than BCS superconductors, for instance, but the "normal" state from which they have condensed is quite different from that of the metals which condense into BCS superconductors. In addition, the phase diagram is filled with evidence of additional ordered states; some even coexisting with the superconductivity.To date, no single microscopic theory has been developed which conclusively explains all of this bizarre behavior, although the physics is generally agreed to be that of adding dopant "holes" to a half-filled Mott insulator

One of the observed properties of cuprate superconductors is the unconventional "d-wave" symmetry of the superconducting order parameter, which causes the low energy properties of cuprates to be very different from those of BCS superconductors. In contrast to conventional superconductors, which cannot be excited without bridging an energy gap, in cuprates there are excitations which lie at low energies. These low lying excitations may cause the

transport properties of cuprates to possess the extremely unusual property of being independent of the imperfections and disorder which vary from sample to sample. Previous research has indicated that this is likely to be the case for the thermal conductivity in particular. Measurements of the low temperature thermal conductivity in various superconductors affirm that a residual resistance attributed to a quasiparticle current is observed in d-wave superconductors, but not observed in s-wave superconductors. This distinction helps to establish the low temperature thermal conductivity as yet another means of testing the order parameter symmetry of a superconductor.

While some measurements find a universal limit thermal conductivity which agrees with the predicted value, others have found that it is smaller than expected, or not seen at all. Many experiments on cuprates indicate that they are complex materials, and that other ordered phases (in addition to superconducting) may be present as well. These additional order parameters may play a role in this suppression. In this thesis, we will develop models which account for the presence of coexisting orders, and will investigate their effects on the low energy properties, and on the thermal conductivity of the cuprates.

Summary of Thesis

In Chapter 1, we provide an introduction to d-wave superconductors. We begin by providing a brief history of major developments in superconductivity. We then go on to discuss some of the phenomenology of cuprate superconductors, in particular, the impact of their unusual pairing symmetry, and describe the phase diagram. Next, we explain the concept of universal limit transport in d-wave superconductors, a phenomenon which arises due to the impurity induced low energy excitations. We then briefly discuss the history of stripes and other spatial orderings in d-wave superconductors.

In Chapter 2, we review the situation regarding transport in a disordered d-wave superconductor. We begin with some background on linear response formalism, and derive the appropriate Kubo formula for the conductivity. We describe how Matsubara formalism is used to calculate the requisite correlation functions. We then review the low-energy model of a d-wave superconductor, and describe how self-energy corrections are applied to the single-particle and two-particle Green's functions. We then calculate the density of states and thermal conductivity, and find the universal limit result. Lastly, we review the relation between the Boltzmann equation and different field-theoretic techniques of computing conductivities, and the implications in dSC systems.

In Chapter 3 we calculate the universal limit thermal conductivity of a d-wave superconductor as a $\mathbf{Q} = (\pi, 0)$ site-centered charge density wave is

turned on. As the density wave's magnitude increases, the quasiparticle spectrum remains gapless up until a critical value, ψ_c. We calculate the vertex corrections within the self-consistent Born approximation, and find that the vertex corrections are not important for slowly and moderately varying scattering potentials. The effect of the self-consistency in the disorder calculation is to renormalize the transition point at which the thermal conductivity vanishes.

In Chapter 4 we consider the coexistence of d-wave superconductivity with a variety of different orders, such as charge, spin and pair density waves. We expand the formalism to include different wave vectors, including checkerboard order. The universal limit thermal conductivity in such competing order scenarios is then derived. We then compare the evolution of the quasiparticle spectrum with respect to the incipient order parameter to the universal limit thermal conductivity.

Acknowledgements

In presenting this thesis, I would like to thank those who have made its preparation possible. First, I would like to thank my advisor, Adam Durst, under whose guidance I have reached adulthood as a physicist and a person. What I have learned from him was not limited to the instruction of a particular fact or set of skills, although there is an immense amount of that which he imparted upon me in our years together. I hope to repay him for his patience in dealing with my own eccentricities by effecting his example as I go on in life.

In addition to Adam's teaching, I have benefitted from and enjoyed many courses at Stony Brook. These courses have helped provide a background for what I hope will be a lifetime of learning. Therefore I am grateful to Peter Stephens, Konstantin Likharev, Ismail Zahed, Dmitri Averin, George Sterman, Barry McCoy, Robert Schrock, Gerry Brown and Barbara Jacak, Hal Metcalf and László Mihály, and again Adam Durst, for their excellent instruction.

Also, I have been lucky enough to have very intrepid and good colleagues in condensed matter theory. In particular, I thank Xiao Shen, Tom Berlijn, Manas Kulkarni, Fabio Franchini, Sriram Ganeshan, Nikita Simonian, Jim Nesteroff, Jue Wang and Li Li for their solidarity in sorting out the problems of "the squalid state". Also, there were many others in our department with whom I developed a close bond. While there are too many to list entirely, I am happy to thank Nathan Borggren, Constantinos Constantinou, Matt Durham, Dominik Geißler, Saul Lapidus, Jason Reeves and Clint Young for all of the discussions and camaraderie.

This department would not last, and I would not have endured if not for the fine work of our front office and maintenance workers. While they are all essential to the operations of our department, I specifically want to thank Pat Peiliker and Pernille Jensen for their help in navigating the mazes of bureaucracy that accompanies academic life.

A house would not be a home without endless arguments about the relative importance of the different subfields of physics, the merits and demerits of different schools of thought on geopolitics, gender, and every other topic under

the sun. I thank my housemates, Elli Pomoni, Luis López, Ovidiu Pâţu and especially Marija Kotur for assistance in these matters.

Finally, I thank my parents Michael and Teresa, and my siblings Harris, Rosina and Erica for a lifetime of encouragement. I really would not have made it without them.

Chapter 1

Introduction

1.1 Conventional superconductors

Superconductivity was discovered in 1911 due to the pioneering work of Kamerlingh Onnes. As he measured the low temperature resistance of mercury, he found that the zero-frequency resistance vanished below a critical temperature of 4.2 K[1]. By lowering the temperature of a metal, Onnes had uncovered a phase transition to a then-unknown state of matter, now known as the superconducting state. In 1933 Meissner and Oschenfeld found that elemental superconductors were perfect diamagnets, meaning that an applied magnetic field would be excluded from the volume of a superconductor, being non-vanishing only on a nanometer scale "penetration depth" from the outside[2]. The Meissner effect demonstrates the rigidity of the phenomenon, as the sample works cooperatively to expel the magnetic field.

Phenomenological theories were constructed in an attempt to resolve these peculiar observations. A model of Gorter and Casimir postulated that there were two seas of electrons: a normal fluid, and a superconducting fluid, whose different behavior could account for some of the thermodynamic properties observed, such as the specific heat[3]. Soon afterward, an expansion of their model which would account for the Meissner effect was posited by Fritz and Heinz London[4]. Pippard refined the London theory to take non-localities into account, and was thereby able to explain the larger penetration depths observed in samples with impurities[5]. Lev Landau and Vitaly Ginzburg proposed a theory allowing for variations in the superfluid density. This theory casts the problem as that of a phase transition occurring with the appearance of an order parameter. Valid near the critical temperature T_c, it was found to be useful in problems where the magnetic field could not be handled pertubatively, and has been enormously useful in many other circumstances[6].

Until the 1950's, however, no single theory was able to explain all of the experimental observations simultaneously. This situation changed after theorists began looking at the problem from the point of view of condensation, as was suggested by Frölich[7]. Leon Cooper's discovery that the electron-electron interaction could be made attractive rather than repulsive was a giant piece in the puzzle. Working with Robert Schrieffer and the eminent John Bardeen, they found that a spin-singlet bound state of electrons with zero net angular momentum could result from this attraction. With all of the phase- space-accessible electrons condensed into these paired states, known as Cooper pairs, electrons were not able to scatter from the usual low temperature scatterers: impurities. This explained the drop in resistance. The fact that the condensation was mediated by phonons resolved the then puzzling isotope effect, the dependence on nuclear mass of the critical temperature, something which had not been accounted for in the other theories. The robustness of the Meissner effect was also explained by this phase coherence[8].

1.2 BCS theory and the gap

One of the hallmarks of BCS superconductors is the existence of an energy gap, which accounts for the robustness of the superconducting state to perturbations such as application of a magnetic field, and to degradations of the supercurrent from scatterers. The size of this energy gap can be seen from the BCS pairing hamiltonian,

$$H_{BCS} = \sum_{k\sigma} \epsilon_k c^\dagger_{k\sigma} c_{k\sigma} + \sum_{kk'q} V_q c^\dagger_{k+q\uparrow} c^\dagger_{-k-q\downarrow} c_{-k\downarrow} c_{k\uparrow}, \tag{1.1}$$

where the first term represents the kinetic energy of the constituent electrons, and the second term represents the interactions. The BCS hamiltonian can be diagonalized using the Bogoliubov-Valatin transformation (see Appendix **??**). The diagonalization leads to the self-consistency equation for the gap function,

$$\Delta(k) = -\sum_{k'} V(k-k') \frac{\Delta(k')}{2E(k')} \tanh(\frac{E(k')}{2k_B T}) \tag{1.2}$$

and leads to the quasiparticle energies

$$E(\mathbf{k}) = \sqrt{\epsilon_k^2 + \Delta^2}. \tag{1.3}$$

The existence of an energy gap is exhibited in the density of states,

$$N(\omega) \propto \frac{\omega}{\sqrt{\omega^2 - \Delta^2}} \Theta(\omega - \Delta). \tag{1.4}$$

There are many different ways to observe this gap. One instance is in the activated behavior (exponentially decaying as $T \to 0$) of the specific heat, due to the Boltzmann factor, whereas the specific heat in metals is linear at low temperatures[10]. Another method of observation was based on Leo Esaki's demonstration that electron tunneling occurred in junctions composed of a superconductor and normal metal joined by a thin insulating later (S-I-N). In 1960, Ivar Giaever followed up on this work in a way which demonstrates the quasiparticle spectrum very clearly. He carefully cooled Niobium below its critical temperature of 9.2 K and measured the tunneling current as he adjusted a bias voltage[9]. While in the metallic state the current-voltage curve is linear, with the slope equal to the inverse of the resistance. As the niobium was cooled past the critical temperature, the onset of a gap in the density of states was observed. An example of this measurement is displayed in part (a) of Fig. 1.1, and the "semiconductor model" method of calculating the tunneling current based on the density of states (which neglects coherence effects in the tunneling) is displayed in part (b) of Fig. 1.1[10].

1.3 Cuprates

The 1986 realization that layered copper oxide materials, known colloquially as cuprates, exhibited superconductivity kicked off a new era in condensed matter physics[11, 12]. This discovery was particularly amazing not only because the critical temperature was much higher than in previously known superconductors, but also due to the complex structure of the cuprates themselves[14]. While the behavior of many elemental superconductors is well described by the Bardeen-Cooper-Schrieffer (BCS) theory, an underlying theory of high temperature superconductors which explains their behavior in all regions of their phase diagrams has not yet been fully formulated. The generally accepted picture, however, is that the high T_c state is obtained by adding holes (or, in some cases, electrons) to a half-filled Mott insulator[14]. Indeed, this recipe for creating high T_c materials can be seen experimentally, via a chemical substitution which contributes the excess carriers. The antiferromagnetic ground state is quenched as doping increases, and soon (but not immediately) afterwards, there is an onset of superconductivity. The critical temperature, T_c, then increases with doping through what is known as the underdoped regime. At some concentration of dopant (usually about 15%), the

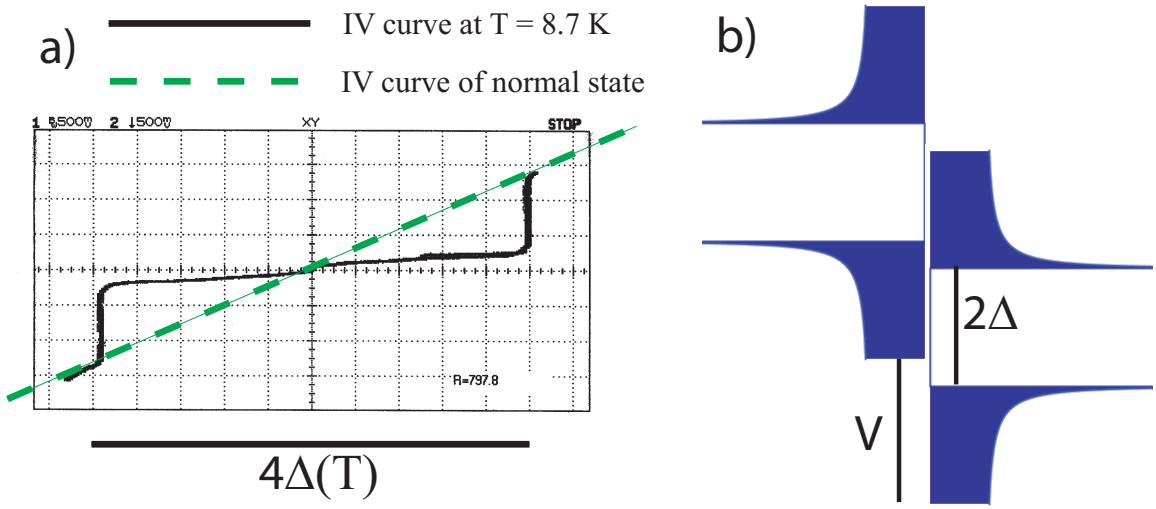

Figure 1.1: a) Current-voltage curve measured in a Niobium-Aluminum-Niobium junction. The excitation energy of a broken pair is $\Delta(T)$, the gap in the density of states is 2Δ, and the gap in between observing the tunneling occurs as 4Δ, in terms of the applied bias voltage V. b) Illustration of the density of states in two BCS superconductors in the presence of a bias voltage V. At $T = 0$, tunneling is possible only after reaching positive or negative bias voltage of magnitude $V = 2\Delta$. At finite temperatures, some tunneling can occur within the gap, as is seen experimentally in a).

critical temperature is maximized (optimal doping), and T_c declines as doping increases through the overdoped regime.

The hamiltonians of the microscopic models used to describe such doped Mott insulators (Mott insulators are those which display insulating behavior due to interactions, rather than because the Fermi level lies in a band gap) contain terms for hopping, antiferromagnetism, and Coulomb repulsion[14].

Although there are literally hundreds of different allotropes of cuprate superconductors, there are some universal features which are more or less shared by all of them. The cuprates are all layered materials which have copper-oxygen planes, where the copper atoms sit on the sites of a square (or rectangular) lattice[14]. The supercurrent is carried within these copper-oxygen planes, as has been verified by a number of experiments[16]. Additionally, the symmetry of the superconducting order parameter is very different than that of BCS superconductors. Experiments based on the interferometry of Josephson currents tunneling between two samples are able to see changes in sign of the order parameter, and indicate that there is a d-wave component present.[15]. A number of such phase sensitive tests, as well as other methods which are sensitive only to the magnitude of the order parameter, all considered together, indicate that the pairing symmetry is solely of $d_{x^2-y^2}$ symmetry[16]. This means that, viewed in momentum space, the superconducting gap (order parameter) necessarily vanishes along the lines $k_x = \pm k_y$. The gap function in momentum space is usually taken to be

$$\Delta(\mathbf{k}) = \frac{\Delta_0}{2}\Big(\cos(k_x a) - \cos(k_y a)\Big), \tag{1.5}$$

although higher harmonics are also sometimes seen in angle-resolved photoemission (ARPES) experiments[17].

This gap is illustrated in Fig. 1.2, along with the Fermi surface implied by a tight-binding model, fit from ARPES data.

One of the consequences of high T_c superconductors having an anisotropic gap is that the excitation spectrum is quite different than that of a BCS superconductor. The excitation energy of the d-wave superconductor is

$$E_k = \sqrt{\epsilon_k^2 + \Delta_k^2}, \tag{1.6}$$

where ϵ_k represents the normal state dispersion, and Δ_k is the gap. These excitions are also very k dependent: in some places, the excitation energy is high, while at four "nodal points", there exist gapless excitations, as seen in Fig. In the vicinity of these nodes, ϵ_k and Δ_k are linear functions in the directions parallel to and perpendicular to the Fermi surface, respectively, so

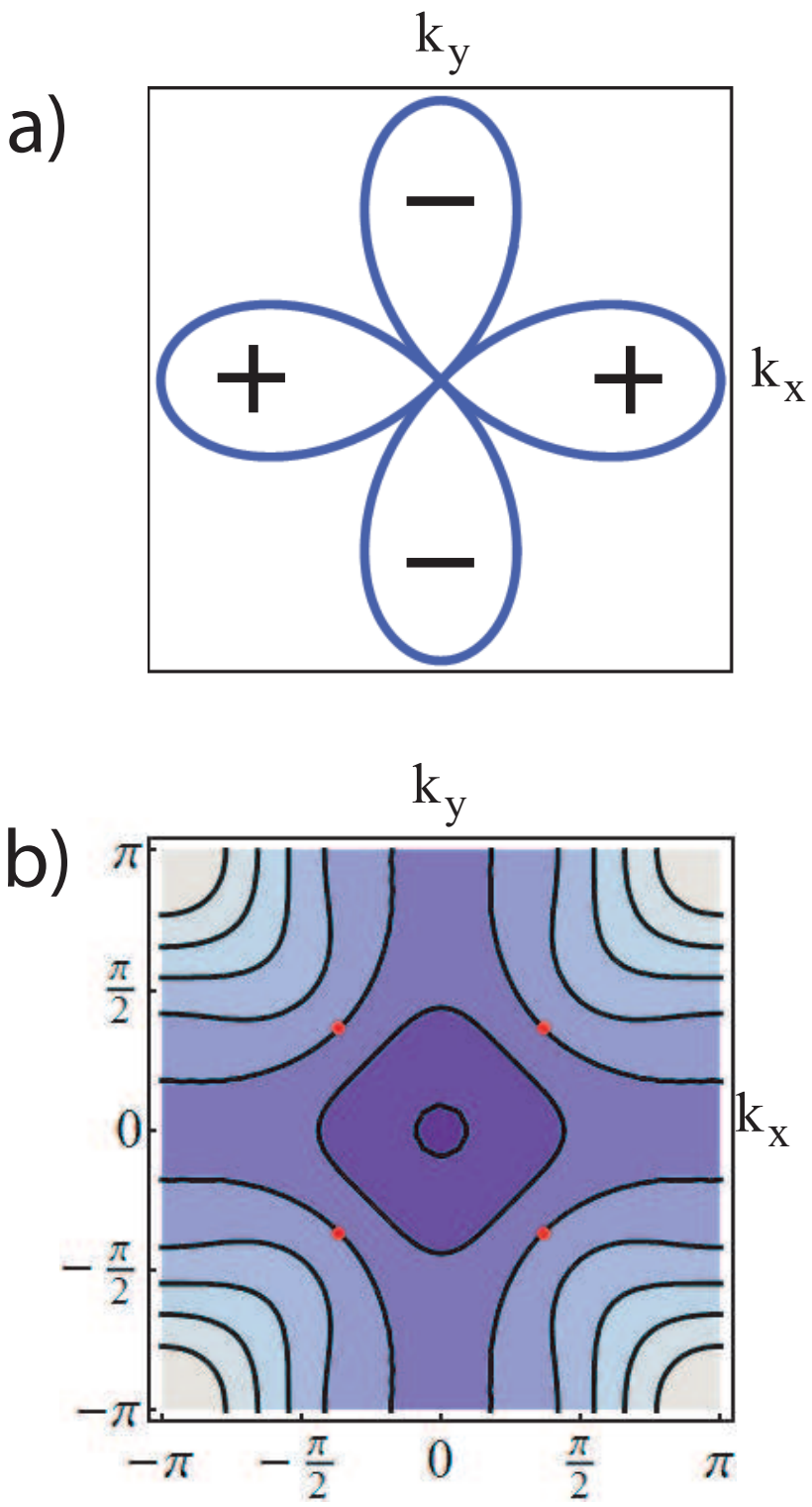

Figure 1.2: a) Illustration of the model d-wave gap. Note that the phase changes from positive to negative at four places; the gap necessarily vanishes along those directions ($k_x = \pm k_y$). b)6Along the directions in which the gap vanishes, and at the places where the normal state dispersion, ϵ_k is zero (the Fermi surface), the quasiparticle energy is zero. Those locations are referred to as nodes, and appear as red dots. The Fermi surface modelled here is taken from Ref. 13; a slightly simpler model will be employed later.

that we could write

$$\epsilon_k \approx v_f k_1 \qquad \Delta_k \approx v_\Delta k_2, \tag{1.7}$$

where k_1 and k_2 represent deviations from the nodal point in the directions perpendicular and parallel to the Fermi surface, respectively. The dispersion of these quasiparticles is therefore the same as that of electrons obeying the Dirac equation, so they may be referred to as Dirac quasiparticles.

If we would perform the tunneling experiments of Giaever using d-wave rather than s-wave superconductors, we would expect that due to the existence of quasiparticles below the gap maximum, tunneling current would not completely vanish, but would include a non-zero current. Scanning tunneling spectroscopy (STS) studies, which measure the tunneling current as a function of bias voltage (meaning that they are essentially the derivative of the tunneling current measured by Giaever) at each point on the sample, have reproduced this prediction qualitatively as well[18]. STS studies of the same compounds which have been raised above the critical temperature for superconductivity see similar current-voltage characteristics as those in the superconducting state, which gives rise to the name of the "pseudogap" phenomenon. The pseudogap may be the consequence of d-wave electron pairs which lack global phase coherence, and is under furious study at present[19].

In addition to observing a non s-wave gap, scanning tunneling microscopy studies have also detected the presence of bound states within the gap[18]. These bound states arise due to the interaction of the quasiparticles with impurities[20, 21].

1.4 Quasiparticles in d-wave superconductors

The order parameter of the cuprates has been well established by a variety of tests to be of $d_{x^2-y^2}$ symmetry, which leads to Dirac quasiparticles described in the previous section. These quasiparticles may have some very unusual properties, as was noticed by Patrick Lee[22]. Let us consider why that is.

The importance of the density of states in solid state physics in determining physical properties is enormous, as we have seen in the Giaever tunneling experiments. Whereas in metals, the density of states is roughly a constant at the Fermi level, the Dirac nature of the quasiparticles gives a density of states which is proportional to the energy[22, 23]. This extra factor of energy affects the power counting involved in estimating transport equations. Such equations are given in terms of the Green's functions (more details on transport are given

in Sec.2

$$\begin{aligned}\sigma &\sim v_f^2 \sum_k G_R(k) G_A(k) \\ &\sim v_f^2 \int \mathrm{d}^d k \frac{1}{\xi_k + \frac{i}{2\tau}} \frac{1}{\xi_k - \frac{i}{2\tau}} \rho(k) \\ &\sim v_f^2 \int \mathrm{d}\xi \frac{1}{\xi^2 + \frac{1}{4\tau^2}} \rho(\xi) \end{aligned} \tag{1.8}$$

where G_R and G_A represent retarded and advanced Green's functions, ξ_k is the energy of a quasiparticle, τ represents the lifetime of a quasiparticle, and $\rho(\xi)$ is the density of states. Clearly, whether the density of states is a constant or is proportional to ξ will affect such a result.

In a metal, only states near the Fermi level are able to contribute, so that $\rho(\xi) \sim \rho(E_f)$, which leads to the Drude result,

$$\sigma \propto \tau; \tag{1.9}$$

the conductivity is proportional to the lifetime. If we estimate the conductivity of the Dirac quasiparticles in this manner, using $\rho(\xi) \sim \xi$, we instead find the conductivity to be independent of the lifetime[22].

Since the modifications to Boltzmann transport due to disorder come about through changes in the inverse lifetime of quasiparticles, this implies the possibility that a universal limit exists, in which the residual conductivity is found to be independent of the details of disorder. By details of disorder we mean: the matrix elements of the scattering potential, the exact configuration of disorder, and the amount of disorder.

A more careful calculation is necessary, however, for the exact result. In fact, in d-wave superconductors, the electrical conductivity has been found to be very sensitive to vertex corrections. The vertex corrections, which account for the weight of backscattering processes in degrading the current, are important because the electrical current is proportional to the Fermi velocity ($\frac{\mathrm{d}\epsilon_k}{\mathrm{d}k}$), rather than the group velocity ($\frac{\mathrm{d}E_k}{\mathrm{d}k}$), to which the spin current and heat current are proportional[24].

The thermal current can thus relax by both intra-nodal and inter-nodal scattering processes. The electronic current, on the other hand, cannot relax by scattering into the same node when it is back scattered. The vertex corrections therefore turn out to be not too important for the thermal conductivity, while they are important even to zeroth order of impurity density for the electrical conductivity. As such, a thermal current due to the Dirac quasiparticles should be present in d-wave superconductors, and persist down

to low temperatures.

To extract the quasiparticle contribution to the low temperature thermal conductivity from experiments, we must first consider the remaining contribution, which is due to the phonons. The entire thermal conductivity goes as

$$\kappa(T) = aT + bT^{\alpha} \tag{1.10}$$

where α is typically three (but can also be a number between two and three, due to boundary scattering)[25–27]. Then, by plotting $\frac{\kappa(T)}{T}$ as a function of $T^{\alpha-1}$, we expect to obtain a linear graph where the intercept is the universal limit thermal conductivity. Note that in materials which lack the quasiparticle contribution, the linear graph should have intercept zero. This is observed plainly in s-wave superconductors[28]. As such, universal limit transport measurements serve as another method to characterize the underlying symmetries of superconductors. These experiments have been performed, and in many instances demonstrate the conduction due to the quasiparticle heat current quite clearly[25–27, 29–36]. Bare-bubble and vertex corrected calculations of the type mentioned in Sec 2.2 indicate that the quasiparticle contribution to the low temperature thermal conductivity is indeed independent of disorder[24], given by the value

$$\frac{\kappa_{00}}{T} = \frac{k_B^2}{3\pi^2\hbar}\frac{v_f^2 + v_\Delta^2}{v_f v_\Delta} \tag{1.11}$$

However, in some circumstances, the universal limit thermal conductivity is measured to be zero, or does not agree with the predicted value[28, 37–40].

1.5 Stripes in superconductors

Cuprates superconductors exhibit many interesting and unusual properties which have made them the subject of intense theoretical and experimental scrutiny for more than twenty years now. In addition to the "off-diagonal long range order" which is the superconducting state, cuprates may contain other kinds of orders. Studies of the Hubbard model predicted that striped phases, that is, uni-directional modulations in charge or spin density, might be found in cuprates[41–44].

Afterwards, stripes in superconductors were observed in LSCO (Lanthanum-Strontium-Copper-Oxide) in neutron scattering experiments[45, 46]. Neutron scattering measures the dynamical structure factor of materials, $S(\Omega)$, using the magnetic moment of an incident beam of neutrons. While only spin density waves are observable in neutron diffraction, charge density waves can be seen indirectly using crystallography, through their induced distortion of

the lattice. Density modulations were not limited to LSCO, however: there is a multitude for evidence of density ordering in a number of materials[47]. Scanning tunneling microscopy has revealed that there are multiple kinds of inhomogeneities present in high temperature superconductors[48–62]. There are spatial modulations in both the superconducing gap, as well as in the local density of states in Bi2212. The fact that density waves are present in different materials means that it is likely a universal trait, and is not just a structural artifact resulting from the structure of one particular superconductor[63].

Different schools of thought exist as to whether or not the ubiquitous stripes are of fundamental importance, or appear incidentally due to the antiferromagnetic background. Some contend that the physics of doping the insulator is the key point[14], while others think that stripe formation is intricately entwined with the superconducting state itself[63]. Investigating the origin of these many ordered phases is well beyond the scope of this thesis. What we aim to do herein is to determine the effects of competing ordered phases on some of the low-energy properties of d-wave superconductors, in particular, on the low temperature thermal conductivity.

Chapter 2

Transport in a disordered d-wave superconductor

2.1 Response functions

2.1.1 Kubo formula

One of the primary ways in which condensed matter physicists study the systems under consideration is to perform transport measurements. By this, we mean we perturb the system with a gradient (of voltage, temperature, etc.) and we measure the response of the system to the perturbation. The most common example is the application of an electric field to a sample and measurement of the induced current. The measured current is proportional to this electric field plus the field arising in the sample due to polarization. The constant of proportionality, which is a tensor quantity, is called the electrical conductivity,

$$j^e_\alpha(\mathbf{r},t) = \sigma_{\alpha\beta}(\mathbf{r},t;\mathbf{r}',t')E_\beta(\mathbf{r}',t'). \tag{2.1}$$

Other kinds of gradients can be applied; in this work we will be concerned instead with the thermal conductivity κ, defined as

$$j^Q_\alpha(\mathbf{r},t) = \kappa_{\alpha\beta}(\mathbf{r},t;\mathbf{r}',t')(-\nabla T)_\beta(\mathbf{r}',t'). \tag{2.2}$$

Response functions are correlation functions which provide information about the system under study. In the language of statistical physics, the poles of single-particle Green's functions inform us of quasiparticle excitations and lifetime[64]. Single-particle Green's functions represent a "first functional derivative" of a free energy[65], and can be used to compute equilibrium properties of a system[64, 66]. Two-particle Green's functions, on the other hand,

represent a second functional derivative of the free energy[65], and can be used to calculate non-equilibrium properties[64, 66].

This last statement is not trivial. For small perturbations, we can derive a Kubo formula, which is a relation between the transport coefficient and a two particle Green's function such as a current-current correlation function,

$$\mathrm{Re}(\sigma_{\alpha\beta}(\omega)) = -\mathrm{Im}\frac{\Pi^{\mathrm{Ret}}_{\alpha\beta}(\omega)}{\omega} \tag{2.3}$$

where

$$\Pi^{\mathrm{Ret}}_{\alpha\beta} \equiv < j_\alpha(\mathbf{r},t) j_\beta(\mathbf{0},0) > \tag{2.4}$$

is the current-current correlation function, taken over the finite temperature ensemble average[66]. Derivations of Kubo formulae can be found in many books[64, 66, 68]. The essence of the formula is summarized here.

To an system which obeys the Schrödinger equation,

$$H_0|\psi(t)> = i\hbar\frac{\partial|\psi(t)>}{\partial t} \tag{2.5}$$

we add a perturbation so that the Schrödinger equation becomes

$$(H_0 + H_{\mathrm{ext}})|\overline{\psi}(t)> = i\hbar\frac{\partial|\overline{\psi}(t)>}{\partial t}, \tag{2.6}$$

where the overbar indicates that the state vector is the eigenstate of the nonequilibrium (perturbed) system. We wish to determine the change in expectation value of a current, j, in the presence of this perturbing field,

$$\delta < j > \equiv < \overline{\psi}(t)|j(t)|\overline{\psi}(t) > - < \psi(t)|j(t)|\psi(t) > . \tag{2.7}$$

We presume that the perturbing part of the hamiltonian is coupled to the current according to

$$H_{\mathrm{ext}} = \int \mathrm{d}\mathbf{r} j_\alpha(\mathbf{r},t) F_\alpha(\mathbf{r},t), \tag{2.8}$$

where $F(\mathbf{r},t)$ is a generalized force. In the instance of electrical conductivity, F would be the electric field, for instance. The perturbed eigenstate is obtained from the unperturbed one via the s-matrix

$$|\overline{\psi}(t)> = T\exp\Big(-i\int_{-\infty}^{t}\mathrm{d}t' H_{\mathrm{ext}}(t')\Big)|\psi(t)> . \tag{2.9}$$

where T here represents the time ordering operator, which orders the operator

series[66]. In linear response, we wish to keep only terms which are linear in the perturbing force. The result, after expanding the s-matrix, is

$$< j_\alpha(t) >= i \int_{-\infty}^{t} \mathrm{d}t' < \psi(t)|[H_{\mathrm{ext}}(t'), j_\alpha(t)]|\psi >, \tag{2.10}$$

where the current in the absence of the perturbation is set to zero. With the use of the assumption of Eq. (2.8) in Eq. (2.10), and the definition of a retarded correlation function

$$\Pi^{\mathrm{Ret}}(\mathbf{r}t;\mathbf{r}'t') = \Theta(t-t')\frac{< \psi(0)|j(\mathbf{r}t), j(\mathbf{r}'t')|\psi(0) >}{< \psi(0)|\psi(0) >}, \tag{2.11}$$

we find that the change in current can be written

$$\delta < j_\alpha(\mathbf{r}t) >= -i \int_{-\infty}^{\infty} \mathrm{d}t' \int \mathrm{d}\mathbf{r} \Pi^{\mathrm{Ret}}_{\alpha\beta}(\mathbf{x},t;\mathbf{x}',t') F_\beta(\mathbf{x}',t'), \tag{2.12}$$

which brings us most of the way to Eq. (2.3).

To complete the derivation, we will Fourier transform into momentum and energy spaces. Let us note that to systems which are translationally invariant in space and time, we can render the simplification

$$\mathcal{G}(\mathbf{r}t;\mathbf{r}'t') = \mathcal{G}(\mathbf{r}-\mathbf{r}', t-t'), \tag{2.13}$$

by a change in coordinates. In other words, the matrix representing the Green's function is Toeplitz, with constant entries along any diagonal[66, 67]. In principle, while we intend to study the effects of density modulations, this simplification can still be made, since we are interested in long wavelength effects only. The Fourier transform of Eq. 2.3 is

$$j_\alpha(\mathbf{q},\omega) = \sigma_{\alpha\beta}(\mathbf{q},\omega) f_\beta(\mathbf{q},\omega). \tag{2.14}$$

The Fourier transform of Eq. 2.8 is

$$H_{\mathrm{ext}} = \frac{i}{\omega} j_\alpha(\mathbf{q}) f_\alpha e^{-i\omega t}, \tag{2.15}$$

where we have assumed that the perturbing force is harmonic,

$$F_\alpha = f_\alpha e^{i(\mathbf{q}\cdot\mathbf{r}-\omega t)}. \tag{2.16}$$

The change in current due to the perturbation is thus

$$\delta < j_\alpha(\mathbf{q},\omega) >= -i\Pi_{\alpha\beta}(\mathbf{q},\omega) f_\beta(\mathbf{q},\omega), \tag{2.17}$$

which leads to Eq. (2.3).

The important simplification of linear response is that for small perturbations we can calculate the non-equilibrium property, $\sigma_{\alpha\beta}$, using only the expectation value of the current-current correlation function evaluated between the unperturbed states. This is a manifestation of the fluctuation-dissipation theorem, whereby we obtain the dissipation (inverse conductivity) from the fluctuations about equilibrium[69].

2.1.2 Thermal currents

In linear response, we measure currents which flow in response to generalized forces which act on the system, according to

$$j_\alpha = X^{\alpha\beta} F_\beta \tag{2.18}$$

where F_α represent generalized forces, such as gradients in the electrical potential, temperature, or particle concentration, and the $X^{\alpha\beta}$ are the transport coefficients, which inform us about how the system responds to perturbations. In order to guarantee agreement with Onsager relations, which govern the thermodynamics of irreversible processes, entropy produced due to irreversible processes must be associated with these forces as

$$\frac{\partial S}{\partial t} = j_\alpha F_\alpha \tag{2.19}$$

where S represents the part of the entropy resulting from irreversibility[66]. We will presume that the systems of interest have only temperature gradients in them. Then, we can define a Kubo formula which will preserve the Onsager relations by associating

$$\frac{\partial S}{\partial t} = -\frac{1}{T^2} J \cdot \nabla T \tag{2.20}$$

Because heat transport occurs only when electrons above the Fermi level move (since electrons below the Fermi level must absorb energy from the surroundings in order to find an unoccupied state, they do not participate in heat transport), we can calculate the thermal conductivity, which we label κ, in a

system perturbed only by a temperature gradient, defined as

$$\mathbf{j}_Q = \frac{-1}{T^2}\kappa\nabla T, \tag{2.21}$$

where J_Q is the heat current, obtained by defining all particle energies relative to the Fermi level. This will be computed in terms of the current-current correlation function. Therefore, the thermal conductivity can be found using the Kubo formula,

$$\frac{\kappa(\Omega)}{T} = -\frac{1}{T^2}\frac{\mathrm{Im}\Pi^{\mathrm{Ret}}(\Omega)}{\Omega}. \tag{2.22}$$

More background on how to compute this correlation function will be given in the next section.

2.1.3 Calculation of correlation functions

In order to calculate thermal conductivity using the Kubo formula (2.3), we must have the retarded Green's function. However, Wick's theorem, which tells us how to decompose the two-particle Green's function in terms of single-particles Green's functions, is only valid for time-ordered Green's functions[64, 66, 70]. In order to make use of diagrammatics, then, we need to realize an indirect way of obtaining the retarded Green's function. The easiest method of doing this is by using an analytic continuation of an imaginary time Green's function; this method is known as the Matsubara method.

In the Matsubara method, the time is effectively taken as a complex temperature variable. To understand why such a bizarre formalism would be used, consider the expression for a finite temperature Green's function,

$$\sum_n < n|e^{-\beta H}e^{iHt}c_k e^{-iHt}c_k^\dagger(t')|n >, \tag{2.23}$$

where the ensemble average is performed over some complete set of states, $|n >$, and c_k's here represent the Schrödinger picture operators. The hamiltonian H is exponentiated in both the Boltzmann weight, and in the time evolution operator. By treating t and β as real and imaginary parts of a single complex variable, the temperature Green's functions can be computed using only a single s-matrix expansion. The definition of complex time $\tau = it$ restricts the time domain of the Green's functions to the range $-\beta \leq \tau \leq \beta$.

Therefore, we define the Matsubara correlation function

$$\Pi_{\alpha\beta}(\mathbf{q}, i\omega_n) = -\int_0^\beta \mathrm{d}\tau e^{i\omega_n\tau} < T_\tau j_\alpha^\dagger(\mathbf{q},\tau)j_\beta(\mathbf{q},0) >, \tag{2.24}$$

where the time ordering operator T_τ is in terms of complex time. The Matsubara frequencies ω_n are limited to

$$\omega_n = \frac{(2n+1)\pi}{\beta} \qquad\qquad \omega_n = \frac{2\pi n}{\beta} \tag{2.25}$$

for bosons and fermions, respectively.

The relation between the imaginary time, real time, and retarded Green's functions is made by the spectral density function, which is the same for each of them. Using a spectral representation, the retarded Green's function is

$$\Pi_{\rm Ret}(\mathbf{q},\omega) = \int_{-\infty}^{\infty} {\rm d}\omega' \frac{A(\mathbf{q},\omega')}{\omega - \omega' + i\delta} \tag{2.26}$$

and the Matsubara correlator is

$$\Pi(\mathbf{q}, i\omega_n) = \int_{-\infty}^{\infty} {\rm d}\omega' \frac{A(\mathbf{q},\omega)}{i\omega_n - \omega'}. \tag{2.27}$$

The spectral function

$$A(\mathbf{q},\omega) = \frac{1}{\mathcal{Z}} \sum_{mn} |< n|j_q|m >|^2 (e^{-\beta E_n} - e^{-\beta E_m}) \delta(\omega + E_n - E_m), \tag{2.28}$$

is the same for both retarded and Matsubara (imaginary time) Green's functions. $A(\mathbf{q},\omega)$ is defined in terms the Grand canonical partition function $\mathcal{Z}$, and the states n and m. Alternatively, we can use a spectral function for the single-particles Green's functions,

$$A(\mathbf{q},\omega) = \frac{1}{\mathcal{Z}} \sum_{mn} |< n|c_k|m >|^2 (e^{-\beta E_n} - e^{-\beta E_m}) \delta(\omega + E_n - E_m). \tag{2.29}$$

In this form, we can see that the spectral function satisfies a sum rule. Integrating (2.29) over all ω and dividing by 2π, and relabeling indices on the second term,

$$\begin{aligned}
\int_{-\infty}^{\infty} \frac{{\rm d}\omega}{2\pi} A(\mathbf{q},\omega) &= \frac{1}{\mathcal{Z}} \sum_{mn} e^{-\beta E_n} \Big(< n|c_q|m >< m|c_q^\dagger|n > + < n|c_q^\dagger|m >< m|c_q|n > \Big) \\
&= \frac{1}{\mathcal{Z}} \sum_{n} e^{-\beta E_n} < n|(c_q c_q^\dagger + c_q^\dagger c_q)|n > \\
, &= \frac{1}{\mathcal{Z}} \sum e^{\beta E_n} < n|n >= 1,
\end{aligned} \tag{2.30}$$

where fermionic anti-commutation relations were used to reach the last line. We can then calculate correlators in terms of Matsubara Green's functions, and obtain the retarded functions which correspond to physical observables by making the appropriate analytic continuation.

2.2 Disordered d-wave superconductor

2.2.1 Model and bare Green's function

We will now begin building the model to describe the low temperature transport in d-wave superconductors. Although there is much evidence that the normal state of the cuprates (i.e., a cuprate above the critical temperature) is far from normal (in the sense of not resembling a Fermi liquid), the superconducting state is remarkably similar to a BCS superconductor[14].

There is vast evidence that the interesting behavior in cuprates is all occurring within the CuO_2 planes[16]. Therefore, we will build an effective field theory in 2+1 dimensions, and will calculate the transport in a single plane. To compare with experimental results, then, we must divide by the stacking density d to obtain the conductivity in three dimensions. The effective theory describes the low-energy properties of the system. Because we are interested in low temperature properties, the high energy modes are thus frozen out.

Since phonon modes are frozen out at low temperatures, and we will not be considering the effects of magnetic fields (which would generate vortices from which quasiparticles could scatter)[71, 72], the only mechanism degrading a quasiparticle current will be impurity scattering. Therefore, we will need to incorporate a randomizing element into our description of the system. As such, the effective hamiltionian has two components: the part describing the d-wave superconductor, and the part describing the disorder (impurities).

$$H_{\text{effective}} = H_{d\text{SC}} + H_{\text{disorder}} \tag{2.31}$$

First, let us explain $H_{d\text{SC}}$. The hamiltonian for a system of interacting electrons is

$$H = \int \mathrm{d}\mathbf{x}\psi^\dagger_\sigma(\mathbf{x})(\frac{-\nabla^2}{2m})\psi_\sigma(\mathbf{x}) + \frac{1}{2}\int \mathrm{d}\mathbf{x}\mathrm{d}\mathbf{x}'\psi^\dagger_\sigma(\mathbf{x})\psi^\dagger_\lambda(\mathbf{x}')V(\mathbf{x}-\mathbf{x}')\psi_\lambda(\mathbf{x}')\psi_\sigma(\mathbf{x}) \tag{2.32}$$

In BCS theory, the electron-electron interaction can become effectively attractive due to an instability in electron-phonon coupling. In this event, the interactions between electrons of zero net angular momentum are the only ones with a sizable phase space. Then, the interacting hamiltonian is simplified to

the pairing hamiltonian, which, due to the restriction on pair momentum, is more easily written in momentum space.

Although cuprates are very different than BCS superconductors, a BCS-like description will be valid in the superconducting state. Therefore, we will make use of the pairing hamiltonian

$$H_{d\mathrm{SC}} = \sum_{k\sigma} \left(\epsilon_k c^\dagger_{k\sigma} c_{k\sigma} + \Delta_k c^\dagger_{k\uparrow} c^\dagger_{-k\downarrow} \right) + \mathrm{h.c.}, \tag{2.33}$$

which differs from the conventional BCS hamiltonian only by the modification to account for a d-wave order parameter, $\Delta \to \Delta_k$.

Such a hamiltonian already represents a vast simplification over that of (2.32), by virtue of the fact that the pairing hamiltonian is quadratic in terms of the electron field operators. This was achieved by requiring self-consistency relations for the order parameter

$$\Delta_k = \sum_{k'} \Delta_{k'} V_{kk'} < c_{k\alpha} c_{-k\beta} > \tag{2.34}$$

The mean-field treatment has eliminated quartic operators from our hamiltonian, but the existence of $c_k c_{-k}$ terms indicates that particle number is no longer conserved: this corresponds to creation and destruction of Cooper pairs. A useful formalism was developed by Yoichiro Nambu, whereby we represent $H_{d\mathrm{SC}}$ in terms of a single field operator,

$$\psi^\dagger_k = \begin{pmatrix} c^\dagger_{k\uparrow} & c_{-k\downarrow} \end{pmatrix}. \tag{2.35}$$

To write $H_{d\mathrm{SC}}$ in terms of the Nambu field operators, we will need to rearrange a little bit. We write out the d-wave hamiltonian,

$$H_{d\mathrm{SC}} = \sum_k \left(\epsilon_k c^\dagger_{k\uparrow} c_{k\uparrow} + \epsilon_k c^\dagger_{k\downarrow} c_{k\downarrow} + \Delta_k c^\dagger_{k\uparrow} c^\dagger_{-k\downarrow} + \Delta^*_k c_{-k\downarrow} c_{k\uparrow} \right). \tag{2.36}$$

Since we are only concerned with bulk properties of a single superconductor, and will not need to consider coherence effects that can arise from Josephson tunneling, we are free to choose the phase of the order parameter. We therefore take $\Delta^*_k = \Delta_k$. Additionally, making use of parity invariance, we also have

$\epsilon_{-k} = \epsilon_k$[99]. Therefore we have

$$\begin{aligned} H_{d\mathrm{SC}} &= \sum_k \Big(\epsilon_k(c^\dagger_{k\uparrow}c_{k\uparrow} + c^\dagger_{-k\downarrow}c_{-k\downarrow}) + \Delta_k(c^\dagger_{k\uparrow}c^\dagger_{-k\downarrow} + c_{-k\downarrow}c_{k\uparrow})\Big) \\ &= \sum_k \Big(\epsilon_k(c^\dagger_{k\uparrow}c_{k\uparrow} - c_{-k\downarrow}c^\dagger_{-k\downarrow}) + \Delta_k(c^\dagger_{k\uparrow}c^\dagger_{-k\downarrow} + c_{-k\downarrow}c_{k\uparrow})\Big) \\ &= \sum_k \begin{pmatrix} c^\dagger_{k\uparrow} & c_{-k\downarrow} \end{pmatrix} \begin{pmatrix} \epsilon_k & \Delta_k \\ \Delta_k & -\epsilon_k \end{pmatrix} \begin{pmatrix} c_{k\uparrow} \\ c^\dagger_{-k\downarrow} \end{pmatrix} \\ &\equiv \sum_k \psi^\dagger_k \widetilde{H}_k \psi_k \end{aligned} \tag{2.37}$$

where we have made use of fermionic anti-commutation relations.

As for the hamiltonian defined in terms of the Nambu field operators, we can likewise consider a Nambu matrix formalism for the Green's functions, which includes the propagators for pairs. We make use of a tilde to signify that an operator is considered in the Nambu space. The bare Green's functions (Matsubara) for the dSC system are thus

$$\begin{aligned} \widetilde{\mathcal{G}}_0(\mathbf{k}, i\omega) &= \widetilde{(i\omega - H_k)}^{-1} \\ &= \frac{1}{((i\omega)^2 - \epsilon_k^2 - \Delta_k^2)} \begin{pmatrix} i\omega + \epsilon_k & \Delta_k \\ \Delta_k & i\omega - \epsilon_k \end{pmatrix} \end{aligned} \tag{2.38}$$

2.2.2 Self energy and impurity scattering

We have just computed the bare Green's function, representing the propagator of the quasiparticles of a system described by $H_{d\mathrm{SC}}$. We must now incorporate the self-energy of the quasiparticles due to impurity scattering.

We therefore introduce a small, but finite density of (identical) impurities,

$$n_{\mathrm{imp}}(\mathbf{r}) = \sum_{i=1}^{N} \delta(\mathbf{r} - \mathbf{r}_i) \equiv n_{\mathrm{imp}}(\mathbf{r}; \mathbf{r}_1, ..., \mathbf{r}_N) \tag{2.39}$$

These impurities generate the random potential

$$V(\mathbf{r}) = \int \mathrm{d}\mathbf{x}' V_{\mathrm{imp}}(\mathbf{x}') n_{\mathrm{imp}}(\mathbf{x} - \mathbf{x}'), \tag{2.40}$$

which is felt by quasiparticles as they move through the system. Inclusion of the impurities destroys the translational invariance, so that the Green's

functions are once again a function of both $\mathbf{k}$ and $\mathbf{k}'$,

$$\widetilde{\mathcal{G}} = \widetilde{\mathcal{G}}(\mathbf{k}, \mathbf{k}'; i\omega). \tag{2.41}$$

The Green's functions, and by extension, the macroscopic observables such as the thermal conductivity, technically now depend not only on the density of impurities, but on their exact configuration within the sample as well. This configuration dependence is important in mesoscopic conductance fluctuations,which can be important in low dimensional systems at low temperatures[68]. If the sample is large enough, however, we can take a configurational average, which will remove this dependence on impurity configuration. The argument runs as follows: divide the entire sample into subcells. In each subcell is a particular impurity configuration of density n_{imp}. Then, in calculating observables, we include a summation over the subcells of the sample. This summation averages over each different configuration included in each subcell (according to its proper probability distribution). Upon doing this configurational average, we restore translation invariance to the Green's functions, that is,

$$< \widetilde{\mathcal{G}}(\mathbf{k}, \mathbf{k}'; i\omega) >_{\text{configuration}} = \widetilde{\mathcal{G}}(\mathbf{k}, i\omega), \tag{2.42}$$

where the brackets represent the configuration average.

Proceeding in this manner, we can calculate the self-energy of the quasiparticles, where we include the effects of the random potential,

$$V(\mathbf{k} - \mathbf{k}') = V_{\text{imp}}(\mathbf{k} - \mathbf{k}') \sum_{i=1}^{N} \exp(-i(\mathbf{k} - \mathbf{k}') \cdot \mathbf{r}_i, \tag{2.43}$$

and average over impurity configurations $\mathbf{r}_i$. The details of this procedure are lengthy, and we refer to Rammer[68]. The result, however is simple: that we obtain the configurational averaged dressed Green's function by including the Green's functions self-consistently in a perturbation series, where the small parameter is the impurity density n_{imp}. Let us then apply this to our model of a disordered d-wave superconductor.

Dyson's equation[64, 66, 68] tells us that the dressed Green's function is given by

$$\widetilde{\mathcal{G}}(\mathbf{k}, i\omega) = (\widetilde{\mathcal{G}}_0^{-1}(\mathbf{k}, i\omega) - \widetilde{\Sigma}(\mathbf{k}, i\omega))^{-1}, \tag{2.44}$$

which is represented diagrammatically in Fig. 2.1. We will guess a form for the self-energy, and then self-consistently compute the Green's functions in terms of that self-energy. The self-energy, like the Green's functions, are Nambu

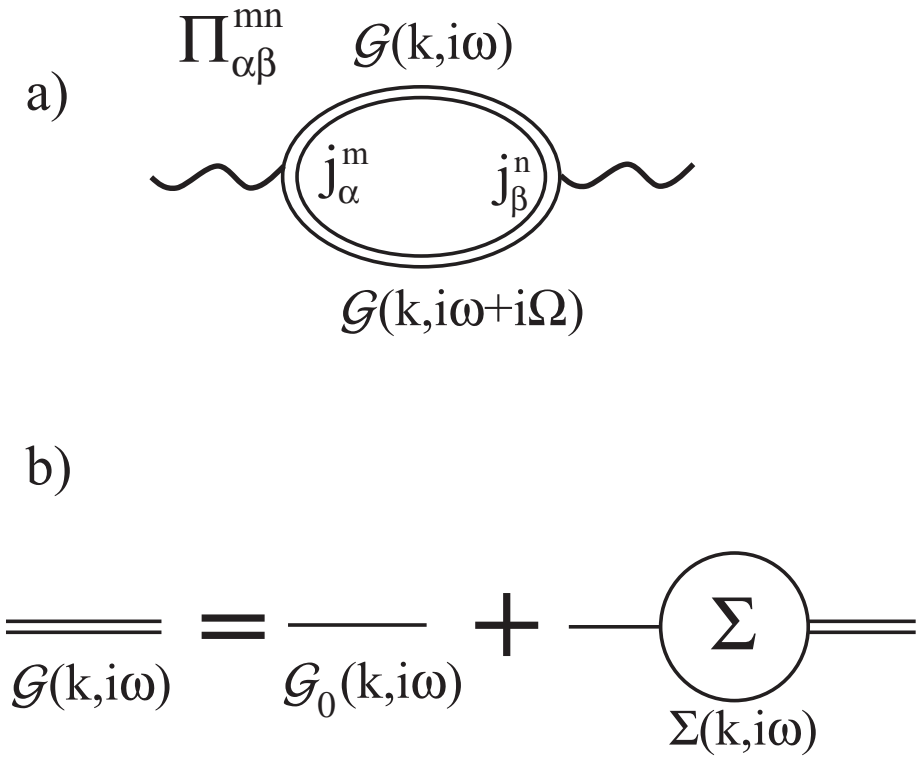

Figure 2.1: a) Bare-bubble approximation of current-current correlation function. The single particle Green's functions include self-energy effects, but the two-particle Green's function (i.e. current-current correlator) does not. b) Self-energy of the single-particle Green's function.

matrices,

$$\widetilde{\Sigma}(\mathbf{k}, i\omega) = \sum_i \Sigma_i(\mathbf{k}, i\omega)\widetilde{\tau}_i \tag{2.45}$$

which we have chosen to expand in terms of Pauli matrices.

Since the self-energy changes the location of the poles of the Green's function, the imaginary part of the self-energy is proportional to the inverse of quasiparticle lifetime, and the real part corresponds to a renormalization of the quasiparticle dispersion[64, 70]. The analog for our Nambu Green's functions is that the imaginary part of the diagonal portion of the self-energy (Σ_0) will correspond to the scattering induced lifetime, and that the other parts (Σ_1 and Σ_3) correspond to some kind of renormalization. It has previously been determined that in the unitary (strong scatterer strength) and Born (weak scatterer strength) limits, that Σ_1 and Σ_3 can be neglected, although this might not be justified for intermediate strength scatterers[73, 74].

We therefore obtain the dressed Green's functions by allowing

$$\widetilde{\Sigma}(\mathbf{k}, \omega) \rightarrow -i\Gamma(\omega)\widetilde{\tau}_0, \tag{2.46}$$

where $\Gamma(\omega)$ is the impurity scattering rate (inverse quasiparticle lifetime). Putting this form of self-energy into Dyson's equation, we obtain

$$\widetilde{\mathcal{G}}(\mathbf{k}, i\omega) = \frac{1}{((i\omega + i\Gamma(i\omega))^2 - E_k^2)} \begin{pmatrix} i\omega + i\Gamma(i\omega) + \epsilon_k & \Delta_k \\ \Delta_k & i\omega + \Gamma(i\omega) - \epsilon_k, \end{pmatrix} \tag{2.47}$$

where we have made use of the definition $E_k = \sqrt{\epsilon_k^2 + \Delta_k^2}$ for the quasiparticle energy.

2.2.3 Density of states

With the self-consistent Green's functions (single particle) in hand, we can proceed to calculate the density of states. The density of states is given by

$$N(\omega) = \sum_k \mathrm{Tr}[\widetilde{A}(\mathbf{k}, \omega)], \tag{2.48}$$

where the spectral function,

$$\widetilde{A}(\mathbf{k}, \omega) = \frac{-1}{\pi}\mathrm{Im}\widetilde{\mathcal{G}}_{\mathrm{Ret}}(\mathbf{k}, \omega) \tag{2.49}$$

is given by

$$\widetilde{A}(\mathbf{k},\omega) = \frac{-1}{\pi}\frac{-\Gamma(\omega)(\omega^2-\Gamma^2(\omega)-E_k^2)\widetilde{\tau}_0 + 2\omega\Gamma(\omega)(\Delta_k\widetilde{\tau}_1+\epsilon_k\widetilde{\tau}_3)}{(\omega^2-\Gamma^2(\omega)-E_k^2)^2+4\omega^2\Gamma^2(\omega)}. \quad (2.50)$$

Noting that it is nonzero only around the four nodal locations (near $(\pm\pi/2,\pm\pi/2)$), we can make use of the fact that the dispersion and gap vary linearly in the vicinity of those points to reparametrize these quantities, and scale out the anisotropy of the Dirac cones. We therefore define $p_1 \equiv \epsilon_k = v_f k_1$ and $p_2 \equiv \Delta_k = v_\Delta k_2$, where $\mathbf{v}_f \equiv \frac{\partial\epsilon_k}{\partial\mathbf{k}}$ and $\mathbf{v}_\Delta \equiv \frac{\partial\Delta_k}{\partial\mathbf{k}}$ are called the Fermi velocity and gap velocity, and point in the directions perpendicular to, and parallel to the Fermi surface, respectively, as depicted in Fig. 2.2.

Using this "nodal" parametrization, summations over momenta $\mathbf{k}$ are replaced by a summation over the four nodes, followed by integration around the local coordinates. Some integrals will be done using angular coordinates, $p_1 \equiv p\cos\theta$ and $p_2 \equiv \sin\theta$, where θ will range from 0 to 2π, and p will range from 0 to p_0, as depicted in Fig. 2.2. The integrand far from the nodes is effectively zero—but we still need to fix the size of each region to match the size of a quarter of the Brillouin zone, in particular for quantities such as Born approximation self-energy, which is logarithmically dependent on the cutoff, p_0. The sum over k-space becomes

$$\begin{aligned}\sum_k f(\mathbf{k}) &= \sum_{j=1}^{4}\int \mathrm{d}^2 p f^{(j)}(\mathbf{p}) \\ &= \sum_{j=1}^{4}\int\frac{\mathrm{d}\theta}{2\pi}\int\frac{p\mathrm{d}p}{2\pi v_f v_\Delta}f^{(j)}(p). \end{aligned} \quad (2.51)$$

With this in mind, we calculate the density of states via the integral over p, with result

$$\begin{aligned}N(\omega) = \frac{2\Gamma(\omega)}{\pi^2 v_f v_\Delta}\Big(\log\frac{p_0}{\Gamma(\omega)} - \log\sqrt{\frac{\Gamma^2(\omega)+\omega^2}{\Gamma^2(\omega)}}\Big) \\ +\frac{|\omega|}{\pi v_f v_\Delta}\Big(\frac{1}{2}-\frac{1}{\pi}\arctan(\frac{\Gamma^2(\omega)-\omega^2}{2|\omega|\Gamma(\omega)})\Big). \end{aligned} \quad (2.52)$$

This result is illustrated in Fig. 2.3. In this form it is particularly clear that there is an energy scale, Γ, in the density of states. For $\omega >> \Gamma(\omega)$, the first term is unimportant, compared with the second term, which goes as $|\omega|\arctan(\omega/\Gamma(\omega)) \sim |\omega|$, which agrees with the prediction of a linear density of states. The density of states does not vanish at zero energy, however. For

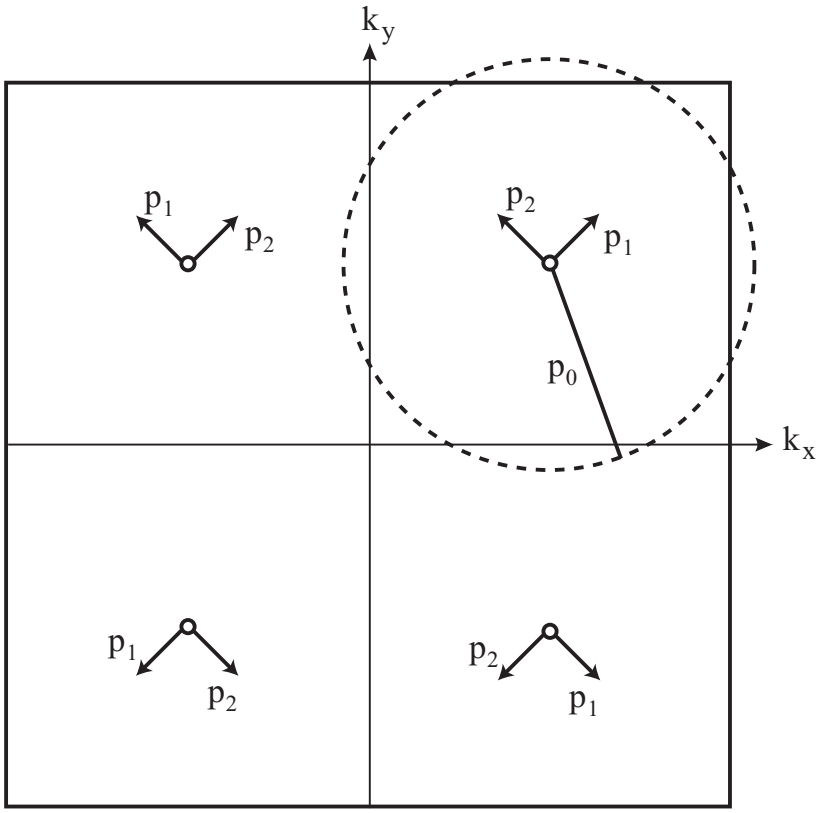

Figure 2.2: Brillouin zone of the model d-wave superconductor. Local coordinates p_1 and p_2 are defined around each node. Summations over k-space can then be converted to a sum over nodes, and an integral about each node. If integrals are done in local polar coordinates with $p_1 \equiv p\cos\theta$ and $p_2 \equiv \sin\theta$, the upper bound of the p integral is the cutoff p_0, as illustrated about the $(\pi/2, \pi/2)$ node.

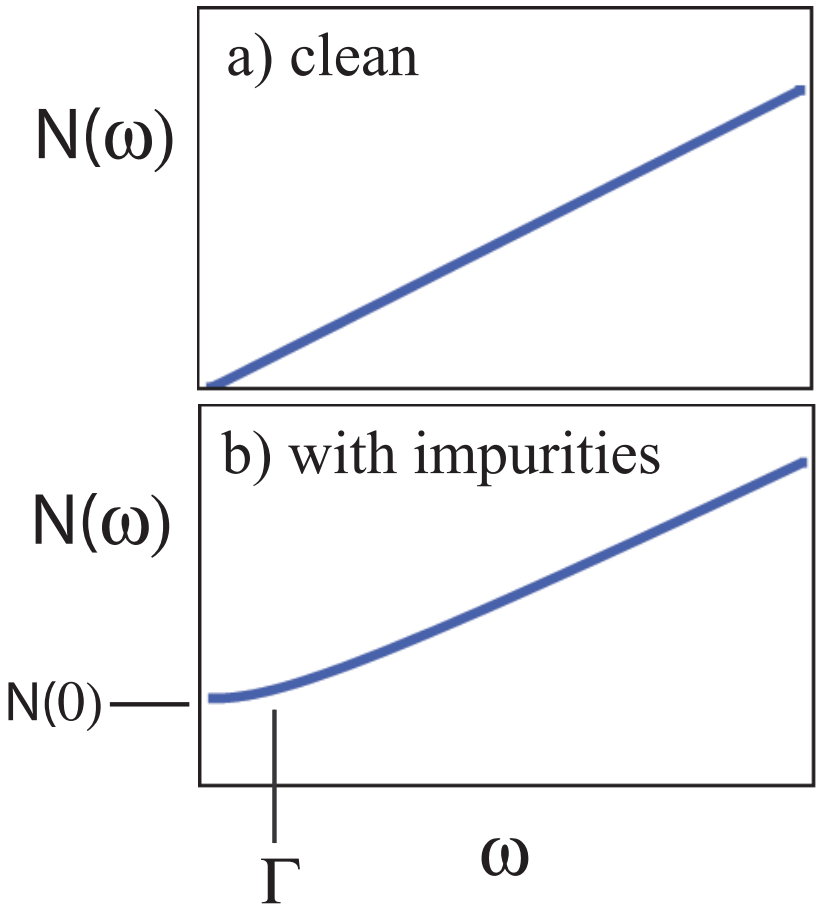

Figure 2.3: a) Illustration of the density of states in a clean (free of impurities) d-wave superconductor ($\Gamma = 0.001$). The density of states is effectively linear down to zero energy. b) Density of states in a disordered d-wave superconductor ($\Gamma = 0.1$). The presence of impurities induces a finite density of states in energies $\omega < \Gamma$.

$\omega << \Gamma(\omega)$, the second term of (2.52) is vanishing, while the first approaches a small constant,

$$N(\omega \to 0) = \frac{2\Gamma_0}{\pi^2 v_f v_\Delta} \log(\frac{p_0}{\Gamma_0}), \tag{2.53}$$

where we adapt the notation $\Gamma_0 \equiv \lim_{\omega \to 0} \Gamma(\omega)$ for the zero frequency limit of the scattering rate. Note that there is a leveling off of the vanishing density of states at zero energy; the zero energy value goes as $\Gamma_0 \log(\Gamma_0/p_0)$. A heuristic argument for the existence of universal limit conductivity is based on the existence of these quasiparticles: the density of these quasiparticles is proportional to the inverse lifetime, so that they are generated and scattered at the same rate, hence leaving the conductivity unaffected by the disorder. This is only a rough estimate—the calculation must be done in full for accuracy.

2.2.4 Thermal conductivity

Having found that there is a finite density of quasiparticle states down to very low energies, we can now determine their contribution to the thermal conductivity. The phononic contribution to thermal conductivity is known: phonons add a term proportional to T^3 in large samples (the power law can be modified due to phonon scattering from boundaries in some samples)[25–27]. By plotting $\frac{\kappa}{T}$ as a function of T^2, then, the quasiparticle contribution can be isolated in experimental data.

We will use the linear response formalism developed in this chapter to calculate the thermal conductivity. As a first estimate, we will use the "bare-bubble" thermal conductivity, meaning that we will include self-energy corrections to the single particle Green's functions, but will not include them for the two-particle Green's functions. In other words, we will neglect the effects of vertex corrections. We will explain the significance of this approximation later in the chapter. The Kubo formula for the thermal conductivity is

$$\frac{\kappa(\Omega, T)}{T} = -\frac{1}{T^2} \frac{\mathrm{Im}(\Pi_{\mathrm{Ret}}(\Omega))}{\Omega}, \tag{2.54}$$

where the (imaginary time) time-ordered current-current correlation function is depicted by the diagram in Fig. 2.1.

The Matsubara correlation function depicted in the figure is

$$\Pi^{mn}(i\Omega) = \frac{1}{\beta} \sum_{i\omega_n} \sum_k \mathrm{Tr}\Big(\widetilde{\mathcal{G}}(\mathbf{k}, i\omega) \widetilde{j}_Q^m(\mathbf{k}, i\omega, i\omega + i\Omega) \widetilde{\mathcal{G}}(\mathbf{k}, i\omega + i\Omega) \widetilde{j}_Q^n(\mathbf{k}, i\omega, i\omega + i\Omega)\Big), \tag{2.55}$$

where $\widetilde{\mathcal{G}}$ are the Matsubara Green's functions for the dSC derived in the pre-

vious section, $\widetilde{j}_Q$ is the dynamic limit of the current operator (derived in Appendix F,

$$\widetilde{j}_Q^m(\mathbf{q}\to 0,\Omega)=\sum_k\sum_{i\omega_n}(i\omega_n+\frac{\Omega}{2})[v_f^m\psi_k^\dagger\widetilde{\tau}_3\psi_{k+q}-v_\Delta^m\psi_k^\dagger\widetilde{\tau}_1\psi_{k+q}] \tag{2.56}$$

The indices m and n are components of the second-rank tensor in position space; while the conductivity should be isotropic for the d-wave superconductor, this situation will change in the next chapter when we include density waves. Defining the notation

$$\widetilde{j}_Q^m=\sum_\alpha\sum_k\sum_{i\omega_n}(i\omega_n+\frac{\Omega_n}{2})v_\alpha^m\psi_k^\dagger\widetilde{\tau}_\alpha\psi_k \tag{2.57}$$

we can write the Matsubara correlation function (breaking it into four pieces: Fermi-Fermi, Fermi-gap, gap-Fermi and gap-gap) as

$$\Pi_{\alpha\beta}^{mn}(i\Omega)=\frac{1}{\beta}\sum_k v_\alpha^m v_\beta^n\sum_{i\omega_n}(i\omega_n+\frac{i\Omega_n}{2})^2\mathrm{Tr}\Big(\widetilde{\mathcal{G}}(\mathbf{k},i\omega)\widetilde{\tau}_\alpha\widetilde{\mathcal{G}}(\mathbf{k},i\omega+i\Omega)\widetilde{\tau}_\beta\Big) \tag{2.58}$$

To compute the bare-bubble thermal conductivity, it is possible to make use of the spectral representation in order to simplify the calculations. With the definition

$$\widetilde{\mathcal{G}}(\mathbf{k},i\omega)=\int \mathrm{d}\omega_1\frac{\widetilde{A}(\mathbf{k},\omega_1)}{i\omega-\omega_1}, \tag{2.59}$$

where the spectral function is given by Eq. 2.49. the correlator becomes

$$\Pi_{\alpha\beta}^{mn}=\sum_k v_\alpha^m v_\beta^n\int \mathrm{d}\omega_1\int \mathrm{d}\omega_2\mathrm{Tr}\Big(\widetilde{A}(\mathbf{k},\omega_1)\widetilde{\tau}_\alpha\widetilde{A}(\mathbf{k},\omega_2)\widetilde{\tau}_\beta\Big)S_0(i\Omega), \tag{2.60}$$

where we defined the function

$$S_0(i\Omega)\equiv\frac{1}{\beta}\sum_{i\omega_n}\frac{(i\omega+\frac{i\Omega}{2})^2}{(i\omega-\omega_1)(i\omega+i\Omega-\omega_2)}. \tag{2.61}$$

$S_0(i\Omega)$ is computed using the standard Matsubara techniques in AppendixE. Analytically continuing $i\Omega\to\Omega+i\delta$ We can make the analytic continuation $i\Omega\to\Omega+i\delta$ in the correlation through its effect on S_0.

$$\mathrm{Im}(S_{\mathrm{Ret}}(\Omega))=-\pi\delta(\omega_1-\omega_2+\Omega)\Big(n_f(\omega_1)(\omega_1+\frac{\Omega}{2})^2-n_f(\omega_2)(\omega_2-\frac{\Omega}{2})^2\Big) \tag{2.62}$$

whereupon we have

$$\mathrm{Im}(\Pi_{\mathrm{Ret}}(\Omega) = \sum_k v_\alpha^m v_\beta^n \int \mathrm{d}\omega_1 \mathrm{Tr}\Big(\widetilde{A}(\omega_1)\widetilde{\tau}_\alpha \widetilde{A}(\omega_1{+}\Omega)\widetilde{\tau}_\beta\Big)\Big(n_f(\omega_1){-}n_f(\omega_1{+}\Omega)\Big)(\omega{+}\frac{\Omega}{2})^2. \tag{2.63}$$

To proceed, we use the parametrization $p_1 \equiv v_f k_1$, and $p_2 \equiv v_\Delta k_2$, so that, noting the alternating handedness of the velocities apparent in Fig.2.2, the sum over the nodes becomes

$$\begin{aligned} \sum_k v_\alpha^m(\mathbf{k}) v_\beta^n(\mathbf{k}) \quad &\rightarrow \quad \sum_{j=1}^4 \int \frac{\mathrm{d}^2 p}{4\pi^2 v_f v_\Delta} v_\alpha^m(j,\mathbf{p}) v_\beta^n(j',\mathbf{p}') \\ &= \quad \int \frac{\mathrm{d}^2 p\, v_\alpha^2}{2\pi^2 v_f v_\Delta} \delta_{mn}, \end{aligned} \tag{2.64}$$

where v_f and v_Δ are the values of the Fermi velocity and gap velocity near the nodal locations at $(\pm\pi/2, \pm/2)$, which is taken to be a constant over the area around the nodes. The low temperature, low frequency thermal conductivity is therefore

$$\lim_{\Omega\rightarrow 0} \frac{\kappa^{mn}(\Omega,T)}{T} = \int \frac{\mathrm{d}^2 p\, v_\alpha^2}{2\pi^3 v_f v_\Delta} \int \mathrm{d}\omega \mathrm{Tr}\Big(\widetilde{A}(\omega)\widetilde{\tau}_\alpha \widetilde{A}(\omega)\widetilde{\tau}_\alpha\Big)(\frac{\partial n_f(\omega)}{\partial \omega})(\frac{\omega}{T})^2 \tag{2.65}$$

The derivative of the Fermi function is sharply peaked at the Fermi energy, so that the only part of the spectral functions bearing any weight is at $\omega = 0$. We will make the assumption that the self-energy at zero energy is of the form

$$\widetilde{\Sigma}(\omega \rightarrow 0) = -i\Gamma(\omega \rightarrow)) \equiv -i\Gamma_0. \tag{2.66}$$

From the form of the spectral function, (2.49), we find that

$$\frac{\kappa(\Omega = 0, T \rightarrow 0)}{T} \equiv \frac{\kappa_{00}}{T} = \int \frac{\mathrm{d}^2 p\, (v_f^2 + v_\Delta^2)}{\pi^3 v_f v_\Delta} \frac{\Gamma_0^2}{(\Gamma_0^2 + p^2)} \mathrm{I}_\omega, \tag{2.67}$$

where we have defined the integral

$$\begin{aligned} \mathrm{I}_\omega &\equiv \int \mathrm{d}\omega (\frac{\omega}{T})^2 (-\frac{\partial n_f}{\partial \omega}) \\ &= \int \mathrm{d}\omega \frac{\beta \omega^2 e^{\beta\omega}}{T^2 (e^{\beta\omega}+1)^2} \\ &= k_B^2 \int_0^\infty \mathrm{d}x (\frac{\log x}{x+1})^2 \\ &= \frac{\pi^2 k_B^2}{3}. \end{aligned} \tag{2.68}$$

We therefore find

$$\begin{aligned} \frac{\kappa_{00}}{T} &= \frac{k_B^2}{3\pi} \frac{v_f^2 + v_\Delta^2}{v_f v_\Delta} \int_0^{p_0} p \mathrm{d}p \frac{\Gamma_0^2}{(\Gamma_0^2 + p^2)^2} \\ &= \frac{k_B^2}{3\pi\hbar} \frac{v_f^2 + v_\Delta^2}{v_f v_\Delta}, \end{aligned} \tag{2.69}$$

where we have evaluated the integral in the limit $p_0 >> \Gamma_0$, and restored a factor of $\hbar$. This result was previously obtained by Durst and Lee[24].

2.3 Boltzmann equation and importance of vertex corrections

2.3.1 Boltzmann equation in metals

In order to gain some physical understanding of the vertex corrections which were neglected in the previous section, we will review some basics of the theory of transport in metals[75, 76]. The simplest description of electronic transport is through the semi-classical picture, whereby the transport of electrons is determined by the non-equilibrium electron distribution function, $f_{\mathbf{k}}(\mathbf{r})$, which measures the probability of an electron in quantum state $\mathbf{k}$ being found at point $\mathbf{r}$ at time t. There are three ways in which $f_{\mathbf{k}}$ can evolve in time. First, electrons are moving in and out of the neighborhood of $\mathbf{r}$. By Liouville's theorem (conserving volumes in phase space),

$$f_{\mathbf{k}}(\mathbf{r}, t) = f_{\mathbf{k}}(\mathbf{r} - \mathbf{v}_{\mathbf{k}} t, 0), \tag{2.70}$$

so that the rate of change of $f_{\mathbf{k}}$ due to diffusion is

$$\Big(\frac{\partial f_{\mathbf{k}}}{\partial t}\Big)_{\text{diff.}} = -\mathbf{v}\cdot\frac{\partial f_{\mathbf{k}}}{\partial \mathbf{r}}. \tag{2.71}$$

The wave-vector of the electrons is affected by external fields as

$$\frac{\mathrm{d}\mathbf{k}}{\mathrm{d}t} \;=\; \frac{1}{\hbar}\mathbf{F}(\mathbf{r},\mathbf{k}), \tag{2.72}$$

this is just the $\mathbf{k}$-gradient of the distribution function,

$$\Big(\frac{\partial f_{\mathbf{k}}}{\partial t}\Big)_{\text{fields}} = -\frac{\partial \mathbf{k}}{\partial t}\cdot\frac{\partial f_{\mathbf{k}}}{\partial \mathbf{k}}. \tag{2.73}$$

The third manner in which the distribution function is affected is due to collisions. We are considering only elastic scattering (assuming impurities to be fixed, and without internal structure), which leads to the collision term

$$\Big(\frac{\mathrm{d}f_{\mathbf{k}}}{\mathrm{d}t}\Big)_{\text{collision}} = 2\pi n_{\text{imp}}\int \mathrm{d}\mathbf{k}'\delta(\epsilon_k-\epsilon_{k'})\Big(f_{\mathbf{k}'}(1-f_{\mathbf{k}})-f_{\mathbf{k}}(1-f_{\mathbf{k}'})\Big)W_{\mathbf{k}\mathbf{k}'}, \tag{2.74}$$

where $W_{\mathbf{k}\mathbf{k}'}$ is the transition rate between states $\mathbf{k}$ and $\mathbf{k}'$.

In a homogenous system, the diffusion term is not present, as the distribution function will not depend on $\mathbf{r}$. The Boltzmann equation is then

$$\frac{\partial \mathbf{k}}{\partial t}\cdot\frac{\partial f}{\partial \mathbf{k}} + \Big(\frac{df_{\mathbf{k}}}{\mathrm{d}t}\Big)_{\text{collision}} = 0 \tag{2.75}$$

The difficulty in solving the Boltzmann equation lies in the evaluation of the collision term. The easiest approximation is to make the relaxation time approximation, which assumes that

$$\Big(\frac{df_{\mathbf{k}}}{\mathrm{d}t}\Big)_{\text{collision}} = \frac{f_{\mathbf{k}}-f^0_{\mathbf{k}}}{\tau_{\mathrm{t}}(\mathbf{k})}, \tag{2.76}$$

where $f^0_{\mathbf{k}} = \frac{2}{e^{\beta\xi_{\mathbf{k}}}+1}$ is the equilibrium distribution function, which is the Fermi function (times a factor of two for spin), and the quantity $\tau_{\mathrm{t}}(\mathbf{k})$ is labelled the transport relaxation time. The Boltzmann equation is

$$f_{\mathbf{k}} = f^0_{\mathbf{k}} - e\tau_{\mathrm{t}}(\mathbf{k})\mathbf{E}\cdot\frac{\partial f_{\mathbf{k}}}{\partial \mathbf{k}} \tag{2.77}$$

For small fields, the system is not disturbed far from the equilibrium, so

that we can approximate

$$\frac{\partial f_{\mathbf{k}}}{\partial \mathbf{k}} \approx \frac{\partial f^0_{\mathbf{k}}}{\partial \mathbf{k}} = \frac{\mathbf{k}}{m}\frac{\partial f^0}{\partial \epsilon_k}, \tag{2.78}$$

so that the current density

$$\begin{aligned} \mathbf{j} &= e\int \frac{\mathrm{d}\mathbf{k}}{(2\pi)^d} f_{\mathbf{k}} \frac{\hbar \mathbf{k}}{m} \\ &= e^2 \int \frac{\mathrm{d}\mathbf{k}}{(2\pi)^d} \tau_{\mathrm{t}}(k) \mathbf{v}_k (\mathbf{v}_k \cdot \mathbf{E}) \Big(-\frac{\mathrm{d}f^0_k}{\mathrm{d}\epsilon_k}\Big), \end{aligned} \tag{2.79}$$

so that the conductivity is proportional to the transport time

$$\sigma = \frac{ne^2}{m}\tau_{\mathrm{t}}. \tag{2.80}$$

Evaluation of the integral in (2.74), and reduction of the common factor $f_{\mathbf{k}} - f^0_{\mathbf{k}}$ leads to the definition

$$\frac{1}{\tau_{\mathrm{t}}(\mathbf{k})} = 2\pi n_{\mathrm{imp}} \int \frac{\mathrm{d}\mathbf{k}'}{(2\pi)^d} \delta(\epsilon_k - \epsilon_{k'}) |W_{\mathbf{k}\mathbf{k}'}|^2 (1 - \cos\theta') \tag{2.81}$$

Note the importance of the factor $(1 - \cos\theta') = 1 - \mathbf{k}\cdot\mathbf{k}'/k^2$. The time in between scattering events (known as the relaxation time) is given by

$$\frac{1}{\tau(k)} = 2\pi n_{\mathrm{imp}} \int \frac{\mathrm{d}\mathbf{k}'}{(2\pi)^d} \delta(\epsilon_k - \epsilon_{k'}) |W_{\mathbf{k}\mathbf{k}'}|^2. \tag{2.82}$$

The $1 - \cos\theta'$ term thus accounts for the fact that small angle scattering does not degrade a current as much as large angle scattering.

In terms of the field-theoretic techniques used in this dissertation, if one uses the bare-bubble method (including only self-energy in the single-particle Green's functions) of calculating the conductivity, we obtain a conductivity which is proportional to the relaxation time,

$$\sigma_{\mathrm{bare-bubble}} \propto \tau_{\mathrm{rel}}, \tag{2.83}$$

whereas if we include self-energy corrections to the two-particle Green's function as well, we get the results in terms of a transport time,

$$\sigma_{\mathrm{vertex-corrected}} \propto \tau_{\mathrm{transport}} \tag{2.84}$$

In using field-theoretic techniques to calculate a conductivity then, we must

include vertex corrections if we want to account for the fact that small angle scattering does not degrade a current as much as large angle scattering[66, 70].

2.3.2 Boltzmann equation in dSC

In a metal, both the charge and energy of the excitations are well defined: this means that elastic collisions which degrade the heat current will have the same effect on the electrical current. Thus, the ratio of electrical to thermal conductivity is fixed,

$$\frac{\kappa}{\sigma} = LT, \tag{2.85}$$

where L is defined as the Lorentz number, and T is the temperature.

In d-wave superconductors, the elementary excitations are nodal quasiparticles, rather than the electron-like excitations of a metal. Because a quasiparticle is a superposition of an electron and hole,

$$\alpha_k^\dagger = u_k c_{k\uparrow}^\dagger + v_k c_{-k\downarrow}, \tag{2.86}$$

its charge is not well-defined. The electron and hole carry opposite charge in opposite directions: this means that the electrical current is proportional to the Fermi velocity, $\mathbf{v}_f \equiv \frac{\partial \epsilon_k}{\partial \mathbf{k}}$. On the other hand, the energy of the quasiparticles remains well-defined, which means that the thermal current is instead proportional to the group velocity, $\mathbf{v}_G \equiv \frac{\partial E_k}{\partial \mathbf{k}}$.

Because the Fermi velocity's magnitude and direction is relatively constant in the vicinity of a single node, an electrical current is degraded much more effectively via inter-node scattering processes. Because the bare-bubble method of calculating the conductivity does not distinguish between inter-nodal and intra-nodal scattering, the vertex corrections are expected to be important for the electrical conductivity: the full computations indeed verify this[24].

The group velocity, on the other hand, varies direction within a single node, so that the thermal current can be degraded through either inter-node or intra-node scattering. This indicates that the bare-bubble conductivity should be sufficient to determine the thermal conductivity.

The calculations and conclusions of this chapter are due to previous work by Adam Durst and Patrick Lee [22, 24]. In the following chapter, we extend the low-temperature transport calculations to models of d-wave superconductors in the presence of additional order parameters.

Chapter 3

Transport in a d-wave superconductor amidst coexisting charge density wave order of wave vector $\mathbf{Q} = (\pi, 0)$

3.1 Introduction

The superconducting phase of the cuprate superconductors exhibits d-wave pairing symmetry[15]. As such, there exist four nodal points on the two-dimensional Fermi surface at which the quasiparticle excitations are gapless, and quasiparticles excited in the vicinity of a node behave like massless Dirac fermions[12, 77, 78]. The presence of impurities enhances the density of states at low energy[23] resulting in a universal limit ($T \to 0, \omega \to 0$) where the thermal conductivity is independent of disorder[22, 24, 79–83]. Calculations have shown that the thermal conductivity retains this universal character even upon the inclusion of vertex corrections[24]. Experiments have confirmed the validity of this quasiparticle picture of transport by observing their universal limit contribution to the thermal conductivity, and thereby measuring the anisotropy of the the Dirac quasiparticles, v_f/v_Δ[25–27, 29–36].

For some time, there has been significant interest[63, 84–88] in the idea of additional types of order coexisting with d-wave superconductivity (dSC) in the cuprates. And in recent years, as the underdoped regime of the phase diagram has been explored in greater detail, evidence of coexisting order has grown substantially[63]. Particularly intriguing has been the evidence of

checkerboard charge order revealed via scanning tunneling microscopy (STM) experiments[48–50, 52–63]. And if charge order coexists with d-wave superconductivity in the underdoped cuprates, it begs the question of how the quasiparticle excitation spectrum is modified. Previous work[89] has shown that even with the addition of a charge or spin density wave to the dSC hamiltonian, the low-energy excitation spectrum remains gapless as long as a harmonic of the ordering vector does not nest the nodal points of the combined hamiltonian, or break the composite symmetry of time-reversal and lattice translation. However, if the coexisting order is strong enough, the nodal points can move to k-space locations where they are nested by the ordering vector, at which point the excitation spectrum becomes fully gapped[89–91].

Such a nodal transition should have dramatic consequences for low-temperature thermal transport, the details of which were studied in Ref.91. That paper considered the caes of a conventional s-wave charge density wave (CDW) of wave vector $\mathbf{Q} = (\pi, 0)$ coexisting with d-wave superconductivity. It showed that the zero-temperature thermal conductivity vanishes, as expected, once charge order is of sufficient magnitude to gap the quasiparticle spectrum. In addition, the dependence of zero-temperature thermal transport was calculated and revealed to be disorder-dependent. Hence, in the presence of charge order, the universal-limit is no longer universal. This result is in line with the results of recent measurements[28, 36**?** –40] of the underdoped cuprates, as well as other calculations [93, 94].

We extend the work of Ref.91 herein. We consider the same physical system, but employ a more sophisticated model of disorder that includes the effects of impurity scattering within the self-consistent Born approximation. We find that this self-consistent treatment of disorder requires that off-diagonal components be retained in our matrix self-energy. These additional components lead to a renormalization of the critical value of charge order beyond which the thermal conductivity vanishes. Furthermore, we include the contribution of vertex corrections within our diagrammatic thermal transport calculation. While vertex corrections become more important as charge order increases, especially for long-ranged impurity potentials, we find that for reasonable parameter values, they do not significantly modify the bare-bubble result.

In Sec. 3.2, we introduce the model hamiltonian of the dSC+CDW system and describe the effect charge ordering has on the nodal excitations. In addition, the model for disorder is presented. In Sec. 3.3.1, a numerical procedure for computing the self-energy within the self-consistent Born approximation is outlined. The results of its application in the relevant region of parameter space are presented in Sec. 3.3.2. In Sec. 3.4, we calculate the thermal

conductivity using a diagrammatic Kubo formula approach, including vertex corrections within the ladder approximation. An analysis of the vertex corrected results, comparison with bare-bubble, and an analysis of the clean limit thermal conductivity is presented in Sec. 3.5. Alo=so in this section, we discuss how our self-consistent model of disorder renormalizes the nodal transition point, the value of charge order parameter at which the nodes effectively vanish. Conclusions are presented in Sec. 3.6.

3.2 Model

We employ the phenomenological hamiltonian of Ref. 91 in order to calculate the low temperature thermal conductivity of the fermionic excitations of a d-wave superconductor with a $\mathbf{Q} = (\pi, 0)$ charge-density wave, in the presence of a small but finite density of point-like impurity scatterers. The presence of d-wave superconducting order contributes a term to the hamiltonian

$$H_{dSC} = \frac{1}{2} \sum_{k\alpha} \left(\epsilon_k c^\dagger_{k\alpha} c_{k\alpha} + \Delta_k c^\dagger_{k\alpha} c^\dagger_{-k\beta} \right) + \text{h.c.} \tag{3.1}$$

where ϵ_k is a typical tight-binding dispersion, and Δ_k an order parameter of $d_{x^2-y^2}$ symmetry. Due to the d-wave nature of the gap, nodal excitations exist in the $(\pm\pi, \pm\pi)$ directions with respect to the origin. The locations of these nodes in the absence of charge ordering are close to the points $(\pm\pi/2, \pm\pi/2)$, and are denoted with white dots in Fig. 3.1. These low energy excitations are massless anisotropic Dirac fermions. That is, the electron dispersion and pair function are linear functions of momentum in the vicinity of these nodal locations. We will refer to the slopes of the electron dispersion and pair function, defined by $\mathbf{v}_f \equiv \frac{\partial \epsilon_k}{\partial \mathbf{k}}$ and $\mathbf{v}_\Delta \equiv \frac{\partial \Delta_k}{\partial \mathbf{k}}$, as the Fermi velocity and gap velocity respectively. The energy of the quasiparticles in the vicinity of the nodes is given by $E_k = \sqrt{v_f^2 k_1^2 + v_\Delta^2 k_2^2}$, where k_1 and k_2 are the momentum displacements (from the nodes) in directions perpendicular to and parallel to the Fermi surface. The universal limit ($T \to 0, \Omega \to 0$) transport properties of these quasiparticles was explored in Sec. 2.2[24].

While experiments have revealed evidence of a number of varieties of spin and charge order, the system described in this chapter will be restricted to the addition of a site-centered charge density wave of wave vector $\mathbf{Q} = (\pi, 0)$, which contributes a term to the hamiltonian

$$H_{CDW} = \sum_{k\alpha} a_k c^\dagger_{k\alpha} c_{k+Q\alpha} + \text{h.c.} \tag{3.2}$$

In real space, this corresponds to the charge being modulated as $\rho(\mathbf{x}) = \rho_0 + \delta\rho(\mathbf{x})$, with $\delta\rho(\mathbf{x}) \propto \cos(\pi x)$. The charge density wave doubles the unit cell, reducing the Brillouin zone to the shaded portion seen in Fig. 3.1. Restricting summations over momentum space to the reduced Brillouin zone, and invoking the charge density wave's time-reversal symmetry and commensurability with the reciprocal lattice, we are able to write the hamiltonian as

$$H = \sum_k \Psi_k^\dagger H_k \Psi \quad H_k = H_k^{dSC} + H_k^{CDW}, \tag{3.3}$$

where

$$H_k = \begin{pmatrix} \epsilon_k & \Delta_k & \psi & 0 \\ \Delta_k & -\epsilon_k & 0 & -\psi \\ \psi & 0 & \epsilon_{k+Q} & \Delta_{k+Q} \\ 0 & -\psi & \Delta_{k+Q} & -\epsilon_{k+Q} \end{pmatrix}, \tag{3.4}$$

is a matrix in the basis of extended Nambu vectors,

$$\Psi_k = \begin{pmatrix} c_{k\uparrow} \\ c^\dagger_{-k\downarrow} \\ c_{k+Q\uparrow} \\ c^\dagger_{-k-Q\downarrow} \end{pmatrix} \quad \Psi_k^\dagger = \begin{pmatrix} c^\dagger_{k\uparrow} & c_{-k\downarrow} & c^\dagger_{k+Q\uparrow} & c_{-k-Q\downarrow} \end{pmatrix} \tag{3.5}$$

and ψ represents the constant value taken at the nodes by the charge density order parameter $A_k = a_k + a^*_{k+Q}$.

The onset of the charge order modifies the energy spectrum of the clean hamiltonian so that the locations of the nodes evolve along curved paths towards the $(\pm\frac{\pi}{2}, \pm\frac{\pi}{2})$ points at the edges of the reduced Brillouin zone, as was noted in Ref. 90. "Ghost" nodes, their images in what is now the second reduced Brillouin zone, evolve the same way, until the charge density wave is strong enough that the nodes and ghost nodes collide at those $(\pm\pi/2, \pm\pi/2)$ points. When that occurs, $\mathbf{Q}$ nests two of the nodes, gapping the spectrum so that low temperature quasiparticle transport is no longer possible. We define the value of ψ at which this occurs as ψ_c. Due to the nodal properties of the quasiparticles, all functions of momentum space $\mathbf{k}$ can be parametrized in terms of a node index j, and local coordinates p_1 and p_2 in the vicinity of each node. We choose to parametrize our functions using symmetrized coordinates

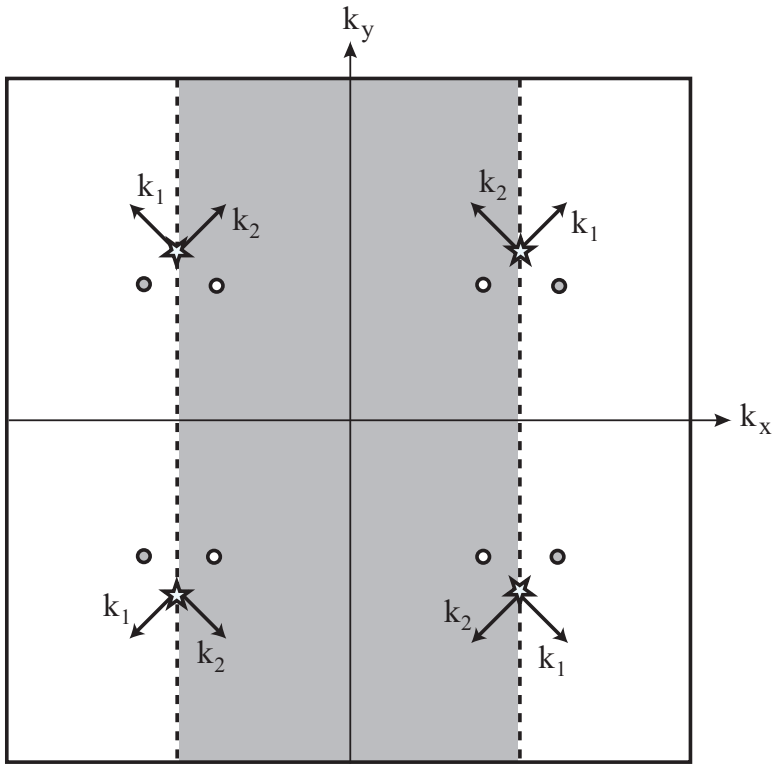

Figure 3.1: Illustrated is the Brillouin zone for our model, reduced to the shaded region by unit-cell doubling charge order. The $\psi = 0$ nodal locations are illustrated by white dots. They are displaced by a distance k_0 from the $(\pm\frac{\pi}{2}, \pm\frac{\pi}{2})$ points (stars). As the charge density wave's amplitude increases, the location of the gapless excitations evolves along curved paths toward the $(\pm\frac{\pi}{2}, \pm\frac{\pi}{2})$ points, until ψ reaches ψ_c, when the spectrum becomes gapped because the nodes are nested by the charge density wave-vector. The gray dots depict the images of the nodes in the second reduced Brillouin zone.

centered at $(\pm\pi/2, \pm\pi/2)$,

$$\begin{aligned} \epsilon_k &= \psi_c + \beta p_1 \qquad & \Delta_k &= \frac{1}{\beta} p_2 \\ \epsilon_{k+Q} &= \psi_c + \beta p_2 \qquad & \Delta_{k+Q} &= \frac{1}{\beta} p_1 \end{aligned} \tag{3.6}$$

where we have rescaled $\sqrt{v_f v_\Delta} k_1 = p_1$ for the coordinate normal to Fermi surface, $\sqrt{v_f v_\Delta} k_2 = p_2$ for the coordinate parallel to Fermi surface, and introduced the definition $\beta \equiv \sqrt{\frac{v_f}{v_\Delta}}$. In this coordinate system, the displacement of the original node locations from the collision points is given by ψ_c. A sum over momentum space is therefore performed by summing over nodes, and integrating over each node's contribution, as follows.

$$\begin{aligned} \sum_k f(\mathbf{k}) &\to \frac{1}{2} \sum_{j=1}^{4} \int \frac{\mathrm{d}^2 p}{4\pi^2 v_f v_\Delta} f^{(j)}(p_1, p_2) \\ &= \frac{1}{8\pi^2 v_f v_\Delta} \sum_{j=1}^{4} \int_{-p_0}^{p_0} \mathrm{d}p_1 \int_{-p_0}^{p_0} \mathrm{d}p_2 \; f^{(j)}(p_1, p_2) \end{aligned} \tag{3.7}$$

where the factor of $\frac{1}{2}$ comes from extending the integrals to all p_1 and p_2, rather than just the shaded part depicted in Fig. 3.1, and p_0 is a high-energy cutoff.

At sufficiently low temperatures, the thermal conductivity is dominated by the nodal excitations, since phonon modes are frozen out, and other quasiparticles are exponentially rare. Using this fact, we can calculate the low temperature thermal conductivity of the system using linear response formalism.

We incorporate disorder into the model by including scattering events from randomly distributed impurities. Because the quasiparticles are created and destroyed only in the vicinity of the four nodal locations near $(\pm\pi/2, \pm\pi/2)$, only limited information about the scattering potential is needed. In particular, the scattering potential $V_{kk'}$ can be simplified to contain only the amplitudes V_1, V_2 and V_3, for intra-node, adjacent node, and opposite node scattering respectively[24]. We calculate the thermal conductivity using linear response formalism, wherein we obtain the retarded current-current correlation function by analytic continuation of the corresponding Matsubara correlator.

In previous research,using a simplified model for disorder, where the electron self-energy was assumed to be a negative imaginary scalar, the thermal conductivity was calculated as a function of ψ, and found to vanish for

$\psi > \psi_c$[91]. We now improve upon that result by calculating the self-energy within the self-consistent Born approximation, and by including vertex corrections within the ladder approximation in our calculation of the thermal conductivity.

3.3 Self-energy

3.3.1 SCBA calculation

Within the self-consistent Born approximation (SCBA), the self-energy tensor is given by

$$\widetilde{\Sigma}(\mathbf{k},\omega) = n_{\text{imp}} \sum_{k'} |V_{kk'}|^2 \, (\widetilde{\sigma_0 \otimes \tau_3}) \widetilde{\mathcal{G}}(\mathbf{k},\omega) (\widetilde{\sigma_0 \otimes \tau_3}) \tag{3.8}$$

where n_{imp} is the impurity density and $\widetilde{V}_{kk'} = V_{kk'}(\widetilde{\sigma_0 \otimes \tau_3})$ accompanies each scattering event, as seen in Fig. 3.2. The tilde signifies an operator in the extended Nambu basis, and the σ's and τ's are Pauli matrices in charge-order-coupled and particle-hole spaces respectively. $\widetilde{\mathcal{G}}(\mathbf{k},\omega)$ is the full Green's

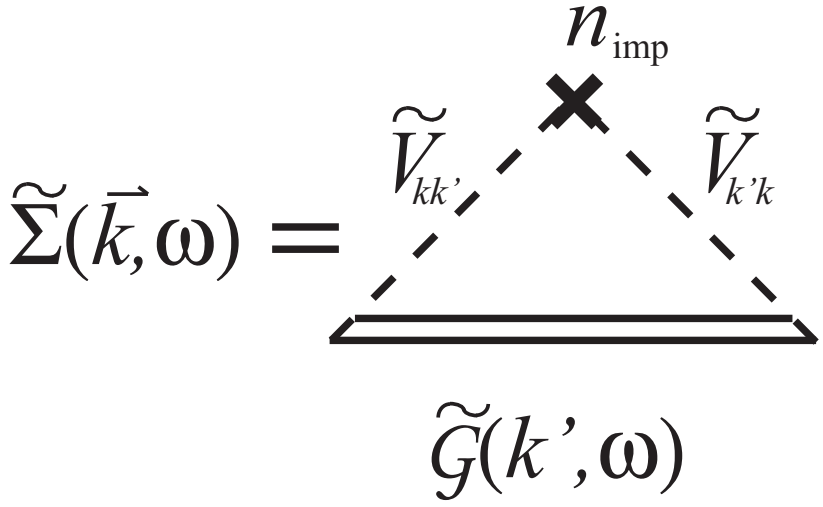

Figure 3.2: Feynman diagram depicting self-energy in the self-consistent Born approximation. The double line represents the dressed propagator, the dashed line represents the interaction with the impurity, and the cross represents the impurity density.

function, whose relation to the bare Green's function $\widetilde{\mathcal{G}}_0(\mathbf{k},\omega)$ and the self-

energy $\widetilde{\Sigma}(\mathbf{k},\omega)$ is given by Dyson's equation

$$\widetilde{\mathcal{G}}(\mathbf{k},\omega) = (\widetilde{\mathcal{G}}_0^{-1}(\mathbf{k},\omega) - \widetilde{\Sigma}(\mathbf{k},\omega))^{-1}, \tag{3.9}$$

the bare Green's function having been determined by

$$\widetilde{\mathcal{G}}_0(\mathbf{k},\omega) = (\omega\widetilde{1} - \widetilde{H}_k)^{-1}. \tag{3.10}$$

Eq. (3.8) and Eq. (3.9) define a set of integral equations for the self-energy $\widetilde{\Sigma}(\mathbf{k},\omega)$.

For the calculation of the universal-limit thermal conductivity, it is sufficient to find the zero-frequency limit of the self-energy. In its present form, $\widetilde{\Sigma}$ has 32 real components. Below, we demonstrate that this number can be reduced further to six components.

If we write the Green's function as

$$\widetilde{\mathcal{G}}(\mathbf{k},\omega) = \frac{1}{\mathcal{G}_{den}} \begin{pmatrix} \mathcal{G}_A & \mathcal{G}_B \\ \mathcal{G}_C & \mathcal{G}_D \end{pmatrix}, \tag{3.11}$$

where

$$\mathcal{G}_\alpha = \sum_{i=0}^{3} \mathcal{G}_{\alpha i}\tau_i \tag{3.12}$$

then the self-energy can be written as the set of 16 complex equations (for $\alpha = \{A,B,C,D\}$, $i = \{0,1,2,3\}$)

$$\begin{aligned} \Sigma_{\alpha i} &= n_{\rm imp} \sum_{k'} |V_{kk'}|^2 \frac{\xi_i}{\mathcal{G}_{den}} \mathcal{G}_{\alpha i} \\ &= \xi_i c \int \mathrm{d}^2 p \frac{\mathcal{G}_{\alpha i}(p_1,p_2)}{\mathcal{G}_{den}(p_1,p_2)} \end{aligned} \tag{3.13}$$

where $\xi_i = \left\{ \begin{array}{l} +1,\ i=0,3 \\ -1,\ i=1,2 \end{array} \right\}$, $c = \frac{n_i(V_1^2+2V_2^2+V_3^2)}{8\pi^2 v_f v_2}$, and the final line is realized by using the notation of Eq. (3.6) and Eq. (3.7) and completing the sum over nodes. From the symmetries of the hamiltonian, we are able to ascertain

certain symmetries the bare Green's function will obey, specifically,

$$\begin{aligned}
\mathcal{G}^{(0)}_{A0}(p_2,p_1) &= \mathcal{G}^{(0)}_{D0}(p_1,p_2) \\
\mathcal{G}^{(0)}_{A1}(p_2,p_1) &= \mathcal{G}^{(0)}_{D1}(p_1,p_2) \\
\mathcal{G}^{(0)}_{A3}(p_2,p_1) &= \mathcal{G}^{(0)}_{D3}(p_1,p_2) \\
\mathcal{G}^{(0)}_{B0}(p_2,p_1) &= \mathcal{G}^{(0)}_{C0}(p_1,p_2) \\
\mathcal{G}^{(0)}_{B1}(p_2,p_1) &= \mathcal{G}^{(0)}_{C1}(p_1,p_2) \\
\mathcal{G}^{(0)}_{B2}(p_2,p_1) &= -\mathcal{G}^{(0)}_{C2}(p_1,p_2) \\
\mathcal{G}^{(0)}_{B3}(p_2,p_1) &= \mathcal{G}^{(0)}_{C3}(p_1,p_2) \\
\mathcal{G}^{(0)}_{\rm den}(p_2,p_1) &= \mathcal{G}^{(0)}_{\rm den}(p_1,p_2)
\end{aligned} \tag{3.14}$$

In addition, the realization that the integration is also symmetric with respect to exchange of p_1 and p_2, coupled with these symmetries, lead to relations for self-energy components

$$\begin{aligned}
\Sigma_{Ai} &= \Sigma_{Di} \\
\Sigma_{Bi} &= \Sigma_{Ci} \qquad\qquad i = 0,1,2,3 \\
\Sigma_{B2} &= \Sigma_{C2} = 0
\end{aligned} \tag{3.15}$$

so that we see a reduction from 32 components of the self-energy to 6 independent components:$\{\Sigma_{\alpha i}\} \equiv \{\Sigma_{A0}, \Sigma_{A1}, \Sigma_{A3}, \Sigma_{B0}, \Sigma_{B1}, \Sigma_{B3}\}$. A self-consistent self-energy must therefore satisfy 6 coupled integral equations given by Eq. (3.13).

The self-consistent calculation of the self-energy proceeds by applying the following scheme: First, a guess is made as to which self-energy components will be included. The full Green's function corresponding to such a self-energy is then obtained from Dyson's equation, Eq. (3.9). The quantitative values of the $\Sigma_{\alpha i}$'s are then determined as follows: An initial guess for the quantitative values of each of the $\Sigma_{\alpha i}$'s is made, and the six integrals of Eq. (3.13) are computed numerically, which provides the next set of guesses for $\{\Sigma_{\alpha i}\}$. This process is repeated until a stable solution is reached. Finally, the resulting solutions must be checked that they are consistent with the initial guess for the form of $\widetilde{\Sigma}$. If they are, the self-consistent calculation is complete.

We begin with the simplest assumption, that $\widetilde{\Sigma}^{(1)}(\omega) = -i\Gamma_0\widetilde{(\sigma_0 \otimes \tau_0)}$, where Γ_0 is the zero-frequency limit of the scattering rate. The superscript indicates that this is the first guess for $\widetilde{\Sigma}$. The Green's function components are computed, which gives the explicit form of Eq. (3.8). Upon evaluating the numerics, it is seen that this first iteration generates a nonzero (real and negative) term for Σ_{B1}. So, the diagonal self-energy assumption turns out to

be inconsistent, in contrast to the situation for $\psi = 0$. We then modify our guess, assuming self-energy of the form $\widetilde{\Sigma}^{(2)} = -i\Gamma_0(\widetilde{\sigma_0 \otimes \tau_0}) - B_1(\widetilde{\sigma_1 \otimes \tau_1})$. The Green's function is computed again, using Dyson's equation, and the self-energy equations are obtained explicitly. It is noted that the symmetries of Eq. (3.14) still hold. Again, the equations (3.13) are solved iteratively; the result is a non-zero Σ_{B3} component as well. Once again, the Green's functions are modified to incorporate this term, and the iterative scheme is applied. Calculation of the self-energy based on the assumption

$$\widetilde{\Sigma}^{(3)} = -i\Gamma_0(\widetilde{\sigma_0 \otimes \tau_0}) - B_1(\widetilde{\sigma_1 \otimes \tau_1}) - B_3(\widetilde{\sigma_1 \otimes \tau_3}) \qquad \Gamma_0, B_1, B_3 > 0 \tag{3.16}$$

generates Γ_0, B_1 and B_3 that are much larger than any remaining terms, and hence provides the self-consistent values of Σ_{A0}, Σ_{B1} and Σ_{B3}. A plot of the 6 components of $\widetilde{\Sigma}$ is displayed in Fig. 3.3 for a representative parameter set, where we see that the three terms of the ansatz are indeed dominant. For the remainder of this chapter, the effect of the Σ_{A1}, Σ_{A3} and Σ_{B0} components will be ignored. The self-consistent Green's functions and bare Green's functions are provided in Appendix D.2, while further characteristics of the self-energy are discussed in Appendix D.1.

3.3.2 SCBA results

In order to discuss the numerical results contained in this chapter, it is necessary to make a note about the units employed. The following discussion of units applies as well to the numerical analysis of the results of the thermal conductivity in Sec. 3.5. Because we are studying the evolution of the system with respect to increasing CDW order parameter ψ, we wish to express energies in units of ψ_c, the value of ψ which gaps the clean system. In order to do this, the cutoff p_0 is fixed such that the Brillouin zone being integrated over in Eq. (3.7) has the correct area. In this way, p_0 sets the scale of the product $v_f v_\Delta$; a parameter $\beta \equiv \sqrt{\frac{v_f}{v_\Delta}}$ is defined to represent the velocity anisotropy. Then, $\frac{p_0}{\psi_c} = \frac{\pi}{2a}\sqrt{v_f v_\Delta}$, so that we may eliminate the frequently occurring parameter $4\pi v_f v_\Delta$ by expressing lengths in units of $\frac{4}{\sqrt{\pi}}a \approx 2.25a$. Impurity density n_{imp} is thus recast in terms of impurity fractions z according to $n_{\text{imp}} = \frac{16}{\pi}z$. Finally, the parameters of the scattering potential are recast in terms of their anisotropy: that is, we define $V_2 \equiv R_2 V_1$ and $V_3 \equiv R_3 V_1$.

With these modifications, the original set of parameters, $\{n_i, V_1, V_2, V_3, v_f, v_\Delta, p_0, \psi, \psi_c\}$ is reduced to $\{z, V_1, R_2, R_3, \beta, p_0, \psi\}$. For the work contained herein, the cutoff

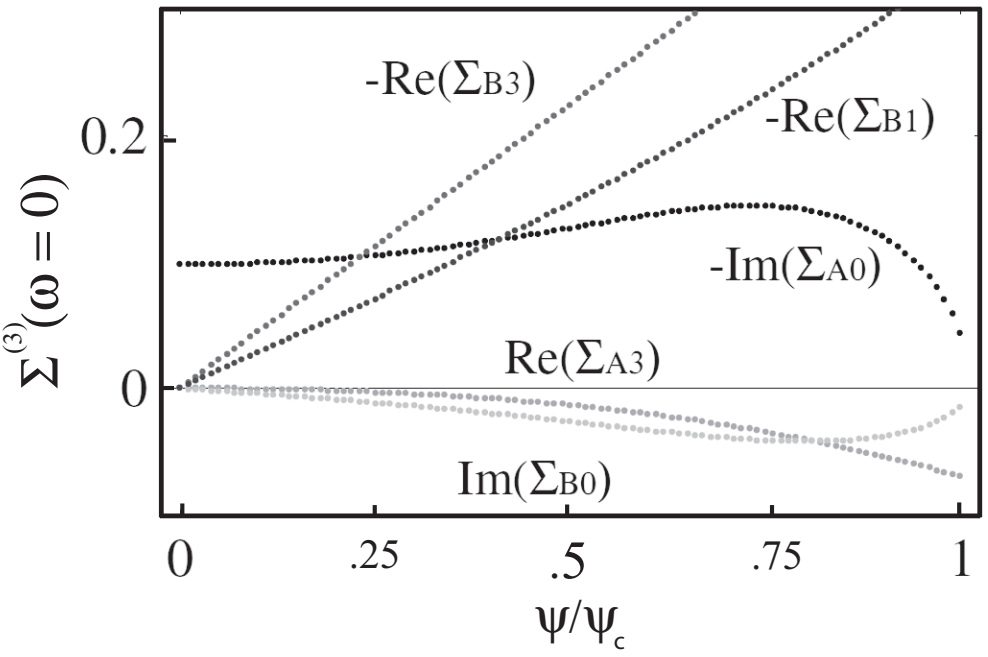

Figure 3.3: Components of self-energy computed using iterative procedure described in Section II. The third iteration self-energy, $\widetilde{\Sigma}^{(3)}$, is shown here. The dominance of $\Gamma_0 = -\mathrm{Im}(\Sigma_{A0}), B_1 = -\mathrm{Re}(\Sigma_{B1})$ and $B_3 = -\mathrm{Re}(\Sigma_{B3})$ over other components establishes this third iteration as yielding the self-consistent value of the self-energy. Σ_{A1} and Σ_{A3} overlap.

p_0 is fixed at $p_0 = 100$. The self energy in the self-consistent Born approximation was computed for different scattering potentials as a function of impurity fraction and CDW order parameter ψ. Since it was found that three of the components, Σ_{A0}, Σ_{B1} and Σ_{B3}, dominate over the others, we will subsequently analyze only those three components, referring to their magnitudes as Γ_0, B_1 and B_3 respectively.

As $z \to 0$, the Green's functions become impossibly peaked from a numerical point of view. For sufficiently large z, depending on the strength of the scatterers, the Born approximation breaks down. Given a scattering strength of $V_1 = 110$, cutoff $p_0 = 100$, scattering potentials that fall off slowly in k-space and velocity anisotropy ratios $\beta \equiv \sqrt{v_f/v_\Delta} = 1, 2, 3, 4$, this puts the range of z in which our numerics may be applied at roughly between one half and one percent.

Some results for $\widetilde{\Sigma}(\psi)$, for several values of z, are shown in Figs. 3.4 and 3.5. These graphs correspond to the same parameters, except that Fig. 3.4 illustrates the $v_f = v_\Delta$ case, and Fig. 3.5 illustrates $v_f = 16 v_\Delta$. In all cases it is seen that

$$\begin{aligned} B_1(\psi, z) &\simeq b_1(z)\psi \\ B_3(\psi, z) &\simeq b_3(z)\psi \end{aligned} \tag{3.17}$$

where the dependence of B_1, B_3, b_1, and b_3 on the remaining parameters is implicit. For much of the parameter space sampled, Γ_0 does not have much ψ dependence, except that it typically rises and then falls to zero at some sufficiently large $\psi < \psi_c$. This feature will be revisited in Sec. 3.5, wherein it is explained that this vanishing scattering rate coincides with vanishing thermal conductivity, and corresponds to the effective gapping of the system by the self-consistent disorder. The value of ψ at which this occurs depends on the entire set of parameters used, and will be referred to as ψ_c^*. The observed z dependence is not very surprising, in light of Eq. (3.13). Σ depends on z roughly according to

$$\begin{aligned} \Gamma_0 &\sim p_0 \exp\left(-\frac{1}{z}\right) \\ B_1 &\sim z \\ B_3 &\sim z \end{aligned} \tag{3.18}$$

as can be seen in Fig. 3.6. When $\psi = 0$, Γ_0 is given exactly by $\Gamma_0 = p_0 \exp(\frac{-1}{2\pi c})$, where c is defined following Eq. (3.13), which is the same result found in Ref. 24, up to a geometric factor in the definition of high-energy cutoff. For finite ψ, this exact form does not hold, but the strong z dependence of Γ_0

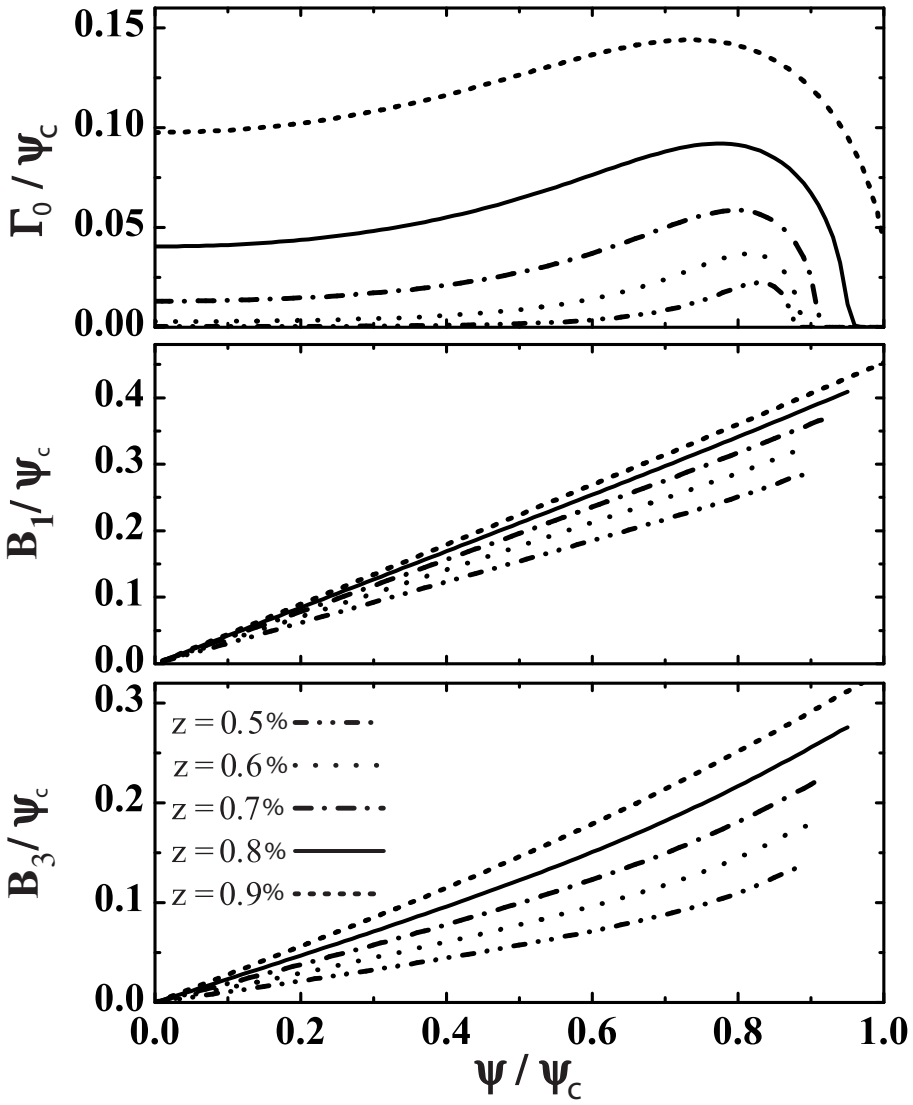

Figure 3.4: Effects of disorder on charge-order-dependence of self-energy components. To satisfy Dyson's equation, it is necessary to include three (Nambu space) components of the self energy. Their self-consistent values are plotted here for several different values of impurity fraction z. Here, the scattering potential is given in our three parameter model as $\{V_1, R_2, R_3\} = \{110, 0.9, 0.8\}$, which represents a fairly short-ranged potential. These results are for the case of isotropic nodes ($v_f = v_\Delta$). The energies of $\widetilde{\Sigma}$ are in units of ψ_c.

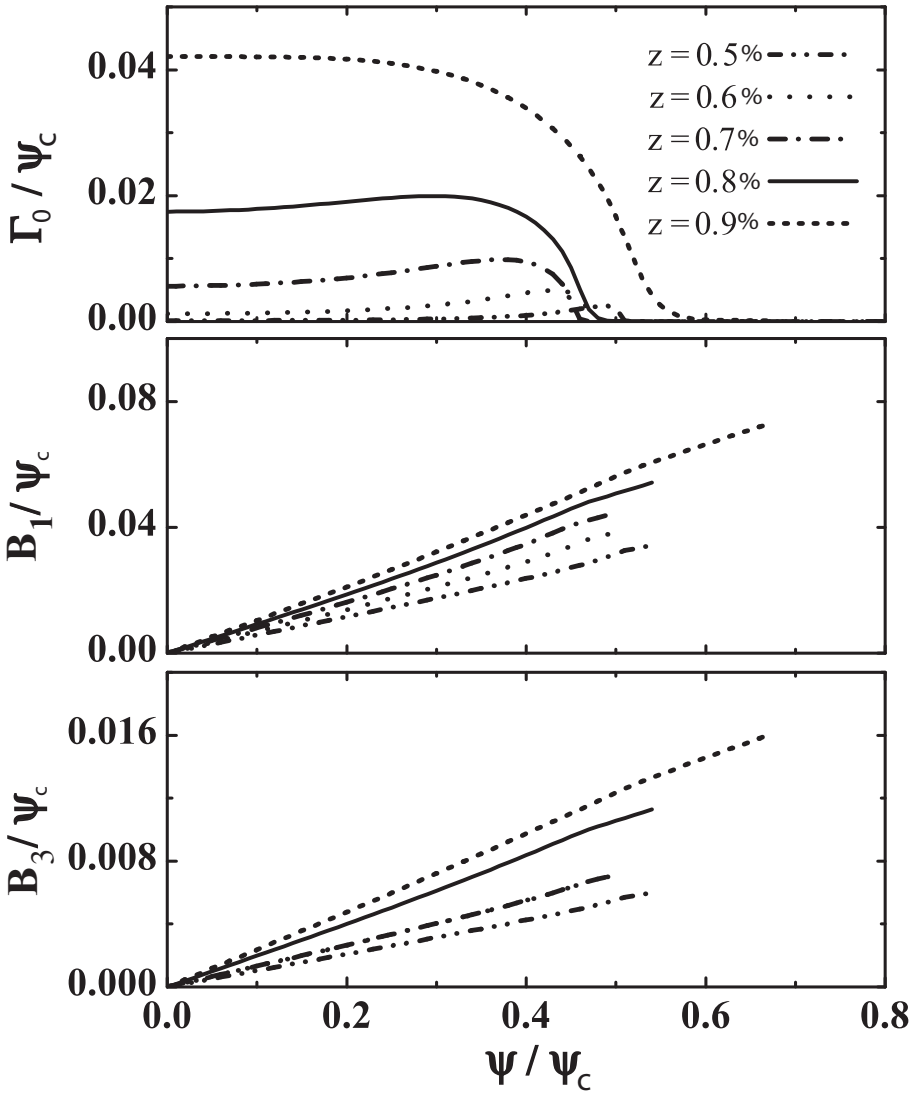

Figure 3.5: Effects of disorder on charge-order-dependence of self-energy components. This figure illustrates the case where $v_f = 16v_\Delta$. The scattering potential is again given by $\{V_1, R_2, R_3\} = \{110, 0.9, 0.8\}$, representing a fairly short-ranged potential. The plots for B_1 and B_3 terminate before ψ reaches ψ_c because for sufficiently large ψ, the excitations become gapped and the quasiparticle density of states goes to zero. The energies of $\tilde{\Sigma}$ are in units of ψ_c.

remains, in contrast to that of B_1 and B_3. Note that the z dependence of B_1 and B_3 is roughly linear for $\psi \ll \psi_c^*$. As ψ approaches ψ_c^* the functions diverge slightly from linearity. Results are shown in increments of 0.2 for $\psi < \psi_c^*$.

3.4 Thermal conductivity

Thermal conductivity was calculated using the Kubo formula [**?**],

$$\frac{\kappa(\Omega, T)}{T} = -\frac{\mathrm{Im}\Pi_{\mathrm{Ret}}(\Omega)}{\Omega\, T^2}, \tag{3.19}$$

where $\Pi_{\mathrm{Ret}}(\Omega)$ is the retarded thermal current-current correlation function. To find this correlator, it is necessary to first compute the appropriate current operator, which is done in Appendix F. In second quantized form,

$$\widetilde{\mathbf{j}}_0^{\kappa} = \lim_{\substack{q\to 0\\ \Omega\to 0}} \sum_{k,\omega} (\omega + \frac{\Omega}{2}) \psi_k^{\dagger} \left(\widetilde{\mathbf{v}}_{fM} + \widetilde{\mathbf{v}}_{\Delta M}\right) \psi_{k+q}, \tag{3.20}$$

where a generalized velocity is defined as

$$\begin{aligned} \widetilde{\mathbf{v}}_{\alpha M} &= v_\alpha^x \widetilde{M}_3^x \hat{x} + v_\alpha^y \widetilde{M}_3^y \hat{y} \\ \widetilde{M}_\alpha^x \equiv \widetilde{(\sigma_3 \otimes \tau_\alpha)} \quad & \widetilde{M}_\alpha^y \equiv \widetilde{(\sigma_0 \otimes \tau_\alpha)} \end{aligned} \tag{3.21}$$

with $\alpha = f, \Delta$ for Fermi and gap velocities respectively.

3.4.1 Vertex correction

To calculate a conductivity that satisfies Ward identities, vertex corrections must be included on the same footing as the self-energy corrections to the single particle Green's function. The details of this calculation are similar to those performed in Appendix B of Ref. 24. The impurity scattering diagrams which contribute to the ladder series of diagrams are included by expressing the correlation function in terms of a "dressed vertex", as shown in part (a) of Fig. 3.7. The current-current correlation function is obtained from this "dressed bubble". The bare current operator of Eq. 3.20 is associated with one vertex of the bubble, while the dressed vertex depicted in Fig. 3.7 (b) is associated with the other. Evaluating the dressed vertex, we find that the

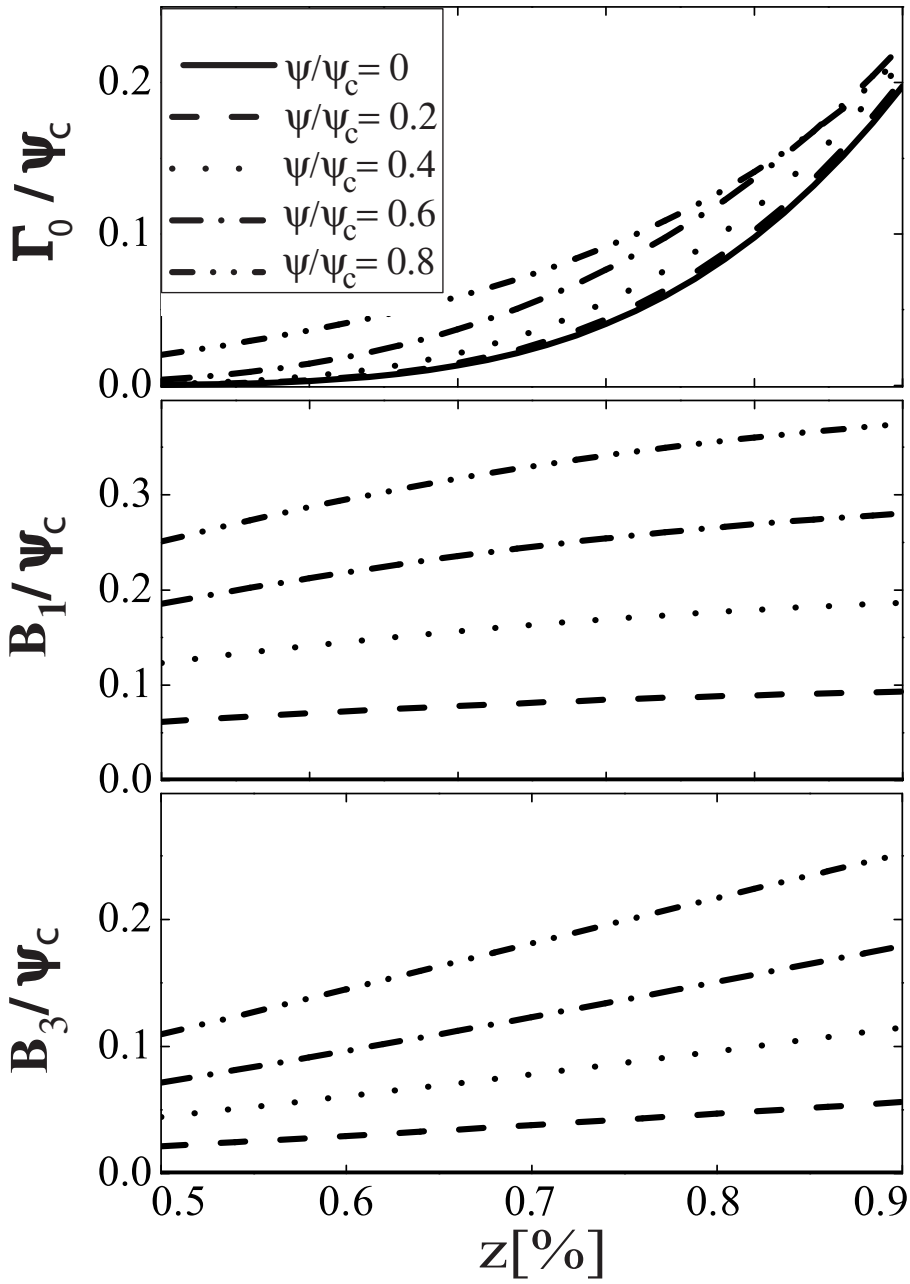

Figure 3.6: Disorder dependence of self-energy components, at different amplitudes of CDW. Nonzero components of $\widetilde{\Sigma}(z)$ are shown for impurity fraction z ranging from 0.5 to 1.0 %, for CDW strength $\psi = 0, 0.2, 0.4, 0.6$ and 0.8 (in units of ψ_c). These results are for scattering parameters $\{V_1, R_2, R_3\} = \{110, 0.9, 0.8\}$ and $v_f = v_\Delta$. Similar results follow for anisotropic Dirac particles. Energies are measured in units of ψ_c. The $\psi = 0$ data here agrees with the exact result, $\Gamma_0 = p_0 \exp(\frac{-1}{2\pi c})$, which appeared in Ref.24.

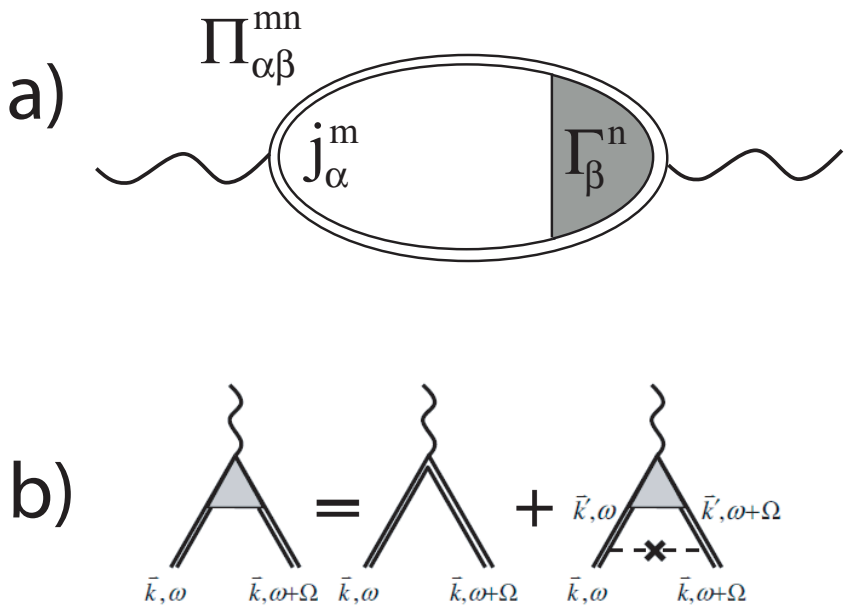

Figure 3.7: (a) Feynman diagram representing the correlation function $\Pi^{mn}_{\alpha\beta}$ in terms of a bare vertex j^m_α, and a dressed vertex Γ^n_β. (b) Feynman diagram representing the (ladder series) dressed vertex in terms of the bare vertex and the Born scattering event.

current-current correlation function takes the form

$$\Pi^{mn}(i\Omega) = \sum_{\alpha,\beta=f,\Delta} \Pi^{mn}_{\alpha\beta}(i\Omega)$$
$$\Pi^{mn}_{\alpha\beta}(i\Omega) = \frac{1}{k_B T}\sum_{i\omega}(i\omega + \frac{i\Omega}{2})^2 \sum_{k}$$
$$\mathrm{Tr}\left[\widetilde{\mathcal{G}}_1 v_\alpha k^m_\alpha \widetilde{M^m_\alpha}\widetilde{\mathcal{G}}_2 v_\beta \widetilde{M^n_\beta}\widetilde{\Gamma^n_\beta}\right] \tag{3.22}$$

where $\widetilde{\mathcal{G}}_1 \equiv \widetilde{\mathcal{G}(\mathbf{k}, i\omega)}$, $\widetilde{\mathcal{G}}_2 \equiv \widetilde{\mathcal{G}}(\mathbf{k}, i\omega + i\Omega)$, and $\widetilde{\Gamma^n_\beta} = \widetilde{\Gamma^n_\beta}(\mathbf{k}, i\omega, i\Omega)$ represents the dressed vertex depicted in Fig. 3.7. The Greek indices denote "Fermi" and "gap" terms, while the Roman indices denote the position space components of the tensor. We use Fig. 3.7 to find the form of the vertex equation, and then make the ansatz that

$$\widetilde{\mathbf{\Gamma}_\beta}(\mathbf{k}, i\omega, i\Omega) = \Big(\widetilde{1} + \widetilde{\Lambda}(|\mathbf{k}|, i\omega, i\Omega)\Big)\hat{k}, \tag{3.23}$$

which leads to the scalar equations

$$\widetilde{\Gamma}^n_\beta(\mathbf{k}, i\omega, i\Omega) = k_n(\widetilde{1} + \widetilde{\Lambda}^n_\beta). \tag{3.24}$$

Looking for solutions of this form, we see that the scalar vertex function is

$$\widetilde{\Lambda}^n_\beta = \mathrm{n}_i \sum_{k'} \widetilde{M^n_\beta}\widetilde{V}_{kk'}\widetilde{\mathcal{G}}_2\widetilde{M^n_\beta}(\widetilde{1} + \widetilde{\Lambda}^n_\beta)\widetilde{\mathcal{G}}_1\widetilde{V}_{k'k}\frac{k'^n_\beta}{k^n_\beta}. \tag{3.25}$$

Since we are working with nodal quasiparticles, we utilize the parametrization of Eq. (3.7), so that the vertex function is now a function of node index j and local momentum $\mathbf{p}$

$$\begin{aligned}\widetilde{\Lambda}^n_\beta &= n_{\mathrm{imp}} \sum_{j'=1}^{4} \underline{V}_{jj'}\underline{V}_{j'j}(\frac{k^{(j')}_{\beta n}}{k^{(j)}_{\beta n}}) \int \frac{\mathrm{d}^2 p'}{8\pi^2 v_f v_2} \\ &\widetilde{M^n_\beta}(\widetilde{\sigma_0 \otimes \tau_3})\widetilde{\mathcal{G}}_2\widetilde{M^n_\beta}(\widetilde{1} + \widetilde{\Lambda}^n_\beta)\widetilde{\mathcal{G}}_1(\widetilde{\sigma_0 \otimes \tau_3}).\end{aligned} \tag{3.26}$$

Arbitrarily choosing $j = 1$, then for $j' = \{1, 2, 3, 4\}$

$$\begin{aligned} \frac{k_{1x}^{(j')}}{k_{1x}^{(1)}} &= \{1, -1, -1, 1\} \qquad \frac{k_{1y}^{(j')}}{k_{1y}^{(1)}} = \{1, 1, -1, -1\} \\ \frac{k_{2x}^{(j')}}{k_{2x}^{(1)}} &= \{1, -1, -1, 1\} \qquad \frac{k_{2y}^{(j')}}{k_{2y}^{(1)}} = \{1, 1, -1, -1\}. \end{aligned} \tag{3.27}$$

Using the node space matrix representing the 3-parameter scattering potential

$$\underline{V}_{jj'} = \begin{pmatrix} V_1 & V_2 & V_3 & V_2 \\ V_2 & V_1 & V_2 & V_3 \\ V_3 & V_2 & V_1 & V_2 \\ V_2 & V_3 & V_2 & V_1 \end{pmatrix} \tag{3.28}$$

we obtain for the vertex equation

$$\widetilde{\Lambda}_\beta^n = \gamma \int \frac{\mathrm{d}^2 p'}{\pi} \widetilde{M}_\beta^n (\widetilde{\sigma_0 \otimes \tau_3}) \widetilde{\mathcal{G}}_2 \widetilde{M}_\beta^n (\widetilde{1} + \widetilde{\Lambda}_\beta^n) \widetilde{\mathcal{G}}_1 (\widetilde{\sigma_0 \otimes \tau_3}) \tag{3.29}$$

where $\gamma \equiv n_{\mathrm{imp}} \frac{V_1^2 - V_3^2}{8\pi v_f v_2}$. The correlator then becomes

$$\begin{aligned} \Pi_{\alpha\beta}^{mn}(i\Omega) &= v_\alpha v_\beta \frac{1}{\beta} \sum_{i\omega} (i\omega + \frac{i\Omega}{2})^2 \sum_k (k_{\alpha m} k_{\beta n}) \\ &\quad \mathrm{Tr} \left(\widetilde{\mathcal{G}}_1 \widetilde{M}_\alpha^m \widetilde{\mathcal{G}}_2 \widetilde{M}_\beta^n (\widetilde{1} + \widetilde{\Lambda}_\beta^n) \right) \\ &= v_\alpha v_\beta \frac{1}{\beta} \sum_{i\omega} (i\omega + \frac{i\Omega}{2})^2 \sum_{j=1}^{4} (k_{\alpha m}^{(j)} k_{\beta n}^{(j)}) \\ &\quad \int \frac{\mathrm{d}^2 p}{8\pi^2 v_f v_\Delta} \mathrm{Tr} \left(\widetilde{\mathcal{G}}_1 \widetilde{M}_\alpha^m \widetilde{\mathcal{G}}_2 \widetilde{M}_\beta^n (\widetilde{1} + \widetilde{\Lambda}_\beta^n) \right). \end{aligned} \tag{3.30}$$

Since

$$\sum_{j=1}^{4} k_{\alpha m}^{(j)} k_{\beta n}^{(j)} = 2 \left((1 - \delta_{\alpha\beta}) \eta_m + \delta_{\alpha\beta} \right) \delta_{mn} \tag{3.31}$$

we can write

$$\Pi_{\alpha\beta}^{mn}(i\Omega) = 2\pi c_{\alpha\beta}^{mn} \frac{1}{\beta} \sum_{i\omega} (i\omega + \frac{i\Omega}{2})^2 \mathrm{Tr} \left(\widetilde{I}_{\alpha\beta}^{mn} (\widetilde{1} + \widetilde{\Lambda}_\beta^n) \right) \tag{3.32}$$

where

$$c^{mn}_{\alpha\beta} \equiv \frac{1}{8\pi^2}\frac{v_\alpha v_\beta}{v_f v_\Delta}\Big((1-\delta_{\alpha\beta})\eta_m + \delta_{\alpha\beta}\Big)\delta_{mn} \tag{3.33}$$

and

$$\widetilde{I}^{mn}_{\alpha\beta}(i\omega, i\omega + i\Omega) \equiv \int \frac{\mathrm{d}^2 p}{\pi}\widetilde{\mathcal{G}}_1 \widetilde{M}^m_\alpha \widetilde{\mathcal{G}}_2 \widetilde{M}^n_\beta. \tag{3.34}$$

To calculate the conductivity, we will need $\mathrm{Tr}(\widetilde{I}^m_{\alpha\beta})$ and $\mathrm{Tr}(\widetilde{I}^m_{\alpha\beta}\widetilde{\Lambda}^n_\beta)$. For $\psi = 0$, it is possible to compute the integral in Eq. (3.34) analytically, but for general ψ we had to compute the integrals numerically. We note that if we write

$$\widetilde{I} = \begin{pmatrix} I_A & I_B \\ I_C & I_D \end{pmatrix}, \tag{3.35}$$

apply the symmetry properties of Eq. (3.14) and reverse the order of integration of p_1 and p_2, then $I_A = I_D$, and $I_B = I_C$, so that the most general expansion of $\widetilde{I}^{mn}_{\alpha\beta}$ in Nambu space is

$$\widetilde{I}^{mn}_{\alpha\beta} = \sum_{i=0}^{1}\sum_{i'=0}^{3}(I^{mn}_{\alpha\beta})_{ii'}(\widetilde{\sigma_i \otimes \tau_{i'}}). \tag{3.36}$$

Then

$$\begin{aligned}\mathrm{Tr}(\widetilde{I}^{mn}_{\alpha\beta}) &= \mathrm{Tr}\left(\sum_{i=0}^{1}\sum_{i'=0}^{3}(I^{mn}_{\alpha\beta})_{ii'}(\widetilde{\sigma_i \otimes \tau_{i'}})\right) \\ &= 4(I^{mn}_{\alpha\beta})_{00},\end{aligned} \tag{3.37}$$

while if we use the same expansion for

$$\widetilde{\Lambda}^n_\beta = \sum_{i=0}^{1}\sum_{i'=0}^{3}(\Lambda^n_\beta)_{ii'}(\widetilde{\sigma_i \otimes \tau_{i'}}), \tag{3.38}$$

we find

$$\begin{aligned}\mathrm{Tr}(\widetilde{I}^{mn}_{\alpha\beta}\widetilde{\Lambda}^n_\beta) &= \sum_{ij=0}^{1}\sum_{i'j'=0}^{3}(I^{mn}_{\alpha\beta})_{ii'}(\Lambda^n_\beta)_{jj'} \\ &\qquad \mathrm{Tr}(\sigma_i\widetilde{\sigma_j\otimes\tau_{i'}\tau_{j'}}) \\ &= 4\sum_{i=0}^{1}\sum_{i'=0}^{3}(I^{mn}_{\alpha\beta})_{ii'}(\Lambda^n_\beta)_{ii'}. \end{aligned} \tag{3.39}$$

Then Eq. (3.29) becomes

$$\begin{aligned}4(\Lambda^n_\beta)_{ii'} &= \mathrm{Tr}\left((\widetilde{\sigma_i\otimes\tau_{i'}})\widetilde{\Lambda}^n_\beta\right) \\ &= \gamma\int\frac{\mathrm{d}^2p}{\pi}\mathrm{Tr}((\widetilde{\sigma_i\otimes\tau_{i'}})\widetilde{M}^n_\beta(\widetilde{\sigma_0\otimes\tau_3}) \qquad (3.40)\\ &\qquad \widetilde{\mathcal{G}}_2\widetilde{M}^n_\beta(\widetilde{1}+\widetilde{\Lambda}^n_\beta)\widetilde{\mathcal{G}}_1(\widetilde{\sigma_0\otimes\tau_3})) \\ &= \gamma\mathrm{Tr}\left(\widetilde{L}^n_{\beta ii'}(\widetilde{1}+\widetilde{\Lambda}^n_\beta)\right) \qquad (3.41)\end{aligned}$$

where

$$\begin{aligned}\widetilde{L}^n_{\beta ii'} \equiv \int\frac{\mathrm{d}^2p}{\pi}&\widetilde{\mathcal{G}}_1(\widetilde{\sigma_0\otimes\tau_3})(\widetilde{\sigma_i\otimes\tau_{i'}}) \\ &\widetilde{M}^n_\beta(\widetilde{\sigma_0\otimes\tau_3})\widetilde{\mathcal{G}}_2\widetilde{M}^n_\beta. \end{aligned} \tag{3.42}$$

The symmetries of $\widetilde{\mathcal{G}}$ which were used to see which components of $\widetilde{I}^{mn}_{\alpha\beta}$ were 0 can also be applied to $\widetilde{L}^n_{\beta ii'}$ with the result that $(L^n_{\beta ii'})_A = (L^n_{\beta ii'})_D$, $(L^n_{\beta ii'})_B = \eta_i(L^n_{\beta ii'})_C$, where $\eta_i = \left\{\begin{array}{c}+1,\ i=0,1\\ -1,\ i=2,3\end{array}\right\}$. Since all that is required for the conductivity is $i=0,1$, we use the expansion

$$\widetilde{L}^n_{\beta ii'} = \sum_{j=0}^{1}\sum_{j'=0}^{3}(\widetilde{\sigma_j\otimes\tau_{j'}})(L^n_{\beta ii'})_{jj'} \tag{3.43}$$

so that

$$
\begin{aligned}
(\Lambda^n_\beta)_{ii'} &= \frac{1}{4}\gamma \mathrm{Tr}\left(\widetilde{L}^n_{\beta ii'}(\widetilde{1}+\widetilde{\Lambda}^n_\beta)\right) \\
&= \frac{1}{4}\gamma\ \mathrm{Tr}\,(\sum_{j=0}^{1}\sum_{j'=0}^{3}(L^n_{\beta ii'})_{jj'}(\widetilde{\sigma_j\otimes\tau_{j'}}) \\
&\qquad + \sum_{jk=0}^{1}\sum_{j'k'=0}^{3}(L_{\beta ii'})_{jj'}(\Lambda^n_\beta)_{kk'}) \\
&= \gamma\left((L^n_{\beta ii'})_{00} + \sum_{j=0}^{1}\sum_{j'=0}^{3}(L^n_{\beta ii'})_{jj'}(\Lambda^n_\beta)_{jj'}\right). \qquad (3.44)
\end{aligned}
$$

The thermal conductivity is obtained from the retarded current-current correlation function

$$
\frac{\kappa^{mn}(\Omega)}{T} = -\frac{1}{T}\frac{\mathrm{Im}\,(\Pi^{mn}_{\mathrm{ret}}(\Omega))}{\Omega}, \qquad (3.45)
$$

where $\Pi_{\mathrm{ret}}(\Omega) = \Pi(i\Omega \to \Omega + i\delta)$. To get the retarded correlator we first perform the Matsubara summation. Consider the summand of Eq. 3.32, which we redefine according to

$$
J(i\omega, i\omega + i\Omega) = \mathrm{Tr}\left(\widetilde{I}^{mn}_{\alpha\beta}(\widetilde{1}+\widetilde{\Lambda}^n_\beta)\right). \qquad (3.46)
$$

The function $J(i\omega, i\omega+i\Omega)$ is of the form $J(i\omega, i\omega+i\Omega) = f(A(i\omega)B(i\omega+i\Omega))$ where A and B are dressed Green's functions of a complex variable $z = i\omega_n$, so that J is analytic with branch cuts occurring where z and $z + i\Omega$ are real. The Matsubara summation needed is performed by integrating on a circular path of infinite radius, so that the only contribution is from just above and just below the branch cuts,

$$
\begin{aligned}
\Pi^{mn}_{\alpha\beta} &= -c^{mn}_{\alpha\beta}\frac{1}{i}\oint \mathrm{d}z(z+\frac{i\Omega}{2})^2 J(z, z+i\Omega) \\
&= -c^{mn}_{\alpha\beta}\frac{1}{i}\int_{-\infty}^{\infty}\mathrm{d}\epsilon\, n_f(\epsilon)\Big(\\
&(\epsilon+\frac{i\Omega}{2})^2(J(\epsilon+i\delta, \epsilon+i\Omega) - J(\epsilon-i\delta, \epsilon+i\Omega)) \\
&+(\epsilon-\frac{i\Omega}{2})^2(J(\epsilon-i\Omega, \epsilon+i\delta) - J(\epsilon-i\Omega, \epsilon-i\delta))\Big). \qquad (3.47)
\end{aligned}
$$

To obtain the retarded function, we analytically continue $i\Omega \to \Omega + i\delta$. Then we let $\epsilon \to \epsilon + \Omega$ in the third and fourth terms, so that

$$\begin{aligned}\Pi^{mn}_{\alpha\beta}(\Omega)_{\rm ret} &= c^{mn}_{\alpha\beta}\int_{-\infty}^{\infty} {\rm d}\epsilon\, n_f(\epsilon+\Omega) - n_f(\epsilon))(\epsilon+\frac{\Omega}{2})^2 \\ &\quad \times {\rm Re}\Big(J^{AR}_{\alpha\beta}(\epsilon,\epsilon+\Omega) - J^{RR}_{\alpha\beta}(\epsilon,\epsilon+\Omega)\Big) \qquad (3.48)\end{aligned}$$

where J^{AR} and J^{RR} are defined by Eqs. (3.46) and (3.44) and are composed of the universal-limit Green's functions given in Appendix D.2. Taking the imaginary part, we find

$$\begin{aligned}\frac{\kappa^{mn}(\Omega,T)}{T} &= -\int_{-\infty}^{\infty} {\rm d}\epsilon \frac{n_f(\epsilon+\Omega)-n_f(\epsilon)}{\Omega}\left(\frac{\epsilon+\frac{\Omega}{2}}{T}\right)^2 \\ \sum_{\alpha\beta} c^{mn}_{\alpha\beta} &\ {\rm Re}\ \ (J^{AR}_{\alpha\beta}(\epsilon,\epsilon+\Omega)) - J^{RR}_{\alpha\beta}(\epsilon,\epsilon+\Omega)). \qquad (3.49)\end{aligned}$$

In taking the $\Omega \to 0$ limit, the difference in Fermi functions becomes a derivative. Evaluating the integral, $\int {\rm d}\epsilon(-\frac{{\rm d}n}{{\rm d}\epsilon})(\frac{\epsilon}{T})^2 = \frac{\pi^2 k_B^2}{3}$, we find that

$$\frac{\kappa^{mm}_{\alpha\beta}(0,0)}{T} = \frac{\pi^2 k_B^2}{3} c^{mm}_{\alpha\beta} {\rm Re}\left(J^{AR}_{\alpha\beta}(0,0) - J^{RR}_{\alpha\beta}(0,0)\right). \qquad (3.50)$$

That $\kappa^{xy} = \kappa^{yx} = 0$ is seen from Eq. (3.33). Finally, since the $\alpha \neq \beta$ integrals are traceless, the result for the thermal conductivity is

$$\frac{\kappa^{mm}}{T} = \frac{k_B^2}{3}\frac{v_f^2 + v_\Delta^2}{v_f v_\Delta}\frac{1}{8}\left(J^{AR}_{\alpha\beta}(0,0) - J^{RR}_{\alpha\beta}(0,0)\right). \qquad (3.51)$$

3.5 Results

For a discussion of the units employed in the analysis, one can refer to Sec. 3.3.2. The reduced set of parameters for the model is $\{z, V_1, R_2, R_3, \beta, p_0, \psi\}$.

We explored a limited region of this parameter space, calculating the integrals and solving the matrix equation numerically. In particular, we looked at the ψ dependence of κ. To vary the anisotropy of the scattering potential, we considered the $\{R_2, R_3\}$ values of $\{0.9, 0.8\}$, $\{0.7, 0.6\}$, and $\{0.5, 0.3\}$, and kept fixed the constant c (given after Eq. (3.13))by appropriately modifying V_1. For $\{R_2, R_3\} = \{0.9, 0.8\}$, we used $V_1 = 110$. The rationale for keeping c fixed is that the self-energy depends only on c, β and p_0. Additionally, we explored the dependence of the thermal conductivity on impurity fraction z

and velocity anisotropy β. For all computations we set the cutoff $p_0 = 100$; this simply fixes a particular value of the product $v_f v_\Delta$ for these calculations.

3.5.1 Vertex corrections

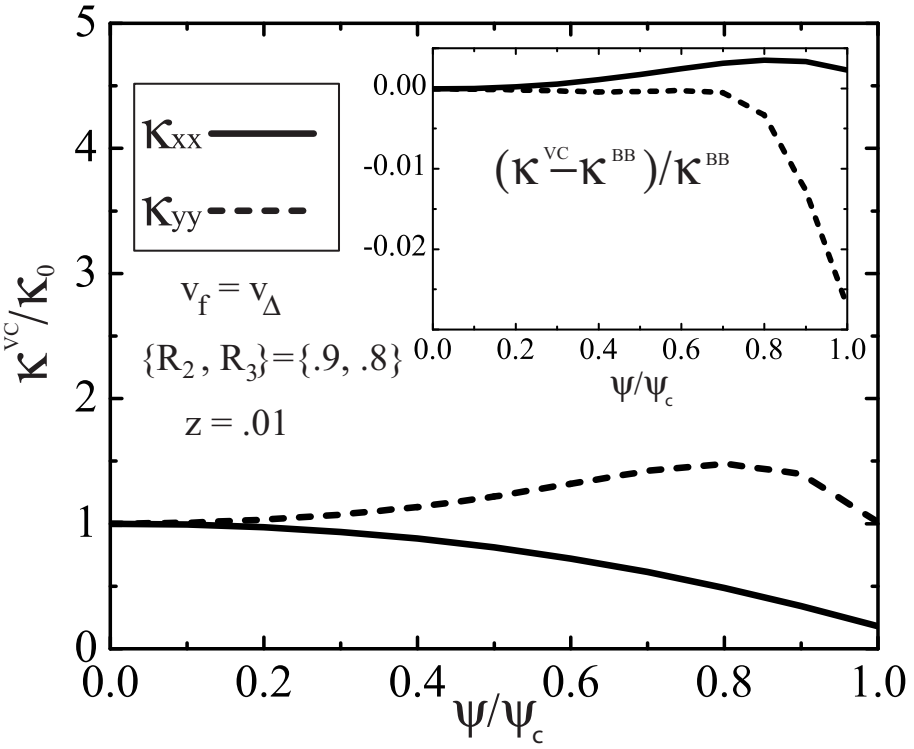

Figure 3.8: Vertex corrected thermal conductivity, in units of the universal conductivity $\kappa_0 \equiv \frac{k_B}{3}(v_f/v_\Delta + v_\Delta/v_f)$. This data reflects a short range scattering potential $\{V_1, R_2, R_3\} = \{110, 0.9, 0.8\}$, impurity fraction z=0.01, and isotropic Dirac quasiparticles ($v_f = v_\Delta$). The inset displays the discrepancy between the bare-bubble and vertex corrected results, in units of the bare-bubble result. It is clear that the vertex corrections are of little quantitative importance for these particular parameters.

The importance of including the vertex corrections is determined by comparing the vertex corrected thermal conductivity with that of the bare-bubble. If $\frac{\kappa^{VC}-\kappa^{BB}}{\kappa^{BB}} << 1$ for a region of parameter space, then in that regime the

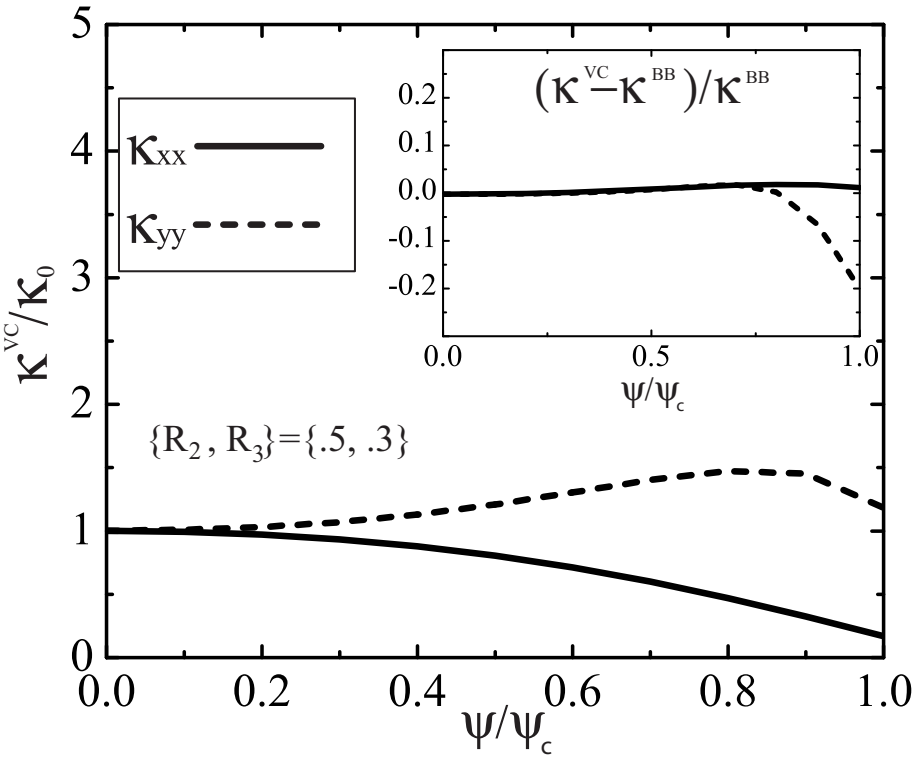

Figure 3.9: Vertex corrected thermal conductivity, in units of the universal conductivity $\kappa_0 \equiv \frac{k_B}{3}(v_f/v_\Delta + v_\Delta/v_f)$. This figure portrays the effect that a different scattering potential has on the importance of vertex corrections. Here, a longer range potential $\{V_1, R_2, R_3\} = \{140, 0.5, 0.3\}$ was used, again with impurity fraction z=0.01 and $v_f = v_\Delta$. The inset displays the discrepancy between the bare-bubble and vertex corrected results, in units of the bare-bubble result. From this, we determine that vertex corrections make a more substantial correction as the forward scattering limit is approached, but only once the charge ordering is quite strong.

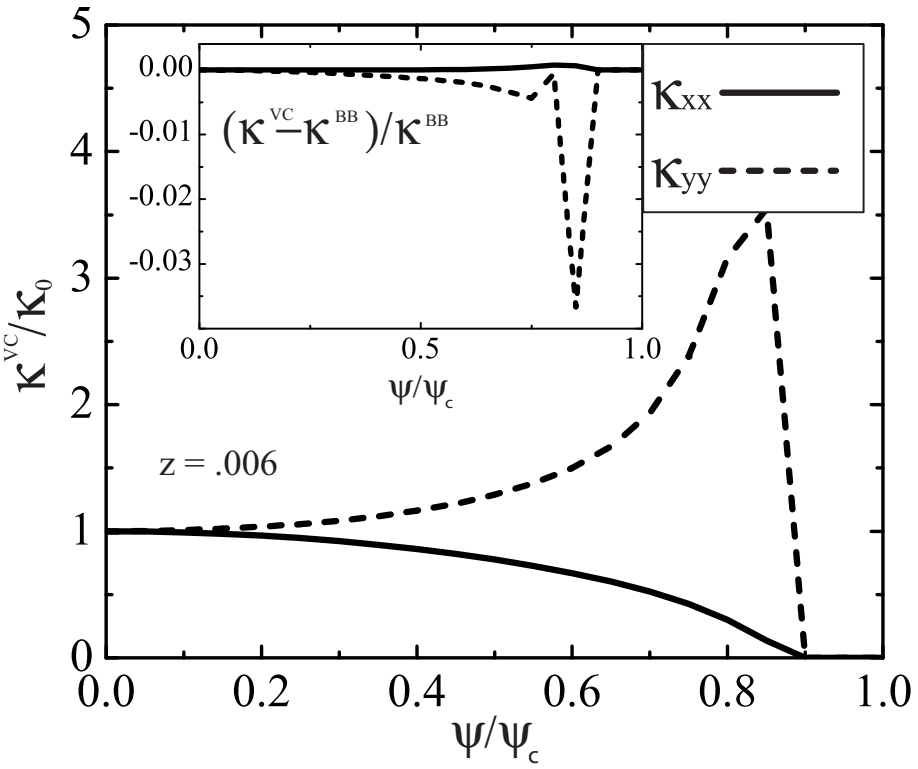

Figure 3.10: Vertex corrected thermal conductivity, in units of the universal conductivity $\kappa_0 \equiv \frac{k_B}{3}(v_f/v_\Delta + v_\Delta/v_f)$. Again, a short-ranged scattering potential, $\{V_1, R_2, R_3\} = \{110, 0.9, 0.8\}$ and isotropic nodes ($v_f = v_\Delta$) are used. This figure displays the effect of a smaller impurity fraction than that depicted in Fig.3.8. The inset displays the discrepancy between bare-bubble and vertex corrected result, in units of the bare-bubble result; since the scattering potential falls off slowly (in k-space) here, the vertex corrections are again quite unimportant.

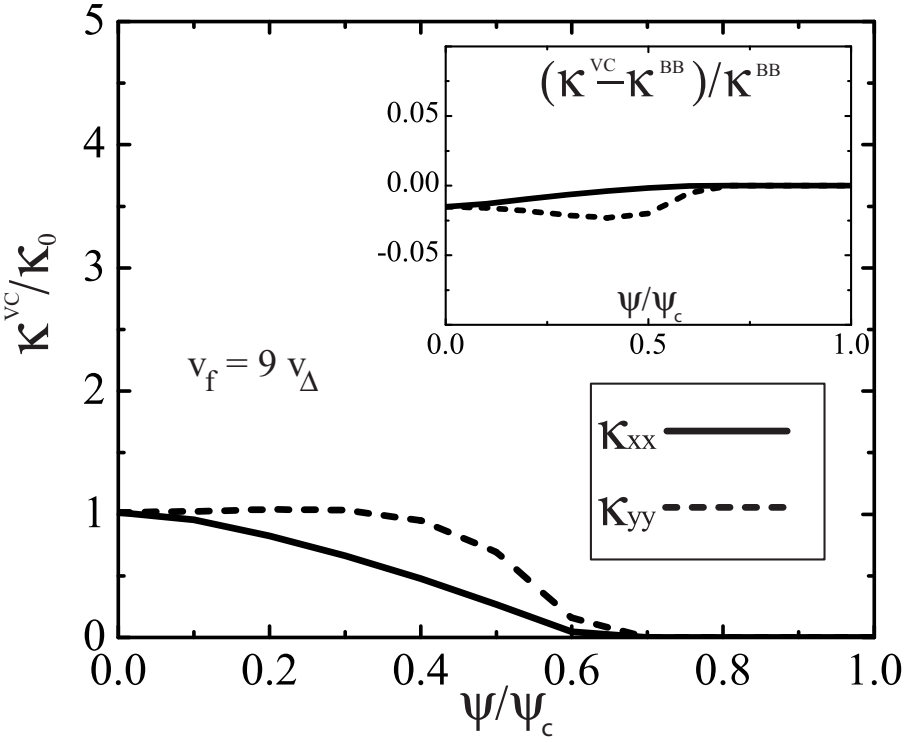

Figure 3.11: Vertex corrected thermal conductivity, in units of the universal conductivity $\kappa_0 \equiv \frac{k_B}{3}(v_f/v_\Delta + v_\Delta/v_f)$, for short-ranged scattering potential, $\{V_1, R_2, R_3\} = \{110, 0.9, 0.8\}$ and impurity fraction $z = 0.01$. These calculations differ from those of Fig.3.8 in that they are for more anisotropic Dirac particles with $v_f = 9v_\Delta$. The thermal conductivity has a qualitatively similar ψ dependence, but vanishes for a smaller value of ψ than for the isotropic case. The inset displays the discrepancy between the bare-bubble and vertex corrected results, in units of the bare-bubble result; again, the vertex corrections do not significantly modify the bare-bubble results.

bare-bubble results can be used instead. This is of threefold practicality: the bare-bubble results are less computationally expensive, the bare-bubble expression is much simpler to analyze, and other hamiltonians could be more easily studied.

The bare bubble thermal conductivity can be obtained by setting $\widetilde{\Lambda}^n_\beta \to \widetilde{0}$ in Eq. (3.46), or by using a spectral representation, as in Ref 91; both methods have the same result. For impurity fraction z ranging from 0.5% to 1%, the importance of the vertex corrections is largely seen to be negligible, which implies that an analysis of the bare bubble results is sufficient.

Figs. 3.8-3.11 illustrate the vertex corrected thermal conductivities, κ^{VC}, in the main graphs, while the insets display the relative discrepancy with respect to the bare bubble thermal conductivities $\frac{\kappa^{VC}-\kappa^{BB}}{\kappa^{BB}}$. Each plot is as a function of the amplitude of the CDW, ψ/ψ_c, where ψ_c indicates the maximal CDW for which the clean system remains gapless. We will postpone analysis of the character of the thermal conductivity until Section V C.

To gauge the importance of the vertex corrections, we look first at Fig. 3.8. The inset indicates that the vertex corrections do not signifigantly modify the bare bubble thermal conductivity. Although their importance grows somewhat with increasing ψ, the correction is still slight.

Next, Fig. 3.8 is used as a reference against which to consider the dependence of vertex corrections on scattering potential, impurity fraction, and velocity anisotropy. The next three figures are the results of computations with each of these parameters modified in turn. By comparing Fig. 3.9 with Fig. 3.8 we conclude that the vertex corrections become more important when the scattering potential is peaked in k-space, but are unimportant for potentials that fall off slowly in k-space.

Fig. 3.8 and Fig. 3.10 correspond roughly to the largest and smallest z for which these calculations are valid. Comparison of these two figures, as well as that of intermediary values of z (not displayed) indicates that the relative importance of the vertex corrections is independent of z. Nor does increasing the velocity anisotropy affect their importance, as seen by making a comparison between Fig. 3.8 and Fig. 3.11.

3.5.2 Clean limit analysis

It is of great interest to consider the behavior of the thermal conductivity in the clean ($z \to 0$) limit. Because the thermal conductivity is composed of integrals over **p**-space of functions which become increasingly peaked in this limit, there exists a sufficiently small z beyond which it is not possible to perform the requisite numerical integrations. However, it is still possible to obtain information about this regime. To that end, we will examine the form

of the bare-bubble thermal conductivity, and consider the $z \to 0$ limit. As we shall see, this will enable us to determine the value of ψ at which the nodal approximation, and hence this calculation, is no longer valid. Additionally, a closed form result for the thermal conductivity in the $z \to 0$ limit in the case $v_f = v_\Delta$ is obtained. The bare-bubble thermal conductivity, identical with setting $\widetilde{\Lambda} \to \widetilde{0}$ in Eq. (3.51), is given by

$$\kappa^{mm} = \frac{k_B}{3} \frac{v_f^2 + v_2^2}{v_f v_2} J^m \tag{3.52}$$

where

$$J^m = \int \frac{\mathrm{d}^2\mathbf{p}}{2\pi} \frac{N_1 + N_2}{D} \tag{3.53}$$

and

$$\begin{aligned}
N_1 &= A\left((A + B + \epsilon_1^2 + \Delta_1^2)^2 + (A + B + \epsilon_2^2 + \Delta_2^2)^2\right) \\
N_2 &= \eta_m A\Big((\psi - B_3)^2((\epsilon_1 + \epsilon_2)^2 - (\Delta_1 - \Delta_2)^2) + B_1^2((\Delta_1 + \Delta_2)^2 - (\epsilon_1 - \epsilon_2)^2) \\
&\quad -4B_1(\psi - B_3)(\epsilon_1\Delta_1 + \epsilon_2\Delta_2))\Big) \\
D &= \Big[(A + B + \epsilon_1^2 + \Delta_1^2)(A + B + \epsilon_2^2 + \Delta_2^2) - B\Big((\epsilon_1 + \epsilon_2)^2 + (\Delta_1 - \Delta_2)^2\Big) \\
&\quad +4B_1\Big(B_1(\epsilon_1\epsilon_2 - \Delta_1\Delta_2) + (\psi - B_3)(\epsilon_1\Delta_2 + \epsilon_2\Delta_1)\Big)\Big]^2,
\end{aligned} \tag{3.54}$$

where $A \equiv \Gamma_0^2$ and $B \equiv (\psi - B_3)^2 + B_1^2$, and $f_1 \equiv f_k$, $f_2 \equiv f_{k+Q}$. Since the results of Section 3.3.2 indicated that $\Gamma_0 \sim \exp(-\frac{1}{z})$ and $B_1, B_3 \sim z$, in the $z \to 0$ limit, $A \to 0$ much faster than $B_1 \to 0$ or $B_3 \to 0$. Therefore in taking the $z \to 0$ limit we will first let $A \to 0$ to obtain a result still expressed in terms of B_1 and B_3. The denominator can be rearranged as

$$\begin{aligned}
D &= \Big((A^2 + A(2B + \epsilon_1^2 + \Delta_1^2 + \epsilon_2^2 + \Delta_2^2) + f\Big)^2, \qquad \text{where} \\
f &= B^2 + (\epsilon_1^2 + \Delta_1^2)(\epsilon_2^2 + \Delta_2^2) - 2B(\epsilon_1\epsilon_2 - \Delta_1\Delta_2) \\
&\quad +4\Big(B_1(\epsilon_1\epsilon_2 - \Delta_1\Delta_2) + (\psi - B_3)(\epsilon_1\Delta_2 + \epsilon_2\Delta_1)\Big) \\
&= \Big((\epsilon_1\epsilon_2 - \Delta_1\Delta_2) - (2B_1^2 - B)\Big)^2 + \Big((\epsilon_1\Delta_2 + \epsilon_2\Delta_1) + 2B_1(\psi - B_3)\Big)^2
\end{aligned} \tag{3.55}$$

We are thus considering, in the limit that $A \to 0$, an integral of the form

$$\int \mathrm{d}^2\mathbf{p} \frac{A\, g(\mathbf{p})}{\big(Ah(\mathbf{p}) + f(\mathbf{p})\big)^2} \tag{3.56}$$

Note that any nonzero contribution to this integral must come from a region in **p**-space in which $f(\mathbf{p}) = 0$. We will consider separately the cases for which $v_f = v_\Delta$ and $v_f > v_\Delta$.

3.5.2.1 Isotropic case

For the special case $v_f = v_\Delta$, it is possible to calculate the integral of Eq. (3.52) exactly, by taking the $A \to 0$ limit, and choosing another parametrization. The coordinates $q_1 \equiv \epsilon_k - \epsilon_{k+Q}$ and $q_2 \equiv \epsilon_k + \epsilon_{k+Q} - 1$, have their origin located at the midpoint of the white and gray dots of Fig. 3.1. Using these coordinates, in the $A \to 0$ limit we find that the elements of Eq. (3.52) become

$$\begin{aligned}
N_1 &= 2A\Big(B^2 + B(q^2+1) + \frac{1}{4}(q^2+1)^2 + q^2 - q_2^2\Big) \\
N_2 &= 2\eta_m A\Big((\psi - B_3)^2((\epsilon_1+\epsilon_2)^2 - (\Delta_1 - \Delta_2)^2) + B_1^2((\Delta_1+\Delta_2)^2 - (\epsilon_1-\epsilon_2)^2) \\
&\quad -4B_1(\psi - B_3)(\epsilon_1\Delta_2 + \epsilon_2\Delta_1)\Big) \\
N_2 &= 2\eta_m\Big((\psi - B_3)^2(q_2^2 + 2q_2 + 1 - q_1^2) + B_1^2(q_2^2 - 2q_2 + 1 - q_1^2) \\
&\quad -4B_1(\psi - B_3)(2q_2^2 - q^2 - 1)\Big) \\
&= 2\eta_m A\Big[(2q_2^2 - q^2 + 1)\Big((\psi - B_3)^2 - 2B_1(\psi - B_3) + B_1^2\Big) \\
&\quad +2q_2\Big((\psi - B_3)^2 - B_1^2\Big) + 4B_1(\psi - B_3)\Big] \\
D &= \Big[2A\Big(1 + B - 2B_1(\psi - B_3)\Big) + \Big(q_2 - (\psi^2 - B_1^2)^2\Big)^2 \\
&\quad +\frac{1}{4}\Big(q^2 - (1 - 4B_1(\psi - B_3))\Big)^2\Big]^2. \qquad (3.57)
\end{aligned}$$

For the special case $v_f = v_\Delta$, the term f in the denominator is zero when

$$q_2 = (\psi - B_3)^2 - B_1^2 \quad \text{and} \quad q^2 = 1 - 4B_1(\psi - B_3). \qquad (3.58)$$

In q_1/q_2 coordinates, these are the equations of a horizontal line and a circle, which must intersect for there to be a nonzero contribution to the integral, since each term is positive definite. In the simplified disorder treatment of Ref. 91 for which $B_1 = B_3 = 0$ and $\Gamma_0 =$ constant, these constraints simplify to $q_2 = \psi^2$ and $q^2 = 1$, so that no contribution occurs when $\psi > 1$ (Note that as in the numerical analysis, ψ, being an energy, is measured in units of ψ_c). With the self-consistent treatment of disorder, there will likewise be a sufficiently large value of ψ beyond which the line and circle no longer intersect; we will

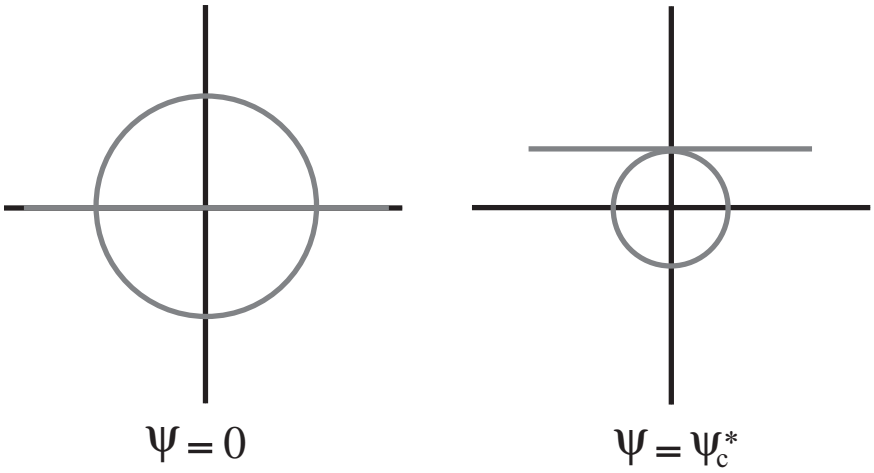

Figure 3.12: Illustrated is a schematic view of the line and circle whose intersection determines whether gapless excitations remain, for the isotropic case ($v_f = v_\Delta$). The left figure indicates the situation in the absence of charge ordering, that is, for $\psi = 0$, where the radius of the circle is 1. The right figure indicates the situation at $\psi = \psi_c^*$, when charge ordering is such that the excitation spectrum becomes gapped. In the clean case, the ψ evolution corresponds to moving the line past the circle. With self-consistent disorder, the radius of the circle and height of the line are both functions of ψ; in each instance, this construction can be used to determine the value of ψ at which the quasiparticle spectrum becomes gapped. This value of ψ is referred to as ψ_c^* in this paper.

call this value ψ_c^* (see Fig. 3.12). We interpret ψ_c^* as the point beyond which the system becomes effectively gapped. This is consistent with the exact result found by computing the eigenvalues of the completely clean hamiltonian (as $\psi_c^* = \psi_c$ in that case).

In Sec. 3.3.2 it was determined that $B_1 \simeq b_1\psi$ and $B_3 \simeq b_3\psi$, where b_1 and b_3 depend on the remaining parameters of the model. Using this approximate form for B_1 and B_3, the condition for the maximum ψ for which the constraints of Eq. (3.58) are satisfied,

$$1 - 4B_1(\psi - B_3) = \Big((\psi - B_3)^2 - B_1^2\Big)^2, \tag{3.59}$$

indicates that

$$\psi_c^{*2} \simeq \frac{\pm\Big((1 - b_3) \mp b_1\Big)^2}{\Big((1 - b_3 - b_1)(1 - b_3 + b_1)\Big)^2}. \tag{3.60}$$

Since $\psi_c^{*2} > 0$, we find that for $v_f = v_\Delta$,

$$\psi_c^* \simeq \frac{1}{1 - b_3 + b_1}. \tag{3.61}$$

We now proceed with the calculation of the clean limit conductivity. Substituting the conditions of Eq. (3.58) into Eq. (3.57), we find that the numerators become

$$\begin{aligned} N_1 &= 4A\Big[\Big(1 - 2B_1(\psi - B_3)\Big)\Big(1 + B - 2B_1(\psi - B_3)\Big)\Big] \qquad (3.62)\\ N_2 &= 4\eta_m A\Big(1 + B - 2B_1(\psi - B_3)\Big)\Big([(\psi - B_3)^2 - B_1^2]^2 + 2B_1(\psi - B_3)\Big) \end{aligned}$$

both of which are independent of $\mathbf{q}$, so that the clean limit result hinges upon the integral

$$I = \int \frac{\mathrm{d}^2q}{4\pi} \frac{A}{\Big(k_1 A + (q_2 - k_2)^2 + \frac{1}{4}(q^2 - k_3)^2\Big)^2}, \tag{3.63}$$

where

$$\begin{aligned} k_1 &= 2\Big(1 + B - 2B_1(\psi - B_3)\Big)\\ k_2 &= (\psi - B_3)^2 - B_1^2\\ k_3 &= 1 - 4B_1(\psi - B_3). \end{aligned} \tag{3.64}$$

The details of this integration are reported in Appendix D.3, with the result

$$I = \frac{1}{2k_1\sqrt{k_3 - k_1^2}}. \tag{3.65}$$

We can now write the anisotropic clean limit thermal conductivity

$$\begin{aligned}
J &= \frac{1 - 2B_1\psi + \eta_m\Big([(\psi - B_3)^2 - B_1^2]^2 + 2B_1(\psi - B_3)\Big)}{\sqrt{1 - 4B_1(\psi - B_3) - [(\psi - B_3)^2 - B_1^2]^2}} \\
&\quad \times\Theta\Big(1 - 4B_1(\psi - B_3) - [(\psi - B_3)^2 - B_1^2]^2\Big) \\
J^{xx} &= \sqrt{1 - 4B_1(\psi - B_3) - [(\psi - B_3)^2 - B_1^2]^2} \\
&\quad \times\Theta\Big(1 - 4B_1(\psi - B_3) - [(\psi - B_3)^2 - B_1^2]^2\Big) \\
J^{yy} &= \frac{1 + [(\psi - B_3)^2 - B_1^2]^2}{\sqrt{1 - 4B_1(\psi - B_3) - [(\psi - B_3)^2 - B_1^2]^2}} \\
&\quad \times\Theta\Big(1 - 4B_1(\psi - B_3) - [(\psi - B_3)^2 - B_1^2]^2\Big),
\end{aligned} \tag{3.66}$$

where the Θ function is the Heaviside step function. Using the definition for ψ_c^* found in Eq. (3.61), and defining

$$\chi \equiv \frac{1}{1 - b_3 - b_1}, \tag{3.67}$$

we are able to rewrite the dimensionless conductivity in terms of parameters easily extrapolated from SCBA calculations

$$\begin{aligned}
J^{xx} &= \frac{K^{xx}}{K_0} = \sqrt{\Big(1 - \frac{\psi^2}{\psi_c^{*2}}\Big)\Big(1 + \frac{\psi^2}{\chi^2}\Big)}\ \Theta[\Big(1 - \frac{\psi^2}{\psi_c^{*2}}\Big)\Big(1 + \frac{\psi^2}{\chi^2}\Big)] \\
J^{yy} &= \frac{K^{yy}}{K_0} = \frac{\Big(1 + \frac{\psi^4}{\psi_c^{*2}\chi^2}\Big)}{\sqrt{\Big(1 - \frac{\psi^2}{\psi_c^{*2}}\Big)\Big(1 + \frac{\psi^2}{\chi^2}\Big)}}\ \Theta[\Big(1 - \frac{\psi^2}{\psi_c^{*2}}\Big)\Big(1 + \frac{\psi^2}{\chi^2}\Big)]
\end{aligned} \tag{3.68}$$

in which form it is clear that the thermal conductivity vanishes for $\psi > \psi_c^*$.

3.5.2.2 Anisotropic case

For the case $v_f > v_\Delta$, the integral of Eq. (3.52) becomes intractable. However, it is still possible to predict ψ_c^*. Using the same q_1/q_2 coordinates, the

f-part of the denominator is again a sum of two positive definite terms. Again, the only contributions to the clean limit thermal conductivity arise when $f = 0$, which again provides two equations

$$\begin{aligned} x^2 + (y-a)^2 &= R^2 \\ (y-b)^2 - x^2 &= c^2 \end{aligned} \tag{3.69}$$

where

$$\begin{aligned} a &= \frac{1}{\beta}(\beta - 1) \\ b &= \frac{\beta^4 - 2\beta^3 - 1}{\beta^4 - 1} \\ c &= \frac{2\beta}{\beta^4 - 1}\sqrt{1 - (\beta^4 - 1)\Big((\psi - B_3)^2 - B_1^2\Big)} \\ R &= \sqrt{(1 - \frac{1}{\beta}(\beta - 1))^2 - 4B_1(\psi - B_3)}. \end{aligned} \tag{3.70}$$

This defines a hyperbola and a circle, again parametrized by ψ. One instance of this is depicted in Fig. 3.13. The value of ψ at which these equations no longer have a solution is ψ_c^*. The computed values for ψ_c^* are included for comparison in the graphs of thermal conductivity in Fig. 3.14 and Fig. 3.15.

3.5.3 Effect of self-consistent disorder

Satisfied that vertex corrections are of little importance, we set about analyzing the form of the thermal conductivity by studying the bare-bubble results. Thermal conductivity κ was computed for $\beta \equiv \sqrt{v_f/v_\Delta}$ values of $1, 2, 3$ and 4 (that is, for v_f/v_Δ=$1, 4, 9$ and 16). In Fig. 3.14 is presented a representative plot of κ for $v_f = v_\Delta$. The clean limit prediction for κ (Eq. (3.68)) is computed by fitting b_1 and b_3 from the self-energy calculations. These clean limit predictions are then plotted on the same graph with the numerical results of the thermal conductivity for the same parameters. In addition, the clean limit results of the simpler disorder model of Ref. 91 are also shown for the $v_f = v_\Delta$ case. Increasing disorder broadens the peak in κ^{yy} near ψ_c^*. For $z = 0.005$, the numerical computation is already almost exactly given by the clean limit results, while for $z = 0.009$, the features of the conductivity are nearly totally smeared out, as seen in Fig. 3.14. In this figure, the value of ψ_c^* given by Eq. (3.61) is indicated with an arrow.

For $v_f > v_\Delta$, the thermal conductivity has the same characteristics as for $v_f = v_\Delta$, except that ψ_c^* is generally smaller with increasing β. The numerically

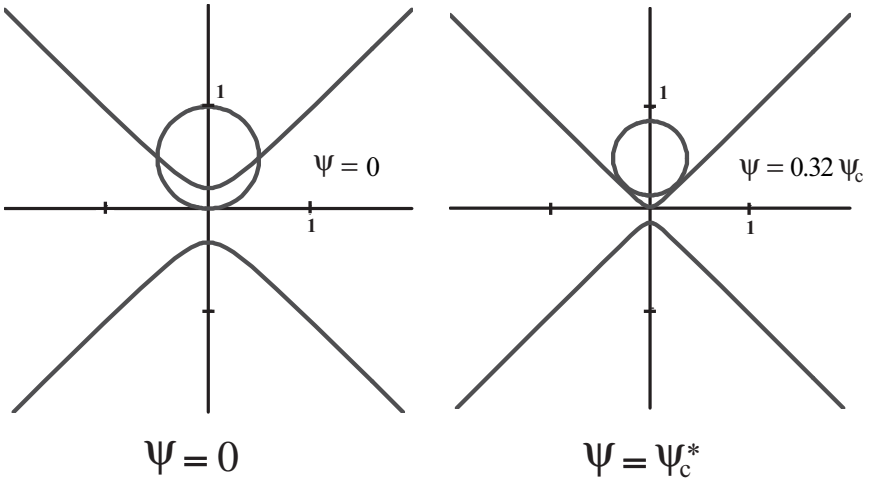

Figure 3.13: For generally anisotropic Dirac quasiparticles, the construction used in Fig.3.12 is modified to contain a hyperbola and circle. When these no longer intersect, the excitation spectrum becomes gapped. Illustrated is the construction for scattering parameter values $\{V_1, R_2, R_3\} = \{110, 0.9, 0.8\}$, impurity fraction $z = 0.01$, and with $v_f = 4v_\Delta$. For these parameters it was determined that this value of ψ at which the spectrum becomes gapped is given by $\psi_c^* = 0.32\psi_c$.

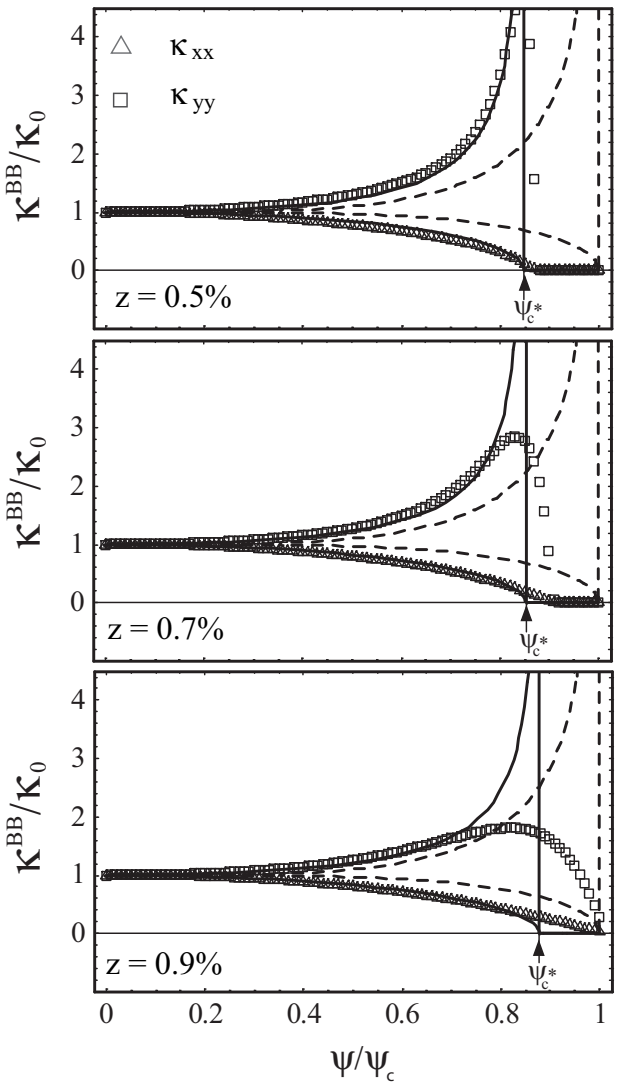

Figure 3.14: Effects of disorder on bare-bubble thermal conductivity's charge-order dependence, isotropic case ($v_f = v_\Delta$). This figure illustrates the case of short-ranged scatterers $\{V_1, R_2, R_3\} = \{110, 0.9, 0.8\}$. Note how an increase in the disorder, z, broadens out the peak in the conductivity. As the disorder becomes sufficiently small, the computed conductivity (triangles and squares) attains a limiting value that closely agrees with the analytic clean limit results of Eq.(3.68) (shown with solid lines). The thermal conductivity obtained by simply letting $\widetilde{\Sigma} \rightarrow$-i$\Gamma_0$ (obtained in Ref. 91) is shown with a dashed line. The effect of the self-consistent disorder is to renormalize the effective ψ at which the thermal conductivity vanishes (from ψ_c to some fraction of it).

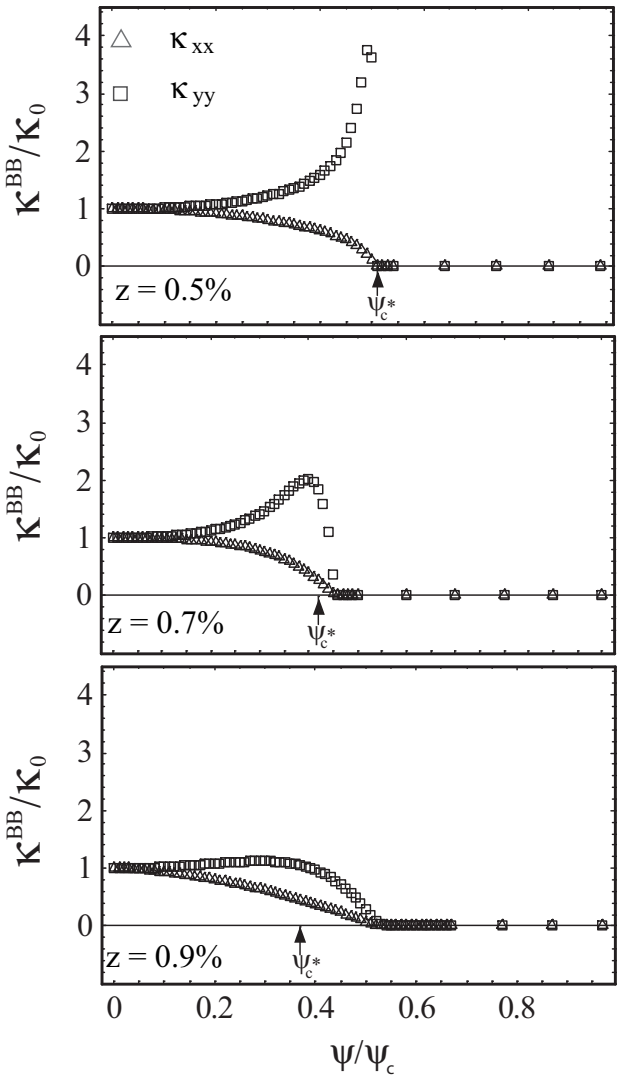

Figure 3.15: Effects of disorder on bare-bubble thermal conductivity's charge-order dependence, anisotropic case ($v_f = 16v_\Delta$). This figure illustrates the case of short-ranged scatters $\{V_1, R_2, R_3\} = \{110, 0.9, 0.8\}$. The effect of disorder is the same as in the isotropic case, which is to mix gapped and gapless states, smearing the peak in κ_{yy} across the renormalized nodal transition point, ψ_c^*. It is interesting to note that for this anisotropic case, ψ_c^* is significantly smaller than ψ_c.

computed thermal conductivities for the case of $\beta = 4$ are shown in Fig. 3.15. In this figure, the value of ψ_c^* is computed by determining the largest value of ψ for which Eqs. (3.69) have a solution, and is indicated with an arrow. It is clear from these graphs that the self-consistent disorder renormalizes the amplitude of charge density wave at which the thermal conductivity vanishes, and that the amount of renormalization is heavily dependent on the velocity anisotropy ratio, and varies only slightly with changing impurity fraction.

3.6 Conclusions

The work described in this chapter investigates the low temperature thermal conductivity of a d-wave superconductor with coexisting charge order in the presence of impurity scattering. We improve upon the model proposed in Ref. 91 by incorporating the effect of vertex corrections, and by including disorder in a self-consistent manner. Inclusion of vertex corrections does not significantly modify the bare-bubble results for short range scattering potentials. The role vertex corrections play increases somewhat for longer range scattering potentials, in particular as the amplitude of charge ordering increases. Nonetheless, for reasonable parameter values, the inclusion of vertex corrections is not found to significantly modify the bare-bubble results. This opens up the possibility of doing bare-bubble calculations for models with different types of ordering.

In the forward scattering limit, where $V_1 >> V_2, V_3$, the vertex corrections played a more significant role, in particular near the nodal transition point. This is consistent with Altland's symmetry classification which finds that pure forward scattering and isotropic scattering d-wave superconductors lie in different universality classes[77].

Our analysis determined that for self-consistency, it is necessary to include off-diagonal (in Nambu space) terms in the self-energy. As the charge ordering increases, the off-diagonal components become more important, and are found to dominate the self-energy in the clean limit. We also find that the thermal conductivity is no longer universal, as it depends on the impurity density and strength of charge ordering, rather than being solely determined by the quasiparticles' anisotropy.

In addition, inclusion of disorder within the SCBA renormalizes the critical value of ordering strength ψ at which the thermal conductivity becomes effectively gapped. This renormalization is seen in the calculated thermal conductivity curves, and depends primarily on the impurity fraction z and velocity anisotropy v_f/v_Δ. For larger v_f/v_Δ, the renormalization becomes significant, which may indicate that these signatures in κ_0 could be observed even

in systems with relatively weak charge order.

Chapter 4

Extension to coexisting density waves of various type and wave vector

4.1 Introduction

The low energy excitations of cuprate superconductors are Dirac fermions, which arise due to the d-wave nature of the superconducting order parameter. One expected signature of these nodal quasiparticles is the presence of a universal term in the low-temperature thermal conductivity, κ_{00}, which depends only on the ratio of the gradient of quasiparticle dispersion to the gradient of the gap, v_f/v_Δ, but not on the disorder[22, 24, 82]. In the optimally doped and overdoped regimes, κ_{00} has been observed in several instances, and agrees closely with its predicted value[25–27, 29–36]. For instance, in $YBa_2(Cu_{1-x}Zn_x)_3O_{6.9}$, κ_{00} is observed to be insensitive to the concentration of Zn atoms.[29]. However, in some cases, the value of the universal limit thermal conductivity, κ_{00}, is smaller than expected, or not observed at all, in particular as one approaches the underdoped regime[28, 37–40]. One possible reason is that localization effects enhance the scattering rate while leaving the density of states unaffected, thus reducing the transport[94].

Another mechanism which might account for non-observation of κ_{00} is the presence of competing order parameters. For years, evidence of the presence of additional symmetry breaking order parameters in cuprates has been compiled in neutron scattering data and scanning tunneling microscopy experiments[48–50, 52–63]. The presence of additional orders other than superconducting may be incidental, yet it also may be intrinsically related to the complex phenomenon of high temperature superconductivity itself. The addition of order

parameters which preserve time-reversal symmetry followed by a lattice translation has been found to preserve the nodal nature of the quasiparticles, for small amplitudes of order[89]. As the strength of such ordering perturbations increases, the locations of the nodal excitations evolve in k-space: for sufficiently large amplitude of order, the quasiparticle spectrum can be entirely gapped[89–92]. This modification of the quasiparticle spectrum will manifest itself in the low temperature thermal conductivity[91–93].

In this chapter, we model a cuprate superconductor using a mean-field formalism describing a BCS-like d-wave superconductor (dSC) perturbed by the addition of an additional order parameter. We then proceed to calculate the low-temperature thermal conductivity, accounting for the presence of several different varieties of competing orders. We affirm that these predictions can then be used as an indirect verification of the presence or absence of various competing orders in cuprates.

The previous chapter's linear response calculation of κ_{00} in a dSC with the addition of a $\mathbf{Q} = (\pi, 0)$ charge density wave showed that vertex corrections were not important for the universal limit thermal conductivitity, within the self-consistent Born approximation[92]. As the charge density wave's amplitude increased beyond a critical value ψ_c, the quasiparticle spectrum became gapped. Correspondingly, the thermal conductivity (made anisotropic by the presence of the density wave) vanished beyond that critical strength of ordering. In addition, a dependence on disorder resulted, in particular for charge orderings near the transition. Armed with this information, we then study the effects of a wider class of density waves on the low-energy properties of cuprates.

In Sec. 4.2, we will develop the mean-field formalism we will use to describe superconductors in the presence of competing orders. We write effective hamiltonians for charge, spin and pair density waves of several wave-vectors. Additionally, we describe configurations with multiple wave vectors, such as checkerboard order. Next, in Sec. 4.3 we will derive the current operators associated with the various kinds of orders, and use this to establish a relation for the bare-bubble thermal conductivity. Finally in Sec. 4.4, we will apply our results to several different cases, and compare and contrast the results.

4.2 Model

4.2.1 States of broken symmetry

States that arise as a result of broken symmetries are characterized by the presence of non-vanishing off diagonal matrix elements. The superconducting

state itself,for instance, can be identified with the non-vanishing "anomalous Green functions", as was learned by Gor'kov[8]. These anomalous Green functions are defined in space and time as

$$< \psi_\alpha(r,t)\psi_\beta(0,0) > . \tag{4.1}$$

Given singlet paired electrons of opposite momenta, this corresponds, in momentum space, to

$$< \psi_\alpha(k,t)\psi_\beta(-k,t) > . \tag{4.2}$$

In a similar fashion, ordered states representing density waves will also admit non-vanishing correlations between states separated by the wave-vector of the density wave. In this chapter, we will consider the subset of those which are defined in momentum space as

$$< \psi^{\alpha\dagger}(k+Q,t)\psi_\beta(k,t) > \equiv \Phi_Q f(k) d(\alpha,\beta), \tag{4.3}$$

representing charge ($d = \delta^\alpha_\beta$) and spin ($d = \delta^\alpha_\beta(\delta^\alpha_\uparrow - \delta^\alpha_\downarrow)$) density waves, as well as pair density waves

$$< \psi^{\alpha\dagger}(k+Q,t)\psi^\dagger_\beta(k,t) > \equiv \Phi_Q f(k)\epsilon^\alpha_\beta. \tag{4.4}$$

For the purposes of simpler classification of orders, we are carefully following some definitions made by Nayak in Ref. 95, so that Φ_Q will represent the magnitude and phase of the density wave and $f(k)$ is an element of a representation of the space group of $\boldsymbol{Q}$ on a square lattice. Certain order parameters obey restrictions. For instance, charge and spin density waves for which $2\mathbf{Q}$ is a member of the reciprocal lattice obey the additional condition

$$\Phi_Q f(k+Q) = \Phi^*_Q f^*(k) \tag{4.5}$$

as was pointed out in Ref. 95.

Written as a sum over real space, the hamiltonian representing a charge density wave system is

$$H_{CDW} = \sum_{\substack{rr\prime \\ \sigma}} \psi e^{-i\boldsymbol{Q}\cdot(\boldsymbol{r}-\boldsymbol{r}_0)} f(r-r\prime) c^\dagger_{r\sigma} c_{r\prime\sigma} + \text{h.c.}. \tag{4.6}$$

Upon Fourier transform this becomes

$$H_{CDW} = \sum_{k\sigma} (\Phi_Q f_k c^\dagger_{k+Q\sigma} c_{k\sigma} + \Phi^*_Q f^*_k c^\dagger_{k\sigma} c_{k+Q\sigma}), \tag{4.7}$$

with the definition $\Phi_Q = \psi e^{i\boldsymbol{Q}\cdot\mathbf{r}_0}$, where $\boldsymbol{r}_0$ describes the shift of the density wave from being site-centered and ψ is the amplitude of the density wave. Coupled with Eq. (4.5), this indicates restrictions on certain density waves' registration with the lattice.

4.2.2 Model

Our starting point is a model for d-wave superconductors

$$H = \sum_{k,\sigma} \left(\epsilon_k c^\dagger_{k\sigma} c_{k\sigma} + \Delta_k c^\dagger_{k\uparrow} c^\dagger_{-k\downarrow} \right) + \text{h.c.} \tag{4.8}$$

where the normal state dispersion is given by a tight-binding hamiltonian,

$$\epsilon_k = -2t(\cos k_x + \cos k_y) - t' \cos k_x \cos k_y - \mu. \tag{4.9}$$

and the superconducting order parameter is of $d_{x^2-y^2}$ symmetry,

$$\Delta_k = \frac{\Delta_0}{2}(\cos(k_x) - \cos(k_y)). \tag{4.10}$$

As given, this hamiltonian has nodal excitations, which are located along the $d_{x^2-y^2}$ symmetry axis in the $(\pm\pi, \pm\pi)$ directions. The nodes' distance from the $(\pm\pi/2, \pm\pi/2)$ points is controlled by the chemical potential μ. These quasiparticles are Dirac fermions in the sense that they have conical dispersion. The excitation energy is

$$E_k = \sqrt{\epsilon_k^2 + \Delta_k^2}, \tag{4.11}$$

and at low energies, $\epsilon_k \sim v_f k_1$ and $\Delta_k \sim v_\Delta k_2$, where k_1 and k_2 are displacementss resulting from the normal state dispersion linear parallel to Fermi surface, and linear gap perpendicular to the Fermi surface, with slopes v_f and v_Δ. For μ on the order of t or smaller, the ratio of Fermi velocity to gap velocity is given as

$$\frac{v_f}{v_\Delta} \approx \frac{4\sqrt{t^2 - \frac{\mu}{t}t'^2}}{\Delta_0}. \tag{4.12}$$

Then, as perturbations are turned on, the locations of the nodes evolves in k-space, although the stability of the nodes is generally preserved for non-nesting perturbations which preserve the composite symmetry of lattice translation followed by time-reversal as was noted by Berg and Kivelson[89].

4.2.3 Density waves of different wave vectors

The presence of a uniform density wave in a superconductor changes the system in both real and momentum space. In real space, the unit cell increases, as the system becomes periodic over a larger distance. In momentum space, we see an effective reduction of the Brillouin zone, also called band folding. Accordingly, our second quantized descriptions of the systems are modified. Whereas in a superconductor we can rewrite a quadratic effective hamiltonian using Nambu field operators,

$$\psi_k^\dagger = \begin{pmatrix} c_{k\uparrow}^\dagger & c_{-k\downarrow} \end{pmatrix} \qquad \psi_k = \begin{pmatrix} c_{k\uparrow} \\ c_{-k\downarrow}^\dagger \end{pmatrix}, \tag{4.13}$$

we could alternatively write extended Nambu vectors, such as

$$\psi_k^\dagger \begin{pmatrix} c_{k\uparrow}^\dagger & c_{-k\downarrow} & c_{k+Q\uparrow}^\dagger & c_{-k-Q\downarrow} \end{pmatrix} \qquad \begin{pmatrix} c_{k\uparrow} \\ c_{-k\downarrow}^\dagger \\ c_{k+Q\uparrow} \\ c_{-k-Q\downarrow} \end{pmatrix} \tag{4.14}$$

where the wave-vector $\mathbf{Q}$ connects each point in the first reduced Brillouin zone with a point in the second reduced Brillouin zone. Sums over k-space are then performed by integrating over the reduced Brillouin zone (the shaded regions in Fig.4.1), and taking the trace of the now-extended Nambu space matrix. The two descriptions are equivalent, but the extended Nambu description naturally fits the effective hamiltonians of systems with non-zero mean-field density waves. In Fig. 4.1, we illustrate four different density waves which are considered in this paper: $\mathbf{Q} = (\pi, 0)$, $\mathbf{Q} = (\pi/2, 0)$, $\mathbf{Q} = (\pi, \pi)$ and $\mathbf{Q} = (\pi, 0) + (0, \pi)$ (checkerboard) orders. These disturbances are illustrated in real space in Fig.4.2.

4.2.3.1 $\mathbf{Q} = (\pi, 0)$ density waves

A density wave of wave vector $\mathbf{Q} = (\pi, 0)$ corresponds to a striped system: the unit cell is doubled in the x-direction, and the Brillouin zone is reduced by 50% as seen in Fig. 4.1. The extended Nambu vector is that of Eq. 4.14, with $\mathbf{Q} = (\pi, 0)$.

4.2.3.2 $\mathbf{Q} = (\pi/2, 0)$ density waves

A density wave of wave vector $\mathbf{Q} = (\pi/2, 0)$ corresponds again to a striped system, one in which the unit cell has increased by a factor of four, and the

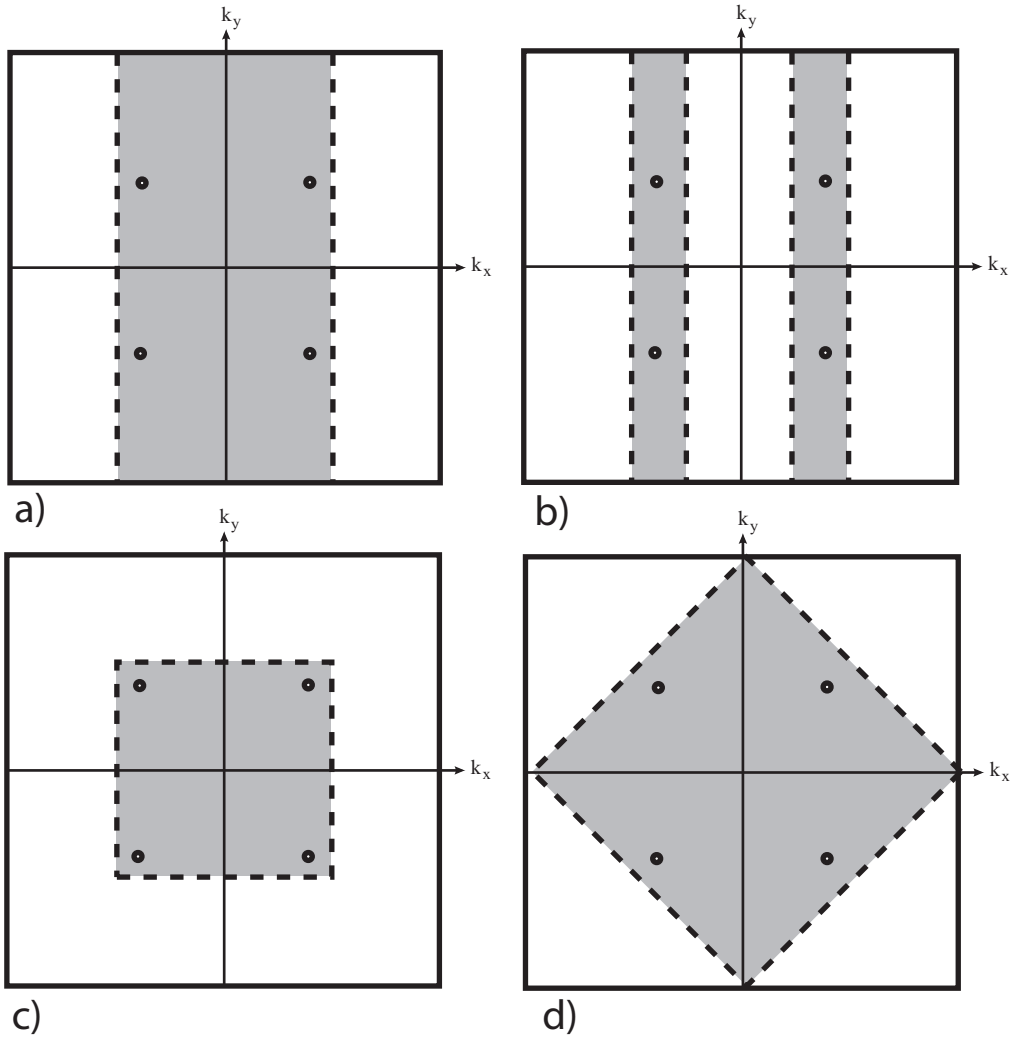

Figure 4.1: Illustrated are the reduced Brillouin zones of a square lattice in the presence of different density waves. The dots illustrate approximately the location of nodal excitations in a plain $d_{x^2-y^2}$-symmetry superconductor; the dashed line is the new zone boundary induced by the density wave. Illustrated are density waves of wave vector: a) $\mathbf{Q} = (\pi, 0)$, b) $\mathbf{Q} = (\pi/2, 0)$, c) $\mathbf{Q}_1 = (\pi, 0)$, $\mathbf{Q}_2 = (0, \pi)$ and d) $\mathbf{Q} = (\pi, \pi)$

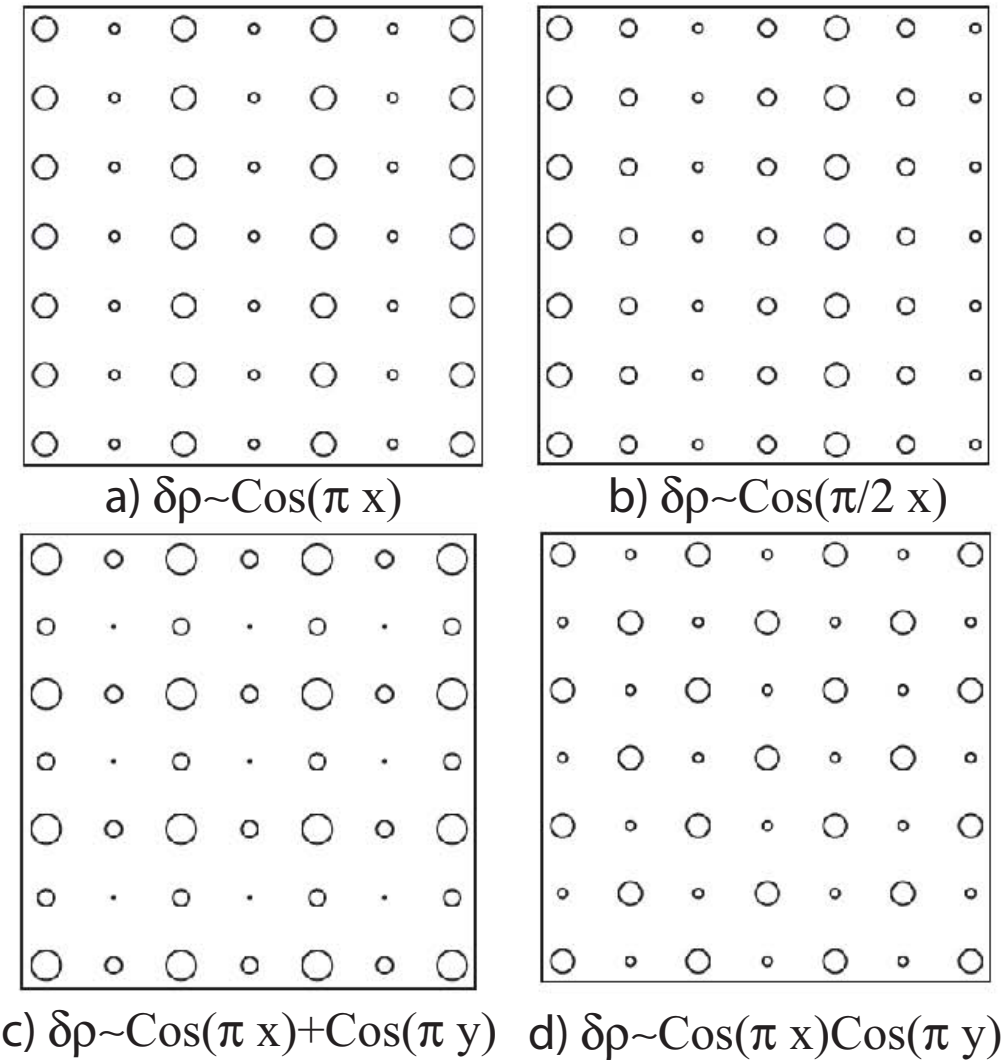

Figure 4.2: Illustrated are the four different density waves considered in this chapter, in real space. Each circle corresponds to the position of a Cu atom, and the size of the circle indicates whether the density at that site is higher or lower than the average. Illustrated are density waves of wave vector: a) $\mathbf{Q} = (\pi, 0)$, b) $\mathbf{Q} = (\pi/2, 0)$, c) $\mathbf{Q}_1 = (\pi, 0)$, $\mathbf{Q}_2 = (0, \pi)$ and d) $\mathbf{Q} = (\pi, \pi)$

Brillouin zone is reduced by the same factor. The reduced Brillouin zone is taken to be the region containing the pre-density-wave nodal quasiparticle excitations of the d-wave superconductor; in Fig. 4.1 (b) this is indicated with shading. The extended Nambu vector is that of Eq. 4.17.

4.2.3.3 $\mathbf{Q}_1 = (\pi, 0); \mathbf{Q}_1 = (0, \pi)$ density waves

Two density waves of equal weight in orthogonal directions corresponds to a checkerboard ordered system. As in the case of the $\mathbf{Q} = (\pi/2, 0)$ case, the Brillouin zone's area is reduced by a factor of four, although it is a different reduced Brillouin zone, illustrated in k-space in Fig. 4.1 (c), and in real space in Fig. 4.2.

4.2.3.4 $\mathbf{Q} = (\pi, \pi)$ density waves

A density wave of wave vector $\mathbf{Q} = (\pi, \pi)$ corresponds to a system which is modulated in both k_x and k_y directions: $\delta\rho \propto \sin(k_x)\sin(k_y)$. The reduced Brillouin zone is indicated in Fig. 4.1 (d) as the shaded region, and the real space modulation is illustrated in Fig.4.2 (d). The extended Nambu vector is as in Eq. 4.14, with $\mathbf{Q}$ now representing the (π, π) density wave.

4.2.4 Charge density waves

A commensurate charge density wave is one for which the charge density is oscillatory in real space and repeats itself after translation by an integer number of lattice constants. In other words, $\rho = \rho_0 + \delta\rho$, where $\delta\rho$ is the oscillatory part. The momentum space description of a mean field hamiltonian for such a system is

$$H_{CDW} = \sum_{k\sigma} \left(\Phi_Q f_k c^\dagger_{k+Q\sigma} c_{k\sigma} + \Phi^*_Q f^*_k c^\dagger_{k\sigma} c_{k+Q\sigma} \right). \tag{4.15}$$

A charge density wave $\rho = \rho_0 + \delta\rho$ which doubles the unit cell (so that $\delta\rho$ alternates sign from cell to cell in the x-direction) has wave-vector $\mathbf{Q} = (\pi, 0)$. A $(\pi, 0)$ CDW perturbation in its 4-component extended Nambu basis (particle, hole, shifted particle, shifted hole) is given by

$$H_{CDW} = \sum_k{}' \psi^\dagger_k \begin{pmatrix} 0 & 0 & A^*_k & 0 \\ 0 & 0 & 0 & -A_{-k} \\ A_k & 0 & 0 & 0 \\ 0 & -A^*_{-k} & 0 & 0 \end{pmatrix} \psi_k, \tag{4.16}$$

where the sum is over the reduced Brillouin zone of Fig. 4.1 a), and we define $A_k \equiv \Phi_Q f_k + \Phi_Q^* f_{k+Q}^*$. A $(\pi/2, 0)$ CDW perturbation written in its 8-component extended Nambu basis

$$\psi_k^\dagger = \begin{pmatrix} c_{k\uparrow}^\dagger & c_{-k\downarrow} & c_{k+2Q\uparrow}^\dagger & c_{-k-2Q\downarrow} & c_{k+Q\uparrow}^\dagger & c_{-k-Q\downarrow} & c_{k+3Q\uparrow}^\dagger & c_{-k-3Q\downarrow} \end{pmatrix} \quad (4.17)$$

is written as

$$H_{CDW}^{(\pi/2,0)} = \sum_k{}' \psi_k^\dagger H_k \psi_k \quad (4.18)$$

where H_k is given by

$$\begin{pmatrix} & & & & A_k^* & 0 & A_{k+3Q} & 0 \\ & & & & 0 & -A_{-k-Q}^* & 0 & -A_{-k} \\ & & & & A_{k+Q} & 0 & A_{k+2Q}^* & 0 \\ & & & & 0 & -A_{-k-2Q} & 0 & -A_{-k-3Q}^* \\ A_k & 0 & A_{k+Q}^* & 0 & & & & \\ 0 & -A_{-k-Q} & 0 & -A_{-k-2Q}^* & & & & \\ A_{k+3Q}^* & 0 & A_{k+2Q} & 0 & & & & \\ 0 & -A_{-k}^* & 0 & -A_{-k-3Q} & & & & \end{pmatrix} \quad (4.19)$$

4.2.5 Pair density waves

Scanning tunneling microscopy experiments have revealed the presence of modulations in the local density of states in the vortex cores of the cuprate $Bi_2Sr_2Ca_1Cu_2O_{8+\delta}$[48, 49, 53, 54, 56, 57], and in some instances, appear in the absence of magnetic field[50, 51]. More recent measurements, conducted in the absence of magnetic field, measured the spatial dependence of the superconducting gap[96]. Their finding was that the superconducting order parameter is modulated, corresponding to superconducting pairs with a net center-of-mass momentum, which has become known as a pair density wave[**?**]. In addition to modulations in the electron density, we can also consider the effects of modulations of the paired electrons. A pair density wave of wave vector **Q** is written as

$$H_{PDW} = \sum_{\substack{k \\ \alpha\beta}} \left(\Theta_Q g_k c_{k+Q\alpha}^\dagger c_{-k\beta}^\dagger + \Theta_Q^* g_k^* c_{-k\beta} c_{k+Q\alpha} \right). \quad (4.20)$$

or, with the definition $B_k \equiv \Theta_Q\,(g_k + g_{-k-Q})$ we can write (for $(\pi,0)$ or (π,π) density waves)

$$H_{PDW} = \sum_k{}' \psi_k^\dagger \begin{pmatrix} 0 & 0 & 0 & B_k \\ 0 & 0 & B_{-k}^* & 0 \\ 0 & B_{-k} & 0 & 0 \\ B_k^* & 0 & 0 & 0 \end{pmatrix} \psi_k \tag{4.21}$$

4.2.6 Spin density waves

The effective hamiltonian corresponding to spin density wave of wave vector $\mathbf{Q}$ is

$$H_{SDW} = \sum_{k\sigma} \sigma\Big(\Phi_Q f_k c_{k+Q\sigma}^\dagger c_{k\sigma} + \Phi_Q^* f_k^* c_{k\sigma}^\dagger c_{k+Q\sigma}\Big). \tag{4.22}$$

For example, a $\mathbf{Q} = (\pi,0)$ or $\mathbf{Q} = (\pi,\pi)$ SDW is represented in its reduced Brillouin zone as

$$H_{SDW}^{(\pi,0)} = \sum_k{}' \psi_k^\dagger \begin{pmatrix} 0 & 0 & A_k^* & 0 \\ 0 & 0 & 0 & A_{-k} \\ A_k & 0 & 0 & 0 \\ 0 & A_{-k}^* & 0 & 0 \end{pmatrix} \psi_k, \tag{4.23}$$

with the definition $A_k \equiv \Phi_Q f_k + \Phi_Q^* f_{k+Q}^*$.

4.2.7 Checkerboard density waves

In addition to broken symmetry states arising due to a single density wave, we can also consider multiple density waves. Scanning tunneling microscopy experiments have previously revealed the presence of checkerboard order in BiSCCoO[48–50, 52–54]. While the wave vectors of the order in those experiments was seen to be near $\mathbf{Q} \approx \frac{\pi}{2}$, for simplicity we first write down the hamiltonian corresponding to $\mathbf{Q}_1 = (\pi,0)$ and $\mathbf{Q}_2 = (0,\pi)$ checkerboard order. The Brillouin zone is reduced to one fourth of its size, as is seen in Fig. 4.1. The extended Nambu vector which describes such a system is

$$\psi_k^\dagger = \Big(c_{k\uparrow}^\dagger \quad c_{-k\downarrow} \quad c_{k+Q_x\uparrow}^\dagger \quad c_{-k-Q_x\downarrow} \quad c_{k+Q_y\uparrow}^\dagger \quad c_{-k-Q_y\downarrow} \quad c_{k+Q_x+Q_y\uparrow}^\dagger \quad c_{-k-Q_x-Q_y\downarrow}\Big) \tag{4.24}$$

and the second quantized hamiltonian which describes the addition of a charge density wave and pair density wave is

$$H_{\mathrm{CDW}}^{\mathrm{checkerboard}} + H_{\mathrm{PDW}}^{\mathrm{checkerboard}} = \sum_{k}{}' \psi_k^\dagger H_k \psi_k, \tag{4.25}$$

where H_k is given by

$$\begin{pmatrix}
0 & 0 & A_k^{(x)*} & B_k^{(x)} & A_k^{(y)*} & B_k^{(y)} & 0 & 0 \\
0 & 0 & B_{-k}^{(x)*} & -A_{-k}^{(x)} & B_{-k}^{(y)*} & -A_{-k}^{(y)} & 0 & 0 \\
A_k^{(x)} & B_{-k}^{(x)} & 0 & 0 & 0 & 0 & A_{k+Q_x}^{(y)*} & B_{k+Q_x}^{(y)} \\
B_k^{(x)*} & -A_{-k}^{(x)*} & 0 & 0 & 0 & 0 & B_{-k-Q_x}^{(y)*} & -A_{-k-Q_x}^{(y)} \\
A_k^{(y)} & B_{-k}^{(y)} & 0 & 0 & 0 & 0 & A_{k+Q_y}^{(x)*} & B_{k+Q_y}^{(x)} \\
B_k^{(y)*} & -A_{-k}^{(y)} & 0 & 0 & 0 & 0 & B_{-k-Q_y}^{(x)} & -A_{-k-Q_y}^{(x)} \\
0 & 0 & A_{k+Q_x}^{(y)} & B_{-k-Q_x}^{(y)} & A_{k+Q_y}^{(x)} & B_{-k-Q_y}^{(x)} & 0 & 0 \\
0 & 0 & B_{k+Q_x}^{(y)*} & -A_{-k-Q_x}^{(y)*} & B_{k+Q_y}^{(x)*} & -A_{-k-Q_y}^{(x)*} & 0 & 0
\end{pmatrix} \tag{4.26}$$

where

$$\begin{aligned}
A_k^{(x)} &\equiv \Phi_{Q_x} f_{k_x} + \Phi_{Q_x}^* f_{k+Q_x}^* \\
A_k^{(y)} &\equiv \Phi_{Q_y} f_{k_y} + \Phi_{Q_x}^* f_{k+Q_y}^* \\
B_k^{(x)} &\equiv \Theta_{Q_x}(g_{k_x} + g_{-k_x-Q_x}) \\
B_k^{(y)} &\equiv \Theta_{Q_y}(g_{k_y} + g_{-k_y-Q_y})
\end{aligned} \tag{4.27}$$

represent the amplitudes of the charge density and pair density waves in the x and y directions.

4.3 Thermal conductivity

At low temperatures, the temperature dependent phonon contribution to thermal conductivity vanishes as a power, $\kappa_{\mathrm{phonon}} \sim T^\alpha$ [26, 28–31, 33, 34, 36–40]. Therefore, the T-linear quasiparticle current can be extracted from experimental data by plotting the measured thermal conductivity over temperature as a function of $T^{\alpha-1}$. In previous work, we considered a site-centered $\mathbf{Q} = (\pi, 0)$ charge density wave and calculated the thermal conductivity using Green's functions obtained from the self-consistent Born approximation, and incorporated vertex corrections within the ladder approximation. Because the results of this work indicated that vertex corrections can usually be

neglected, in what follows we will derive the thermal conductivity using the "bare-bubble" correlation function. This will greatly simplify the calculation, allowing its application to a variety of systems.

4.3.1 Current operators

In order to calculate the thermal conductivity, we first need to derive the heat-current associated with the quasiparticles. Because heat and spin currents are both proportional to the quasiparticle current, we can get the heat-current by calculating the spin-current, and then using the energy measured from the Fermi level as the associated charge (instead of the spin). To calculate the spin current for any particular hamiltonian, we write the density operator in second quantized form, and then use Heisenberg equations of motion to find the momentum space representation of the current, that is

$$\lim_{q\to 0}(\mathbf{q}\cdot\mathbf{j^s}) = [\rho_q^S, H]. \tag{4.28}$$

The density operator is

$$\rho_q^s = \sum_k{}' \left(c_{k\uparrow}^\dagger c_{k+q\uparrow} + c_{-k\downarrow} c_{-k-q\downarrow}^\dagger \right). \tag{4.29}$$

Taking the commutator with the hamiltonians Eqs. (4.8),(4.15), (4.20) and (4.22), using anti-commutation relations, and discarding boundary terms, we find

$$\begin{aligned} [\rho_q^s, H] &= \sum_{\substack{kk'\\ \sigma}} [\sigma c_{k'\sigma}^\dagger c_{k'+q\sigma}, \psi_k^\dagger \widetilde{H}_k \psi_k] \\ &= \sum_k \boldsymbol{q}\cdot\psi_k^\dagger \frac{\partial \widetilde{H}_k}{\partial \boldsymbol{k}} \psi_k \end{aligned} \tag{4.30}$$

for the spin current. The heat current in the Matsubara representation is given by

$$\widetilde{j}(i\omega, i\Omega) = (i\omega + \frac{i\Omega}{2}) \sum_k \frac{\partial \widetilde{H}_k}{\partial \boldsymbol{k}} \tag{4.31}$$

Now we have a generalized velocity operator in the Nambu space, $\widetilde{v}_k = \frac{\partial \widetilde{H}_k}{\partial \boldsymbol{k}}$. For instance, for the $\boldsymbol{Q} = (\pi, 0)$ pair density wave of Eq. 4.21 , the velocity

operator would read

$$\widetilde{v}(\boldsymbol{k}) = \begin{pmatrix} \boldsymbol{v}_{f,k} & \boldsymbol{v}_{\Delta,k} & 0 & \frac{\partial A_k}{\partial \boldsymbol{k}} \\ \boldsymbol{v}_{\Delta,k} & -\boldsymbol{v}_{f,k} & \frac{\partial A^*_{-k}}{\partial \boldsymbol{k}} & 0 \\ 0 & \frac{\partial A_{-k}}{\partial \boldsymbol{k}} & \boldsymbol{v}_{f,k+Q} & \boldsymbol{v}_{\Delta,k+Q} \\ \frac{\partial A^*_k}{\partial \boldsymbol{k}} & 0 & \boldsymbol{v}_{\Delta,k+Q} & -\boldsymbol{v}_{f,k+Q} \end{pmatrix} \tag{4.32}$$

For density waves without internal momentum dependance, or for those where the variation is slight near the nodal locations, the velocity operator reduces to the form found in Refs. 91, 92

$$\widetilde{v}_{f,k} = \begin{pmatrix} \boldsymbol{v}_{f,k} & \boldsymbol{v}_{\Delta,k} \\ \boldsymbol{v}^*_{\Delta,k} & -\boldsymbol{v}_{f,k} \end{pmatrix} \tag{4.33}$$

4.3.2 Universal limit thermal conductivity

The universal limit thermal conductivity is calculated using linear response formalism. The thermal conductivity is given in terms of the retarded correlation function.

$$\frac{K(\Omega, T)}{T} = \lim_{\Omega \to 0} -\frac{\mathrm{Im}(\Pi_{\mathrm{Ret}}(\Omega))}{\Omega T^2} \tag{4.34}$$

We evaluate the correlation function using the Matsubara method. The bare-bubble correlator, given in terms of a spectral representation, is

$$\Pi(i\Omega) = \int \mathrm{d}\omega_1 \mathrm{d}\omega_2 \mathrm{Tr} \sum_k \left[\widetilde{A}(\omega_1) \widetilde{v} \widetilde{A}(\omega_2) \widetilde{v} \right] S(i\Omega) \tag{4.35}$$

where

$$S(i\Omega) \equiv \sum_{i\omega_n} \frac{(i\omega + \frac{i\Omega}{2})^2}{(i\omega - \omega_1)(i\omega + i\Omega - \omega_2)} \tag{4.36}$$

and $A(\boldsymbol{k}, \omega)$ is the spectral function.

It is important to use the correct form of the spectral function in Eq. (4.39) to avoid erroneous results, as is noted in Ref. 91. For example, a bond-centered CDW of wave vector $\boldsymbol{Q} = (\pi, 0)$, which looks like

$$H_{CDW} = \begin{pmatrix} 0 & 0 & i\psi & 0 \\ 0 & 0 & 0 & -i\psi \\ i\psi & 0 & 0 & 0 \\ 0 & -i\psi & 0 & 0 \end{pmatrix} \tag{4.37}$$

leads to a spectral function which is not real, and the spectral function is not given by the formula

$$\widetilde{A}(\boldsymbol{k},\omega) = -\frac{1}{\pi}\mathrm{Im}(G_R(\boldsymbol{k},\omega)), \tag{4.38}$$

but rather by

$$A(\boldsymbol{k},\omega) \equiv \frac{-1}{2\pi i}\Big(G_R(\boldsymbol{k},\omega) - G_A(\boldsymbol{k},\omega)\Big). \tag{4.39}$$

The details of the thermal conductivity calculation are similar to those of Refs. 92. In general, the self-consistent t-matrix approximation can be used to compute the Green's functions, however, here we use a simpler, diagonal self-energy as a first approximation. In terms of a model hamiltonian H_k and incorporating impurity scattering by assuming a finite imaginary part of the self-energy, $\widetilde{\Sigma}_R(\omega \to 0) = -i\Gamma_0$, the universal limit thermal conductivity is

$$\lim_{T\to 0}\frac{\kappa_0}{T} = \frac{k_B^2\pi^2}{3}\sum_k \mathrm{Re}\Big[\mathrm{Tr}[\widetilde{A}(0)\frac{\partial\widetilde{H}_k}{\partial\boldsymbol{k}}\widetilde{A}(0)\frac{\partial\widetilde{H}_k}{\partial\boldsymbol{k}}]\Big] \tag{4.40}$$

where

$$\begin{aligned}\widetilde{G}_R(\mathbf{k},\omega) &= \Big(\omega - \widetilde{H}_k + i\Gamma(\omega)\Big)^{-1}\\ \widetilde{G}_A(\mathbf{k},\omega) &= \Big(\omega - \widetilde{H}_k - i\Gamma(\omega)\Big)^{-1}.\end{aligned} \tag{4.41}$$

4.4 Effects on spectrum and thermal conductivity

Here we modify the dSC hamiltonian (4.8) with the addition of density waves such as (4.15), (4.20) and (4.22), which will be tuned by the real parameter ψ, the strength of the density wave. This is done to study the behavior of the quasiparticle spectrum, and through (4.40), the universal limit thermal conductivity. In each of the figures from Fig. 4.3 to Fig. 4.10, we present a) The trajectory of the nodes in the region $0 < k_x, k_y < \frac{\pi}{2}$, as the density wave is turned on. The starting place (node for dSC system) is indicated with a star. b) (minimum) quasiparticle energy as a function of the order parameter strength ψ; and c) universal limit thermal conductivity as a function of ψ. In all instances, the universal limit conductivity $\frac{\kappa_{00}}{T}$ is given in units of $\frac{v_f^2+v_\Delta^2}{v_f v_\Delta}$, the value for the plain dSC system, and we measure Δ_0, $E_{\min}$, μ and Γ_0 in units of t, the hopping parameter.

4.4.1 $\mathbf{Q} = (\pi, 0)$ density waves

The addition of a $\mathbf{Q} = (\pi, 0)$ charge density wave to a d-wave superconductor has been considered before[90–92]. As the perturbation is turned on, the nodes' locations evolve along curved paths, until they meet the images of the nodes from the second reduced Brillouin zone at the collision point $(\pi/2, \pi/2)$, as seen in Fig. 4.3. The effect is the same, regardless of whether the density wave is of s-wave ($\Phi_Q = \psi$, $f_k = 1$, site-centered), p_x-wave ($\Phi_Q = i\psi$, $f_k = \sin(k_x a)$, bond-centered) or p_y-wave ($\Phi_Q = \psi$, $f_k = \sin(k_y a)$, site-centered) symmetry. The critical value of ψ which gaps the system is $\psi_c = v_f k_0$, where

$$k_0 = \sqrt{2}\Big[\frac{\pi}{2} - \cos^{-1}\Big(\frac{-t}{2t'} + \sqrt{(\frac{t}{2t'})^2 - \frac{\mu}{4t}}\Big)\Big] \tag{4.42}$$

is the distance separating the $\psi = 0$ nodal point from $(\pi/2, \pi/2)$ in k-space. The resulting thermal conductivity is anisotropic, reflecting the stripiness of the system. The nodes are deformed as they approach the collision point, and the thermal conductivity κ_{yy} perpendicular to the direction of the density wave increases at first, before both κ_{xx} and κ_{yy} vanish for larger amplitudes of density wave, ψ. The effect of a $\mathbf{Q} = (\pi, 0)$ pair density wave is similar to that of the charge density wave: the nodes evolve along a curved path until they meet their images in the second reduced Brillouin zone, and the resulting universal limit thermal conductivity is the same. The effects of a site-centered $(\pi, 0)$ pair density wave is shown in Fig. 4.5.

A more unusual case is that of the $\mathbf{Q} = (\pi, 0)$ spin density wave. With this perturbation, the nodal points evolve directly towards the $(\pi/2, k_y)$ line, as seen in Fig.4.6. The quasiparticle spectrum then evolves so that there are two minima. In other words, the node splits in two, and nodes move up and down the $(\pi/2, k_y)$ line. The nodes are nested by $\mathbf{Q}$, but the spectrum remains gapless, and the universal limit thermal conductivity is unaffected. If the perturbation is allowed to become extremely large ($\psi >> \Delta_0$), then the nodes (there are now twice as many) collide with their ghosts, and the thermal conductivity then vanishes. The split-off nodes collide at different strengths of ψ, however, and the spectral weight disappears in two batches, accordingly, as does the thermal conductivity.

4.4.2 $\mathbf{Q} = (\pi, \pi)$ density waves

Adding a $\mathbf{Q} = (\pi, \pi)$ spin density wave was also discussed as an example in Ref. 89. In real space, such a density wave is modulated as $\cos(k_x)\cos(k_y)$,

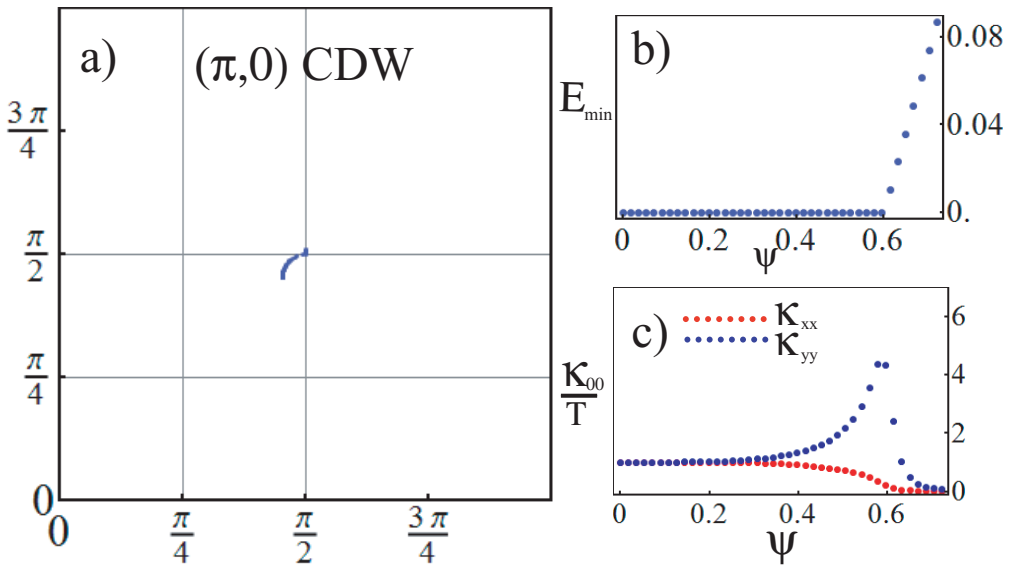

Figure 4.3: Effects on spectrum and low temperature transport of a $\mathbf{Q} = (\pi, 0)$ charge density wave. The results are the same for site centered (s-wave or p_y wave) and bond centered (p_x-wave) density waves, in that the nodes evolve along the same curved paths toward the $(\pm\pi/2, \pm\pi/2)$ points, where they collide with their images from the next reduced Brillouin zone. As this happens, the nodes are nested and the spectrum is gapped. The universal limit thermal conductivity vanishes beyond this point. Disorder Γ_0 broadens the transition. Here we take $\mu = -0.6$, $\Delta_0 = 4$ and $\Gamma_0 = 0.02$.

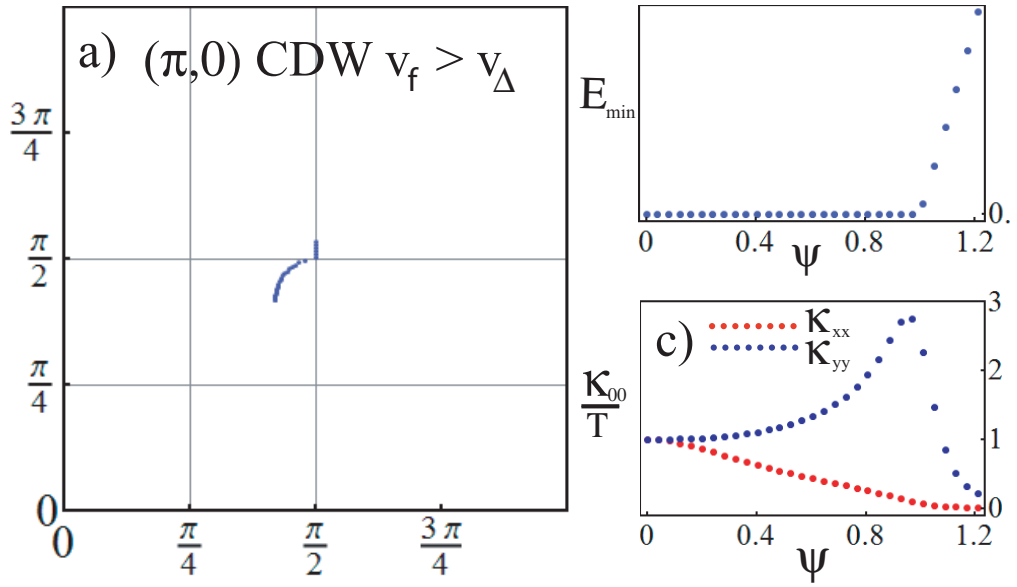

Figure 4.4: Effects on spectrum and low temperature transport of a $\mathbf{Q} = (\pi, 0)$ charge density wave. Depicted are the results for $\mu = -1$, $\Delta_0 = 0.4$ and $\Gamma_0 = 0.02$. These parameters describe anisotropic Dirac quasiparticles, with $v_f/v_\Delta = 10$. The anisotropy tends to suppress κ_{00} slightly.

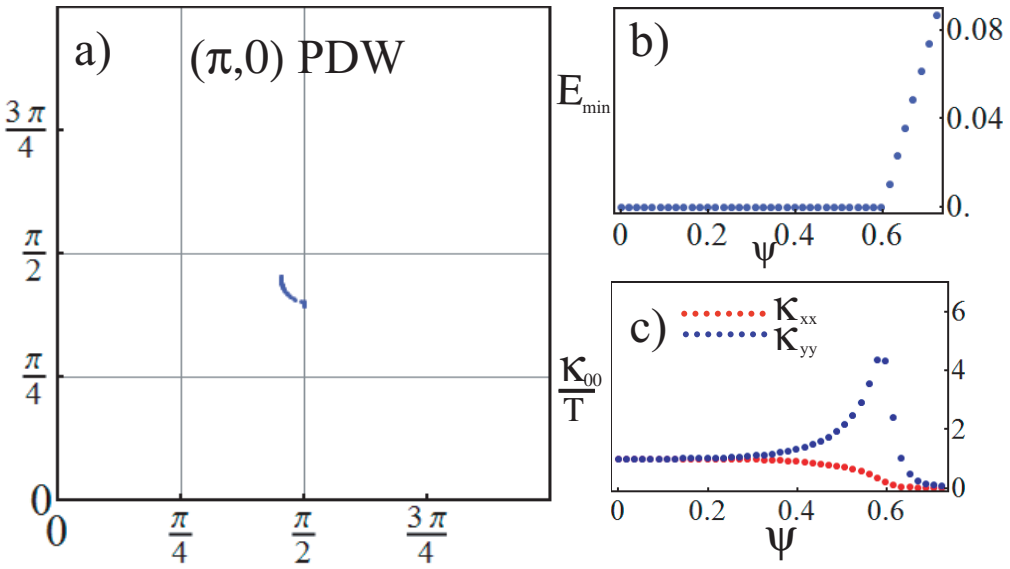

Figure 4.5: Effects on spectrum and low temperature transport of a $\mathbf{Q} = (\pi, 0)$ pair density wave. Depicted are the results for $\mu = -.6$, $\Delta_0 = 4$ ($v_f = v_\Delta$) and $\Gamma_0 = 0.02$. As was the case for the CDW, the nodes evolve along a curved path towards the $(\pi/2, k_y)$ line. Upon reaching $k_x = \pi/2$, the nodes are nested, and the spectrum is gapped. For ψ larger than the critical value ψ_c, the thermal conductivity vanishes, up to disorder broadening.

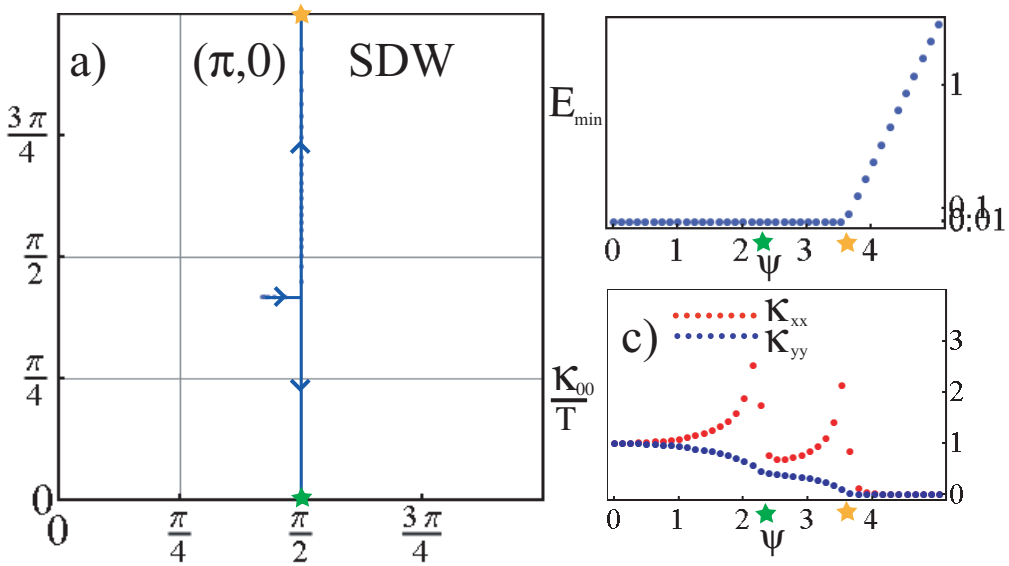

Figure 4.6: Effects on spectrum and low temperature transport of a $\mathbf{Q} = (\pi, 0)$ spin density wave. Depicted are the results for parameters $\Delta_0 = 4$, $\mu = -.6$ and $\Gamma_0 = 0.02$. As the density wave is turned on, the nodes move in a straight line to the $(\pm\pi/2, k_y)$ lines. When they reach that line, each node splits in two, and the two nodes move up and down along that line. The spectrum remains gapless, even though the nodes are nested by the ordering vector. Correspondingly, the thermal conductivity is unaffected at that energy scale. For ψ much larger, these two nodes collide with their ghost nodes (at different values of ψ), and the thermal conductivity is additively reduced by one half of the pure dSC value after each such collision. The locations of the two separate nodal collisions are illustrated by green and orange stars in (a), and the strength at which they appear is given in (b) and (c).

so that nodes remain along the (π, π) direction as the density wave is turned on, as is seen in Fig. 4.7. When the nodes reach $(\pi/2, \pi/2)$, the system is

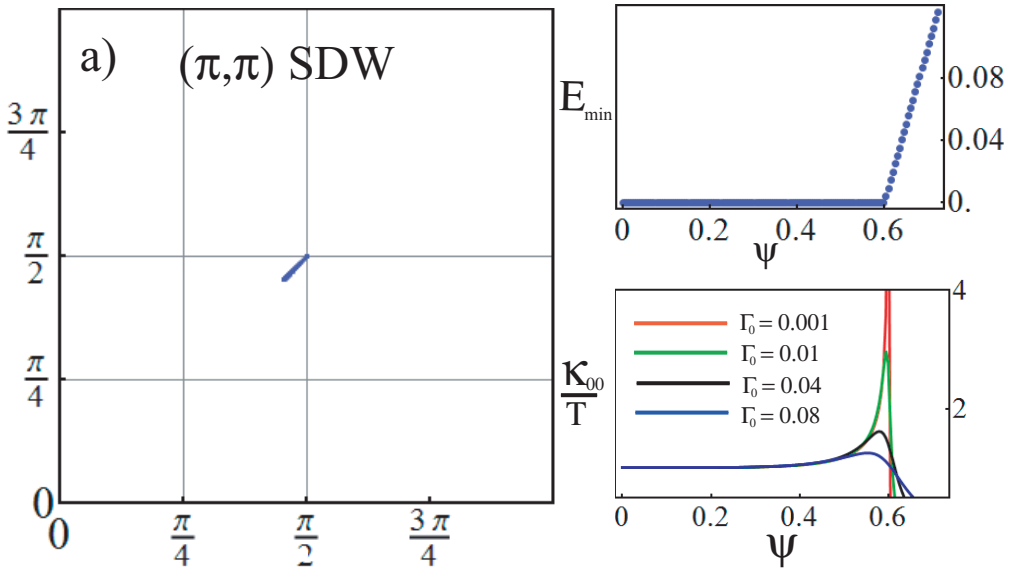

Figure 4.7: Effects on spectrum and low temperature transport of a $\mathbf{Q} = (\pi, \pi)$ spin density wave. As the density wave is turned on, the nodes move along the symmetry lines $k_x = \pm k_y$ toward $(\pm\pi/2, \pm\pi/2)$, where they become gapped. Accordingly, κ_{00} vanishes. In c) the effects of increasing disorder are presented. The disorder tends to smear the thermal conductance around the nodal transition; as such, κ_{00} is no longer universal.

gapped[89], and the thermal conductivity vanishes. On the other hand, a $\mathbf{Q} = (\pi, \pi)$ charge density wave behaves in a similar manner to the $(\pi, 0)$ spin density wave, in that the nodes do not vanish for small perturbations.

The addition of a $\mathbf{Q} = (\pi, \pi)$ pair density wave drives the location of the nodes towards the Γ point at $(k_x, k_y) = (0, 0)$, an effect which is repeated by the addition of the checkerboard pair density wave. In both instances, a large perturbation $\psi >> \Delta_0$ is required to affect the thermal conductivity.

4.4.3 $\mathbf{Q} = (\pi/2, 0)$ charge density wave

A $\mathbf{Q} = (\pi/2, 0)$ density wave behaves slightly differently than the $(\pi, 0)$ case. In this case, the nodes are driven towards the $(\pi/4, k_y)$ line, rather than $(\pi/2, k_y)$. While they would become gapped if they arrived there, for realistic parameters t, μ, and Δ_0, such a density wave would dominate the system, that is, $\psi >> \Delta_0$. The evolution is as seen in Fig. 4.8 and preserves the nodes for

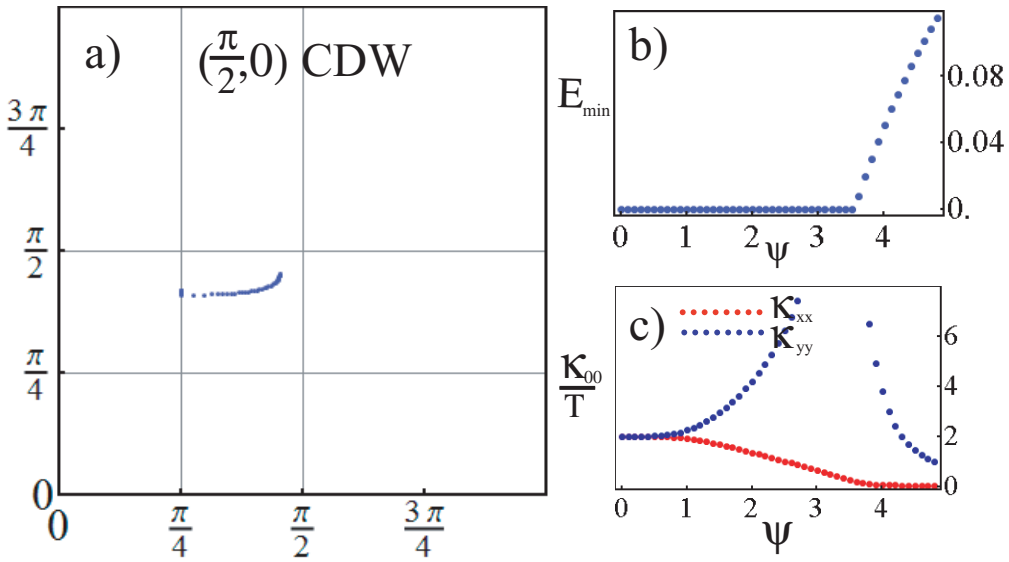

Figure 4.8: Effects on spectrum and low temperature transport of a $\mathbf{Q} = (\pi/2, 0)$ charge density wave. As the density wave is turned on, the nodes move in a curved path to the $(\pm\pi/4, k_y)$ lines. The spectrum becomes gapped at that point, when the node is nested by the ordering vector and the thermal conductivity vanishes for ψ larger than about $4t$. Such a system is out of the range of validity of our model, as it would be dominated by the charge order, rather than the d-wave superconductor. For ψ on the order of ψ_c, κ_{00} retains its dSC value. Here, $\mu = -.6$, $\Delta_0 = 4$ and $\Gamma_0 = 0.05$

$\psi < \Delta_0$. As such, the universal limit thermal conductivity is not significantly affected by this perturbation.

4.4.4 $\mathbf{Q}_1 = (\pi, 0)$, $\mathbf{Q}_2 = (0, \pi)$ checkerboard density waves

Configurations with more than one density wave can also be considered in this formalism. In this paper, we turn our attention to the checkerboard configuration illustrated in part c) of Fig. 4.1. As we turn on two charge density waves of $\mathbf{Q}_1 = (\pi, 0)$ and $\mathbf{Q}_2 = (0, \pi)$ with equal amplitudes, the nodes are perturbed along the symmetry line toward the $(\pi/2, \pi/2)$ point, as shown in Fig. 4.9. When the nodes reach the $(\pi/2, \pi/2)$ point, the spectrum becomes

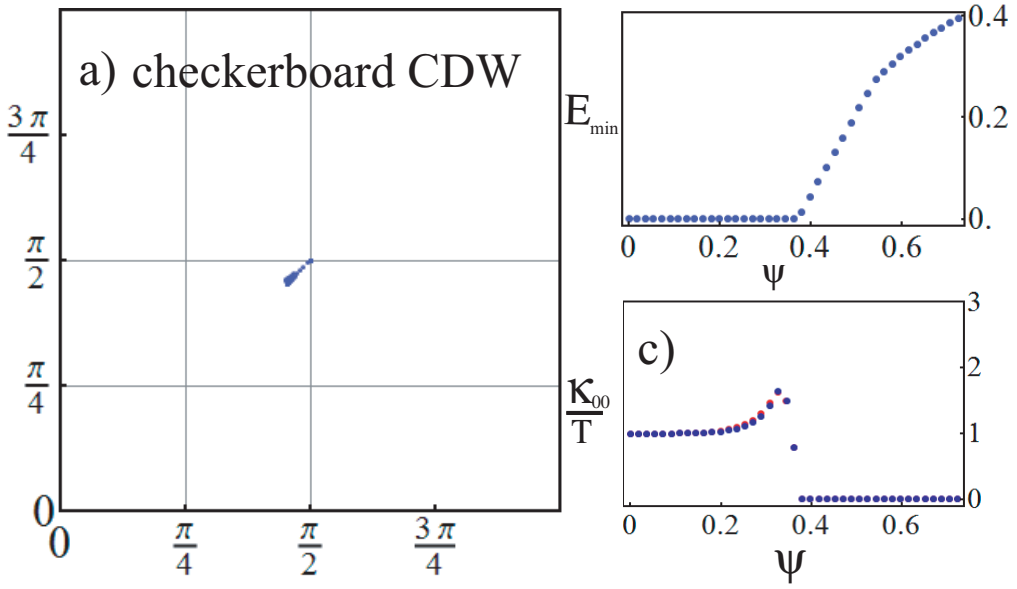

Figure 4.9: Effects on spectrum and low temperature transport of a $\mathbf{Q}_1 = (\pi, 0)$, $\mathbf{Q}_2 = (0, \pi)$ charge density perturbation to the dSC system. The nodes move in straight lines toward the $(\pm\pi/2, \pm\pi/2)$ points. The spectrum becomes gapped at that point, and κ_{00} vanishes for ψ larger than about $0.4t$.

gapped, and the thermal conductivity vanishes, with a value of ψ_c about two-thirds of that for the striped $(\pi, 0)$ CDW. In contrast, the checkerboard pair density wave seen in Fig. evolves the nodes along the same symmetry line, but towards the Γ point $(0, 0)$. At that point, the spectrum would become gapped, and the universal limit thermal conductivity would vanish. However, systems

which more closely resemble a d-wave superconductor than the checkerboard ($\Delta_0 > \psi$) will remain gapless, as the nodal evolution would not be driven that far—about thirty times the critical value for the striped $(\pi, 0)$ PDW .

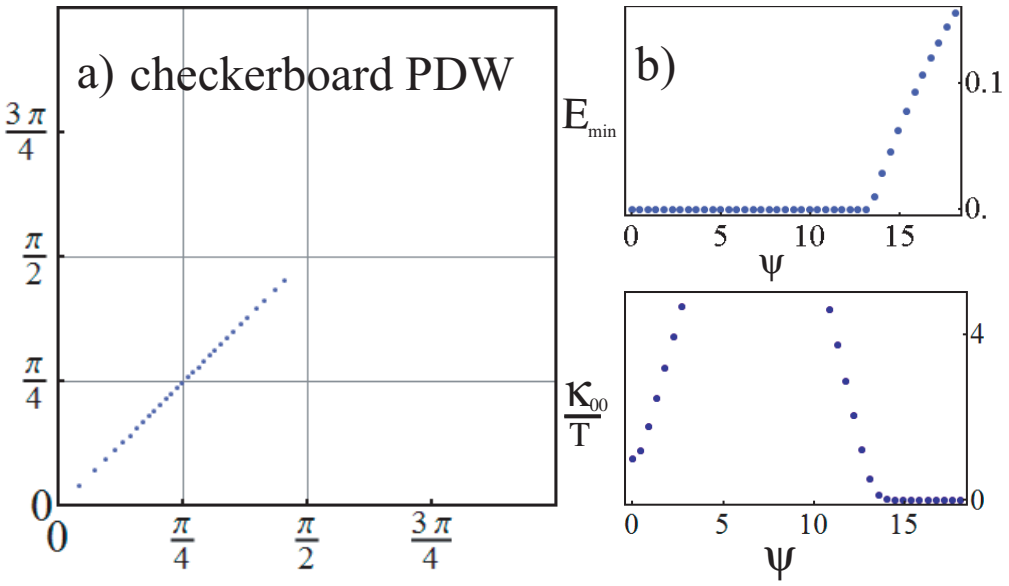

Figure 4.10: Effects on spectrum and low temperature transport of a $\mathbf{Q}_1 = (\pi, 0)$, $\mathbf{Q}_2 = (0, \pi)$ pair density perturbation to the dSC system. The nodes move in straight lines toward the origin at $(0, 0)$ points. The spectrum would become gapped at that point, however, the value of ψ required is much larger than the energy scale on which the system is superconducting. Therefore, for reasonable strengths of the ordering vector, the thermal conductivity is unaffected by this density wave.

4.5 Conclusion

In conclusion, we have written mean-field hamiltonians describing a d-wave superconductor perturbed by a variety of density waves. We noted the effects of such perturbations on the low energy quasiparticle spectrum, and by

calculating the universal limit ($T \to 0, \Omega \to 0$) thermal conductivity, see the effect that density waves can have on the low temperature thermal transport. We learned that whether the universal limit thermal conductivity is robust in the presence of an incipient density wave depends on which density wave, and which wave vector is added. For instance, in the case of $\mathbf{Q} = (\pi, 0)$ pair density waves, the quasiparticle nodes evolve so that their k-space locations move toward $(\pm\pi/2, \pm\pi/2)$, as they do for a CDW of the same wave vector. When they reach this point, which is the point at which the density wave vector nests the nodes, the spectrum becomes gapped. However, for the $\mathbf{Q} = (\pi, 0)$ spin density wave, the nodal structure is preserved beyond this strength, despite the nesting of the nodes. For the $\boldsymbol{Q} = (\pi, \pi)$ density waves, the effects of SDW and CDW are reversed from that of the $(\pi, 0)$ case; the (π, π) CDW preserves nodality beyond the nesting wave vector, while the (π, π) SDW is gapped beyond a critical strength. In the case of $\mathbf{Q} = (\pi/2, 0)$, the different wave vector drives the nodes toward $(\pi/4, k_y)$ instead. Given typical tight-binding parameters, such a charge density wave will not gap the quasiparticle spectrum, and will thus not affect the thermal conductivity, which remains universal. In the case of $\mathbf{Q}_1 = (\pi, 0)$, $\mathbf{Q}_2 = (0, \pi)$ checkerboard charge order, whether or not the universal limit thermal conductivity is robust depends on which type of density wave is present: the CDW checkerboard nodes move toward the $(\pm\pi/2, \pm\pi/2)$ point, and become gapped, however the PDW checkerboard nodes moves away from that direction, and the nodal structure is preserved.

Because the onset of charge ordering is believed to be correlated with underdoping, observations which show that the low temperature thermal conductivity differs from the universal value predicted in Ref. 24 may be due to the influence of coexisting orders. There are some general features that appear in all of the models considered in this paper. (1) In general, the nodal evolution is determined more by the wave-vector $\mathbf{Q}$ than by the chemical potential μ, although μ will determine the amplitude of density wave which will gap the system. (2) The physics still remains nodal in the following sense. Whether the density waves considered were of s-wave or p-wave symmetry did not have any effect; the only thing which mattered was the amplitude of the density wave at the node. (3) It is interesting to note that the universal limit thermal conductivity generally develops a disorder dependence, especially near the nodal transition point. The presence of density waves are therefore one possible explanation of the breakdown of universal limit thermal transport in cuprates. (4) In general, there is an increase in the conductivity near the nodal transitions (for models which have transitions), which is caused by the deformations (effectively increasing v_f/v_Δ) as the nodes meet their images. This feature is consistent with thermal conductivity measurements of Proust

et al.[97] which find a large enhancement in thermal conductivity of Bi-2201 over the pure dSC value.

Chapter 5

Conclusions

We have considered a variety of effective hamiltonians corresponding to d-wave superconductors coexisting with a variety of density waves, which has been inspired by the observation of these symmetries in the cuprate superconductors. We have studied the ways in which the low temperature properties of d-wave superconductors are modified by the addition of these coexisting order parameters. The location of nodal quasiparticles evolves in k-space until the spectrum becomes gapped; this evolution depends on which particular density wave is under consideration.

We have seen that the low temperature thermal conductivity can be affected by coexisting order parameters in two ways. In general, the thermal conductivity which was disorder independent (universal) in a d wave superconductor develops a disorder dependence when density waves are present. Also, for sufficiently large amplitudes, the density waves can suppress κ_{00} entirely by gapping the quasiparticle spectrum.

The inclusion of vertex corrections was found to be unimportant in the dSC + $\mathbf{Q} = (\pi, 0)$ CDW system. This finding is in agreement with the heuristic argument that thermal currents can relax via both internode and intranode scattering, and that it is therefore not important to distinguish between those scattering events.

Because of evidence that the density modulations may increase with underdoping, it is possible that transport measurements on well prepared samples could indirectly observe these density modulations, by observing a low temperature thermal conductivity which changes as more underdoped samples are measured. The thermal conductivity is affected in two ways. First, because our calculations generally predict an upturn in κ_{00} near the nodal/gapped transition (for models which have one) the quasiparticle contribution to thermal conductivity should be enhanced from the pure dSC value as one underdopes the sample. Secondly, our calculations indicate that a non-universality

develops near the nodal/gapped transition. Therefore, variations in κ_{00} are also expected upon the introduction of controlled disorder (along the lines of the kind used in Ref. 29), as long as the doping level puts the sample near the nodal/gapped transition. This signature of ordering in transport is depicted in Fig. 5.1. Experiments on Bi-2201 ($Bi_{2+x}Sr_{2-x}CuO_{6+\delta}$ indicate that there is an enhancement of the universal limit thermal conductivity with underdoping[97]. Our findings indicate that the low temperature thermal conductivity is enhanced near the nodal/gapped transition, which is consistent with this measurement.

Future directions

In real materials, the quasiparticle scattering mechanisms seem to occur due to both in-plane (unitary limit scatters) and out-of-plane (Born limit scatterers), rather than any one of the two[35, 72]. Because of this, a more complete model for the scattering should be considered, whereby the quasiparticle lifetime would be generated by

$$\frac{1}{\tau} = \frac{1}{\tau_{\text{Born}}} + \frac{1}{\tau_{\text{unitary}}}, \tag{5.1}$$

with two impurity densities, n_{in} and n_{out}, representing in and out of plane impurities.

STM experiments indicate that a checkerboard modulation of the local density of states occurs, with the magnitude of the wave vector somewhere in the range from $Q = \frac{2\pi}{4.5}$ to $Q = \frac{2\pi}{4}$[48, 49]. To estimate the effect of $\mathbf{Q}_1 = (\frac{\pi}{2}, 0), \mathbf{Q}_2 = (0, \frac{\pi}{2})$ checkerboard based on the $\mathbf{Q} = (\frac{\pi}{2}, 0)$ CDW, we can compare the effects of the $\mathbf{Q} = (\pi, 0)$ CDW to that of the $\mathbf{Q}_1 = (\pi, 0), \mathbf{Q}_2 = (0, \pi)$ checkerboard. The $(\pi, 0)$ striped CDW drives the nodes along a curved path toward the $(\frac{\pi}{2}, \frac{\pi}{2})$ point. The $(\pi, 0)$ checkerboard CDW adds the direction of the two constituent density waves, and the nodes evolve directly towards $(\frac{\pi}{2}, \frac{\pi}{2})$. The nodal evolution of the pair density wave obeys the same logic: the addition of the nodal direction for the pair density wave sends the $(\pi, 0)$ checkerboard PDW away from $(\frac{\pi}{2}, \frac{\pi}{2})$. This is indeed what our calculations observed. If we apply this to estimate the nodal evolution of $(\frac{\pi}{2}, 0)$ checkerboard, we would not expect to see the nodal collision for a reasonably small density wave perturbation, as the nodes would evolve toward the Γ point at $(0, 0)$.

The quest to understand the unusual behavior exhibited by cuprates is nowhere near its end. By considering the effects of competing orders on the quasiparticle spectrum and low temperature thermal conductivity of d-wave superconductors, we augment our understanding by just one small parcel.

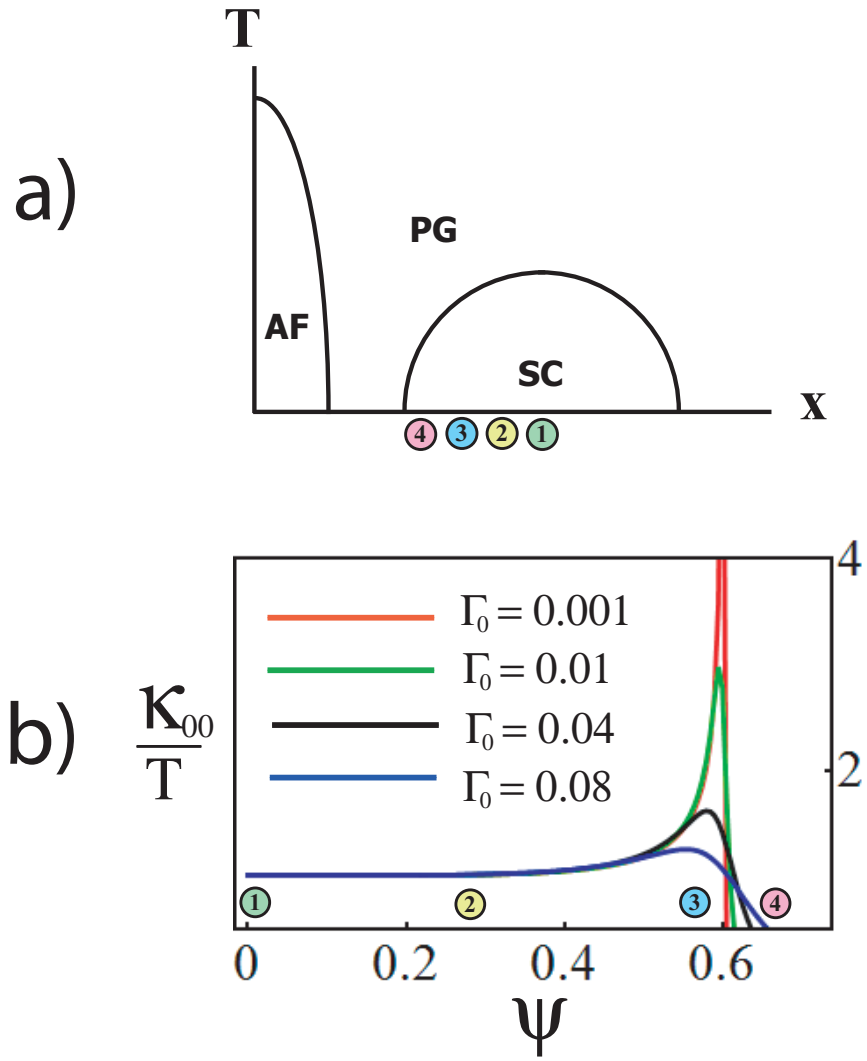

Figure 5.1: a) Generic phase diagram of cuprates, with three prominent phases labeled, and axes T and x representing temperature and doping. AF is the anti-ferromagnetic insulating state present at low doping, SC is the superconducting state, and PG is the pseudogap region. Coexisting or competing order parameters are believed to onset as one underdopes from optimal doping. Four increasingly underdoped samples are thus labeled by numbers one through four.
(b) Samples which are increasingly underdoped might be expected to display an increase in the quasiparticle term in the low temperature thermal conductivity (with respect to the optimally doped value representing a pure d-wave superconductor). In addition, for strong enough ordering (i.e. far from optimal doping), non-universal behavior is expected in the thermal conductivity, as is exhibited by the different values of κ_{00} anticipated for samples with varying Γ_0 for doping level "3".

Bibliography

[1] H.K. Onnes, Comm. Phys. Lab. Univ. Leiden, Nos. 119,120,122 (1911).

[2] W. Meissner and R. Oschenfeld, Naturwiss. **21**, 787 (1933).

[3] C.J. Gorter and H.G.B. Casimir, Phys. Zeits. **35**, 963 (1934).

[4] F. London, *Superfluids, Vol. I*, (Wiley, New York, 1950).

[5] A.B. Pippard, Proceed. Royal Soc. Lond. A **216**, 547 (1953).

[6] V.L. Ginsberg and L.D. Landau, JETP **20** 1064, (1950).

[7] H. Frölich, Phys. Rev. **79** 845, (1950).

[8] R. Schrieffer, *Superconductivity*, W.A. Benjamin Publishers, 1964.

[9] I. Giaever, Phys. Rev. Lett. **5** 147 (1960).

[10] M. Tinkham *Introduction to Superconductivity*, (Dover, New York, 2004).

[11] J.G. Bednorz and K.A. Müller, Z. Phys. B **64**, 189 (1986).

[12] P.A. Lee, Science **277**, 50 (1997).

[13] H. Ding, M.R. Norman, J.C. Campuzano, M. Randeria, A.F. Bellman, T. Yokoya, T. Takahashi, T. Mochiku, and K. Kadowaki, Phys. Rev. B **54**, 9678R (1996).

[14] P.A. Lee, N. Nagaosa and X.G. Wen, Rev. Mod. Phys. **78** 17 (2006).

[15] D.J. Van Harlingen, Rev. Mod. Phys. **67** 515 (1995)

[16] C.C. Tsuei and J.R. Kirtley Rev. Mod. Phys. **72** 970 (2000).

[17] A. Damascelli, Z. Hussain and Z.X. Shen, Rev. Mod. Phys. **75** 473 (2003).

[18] Ø. Fischer, M. Kugler, I. Maggio-Aprile and C. Berthod, Rev. Mod. Phys. **79** 353 (2007).

[19] T. Valla, A. V. Fedorov,J.H. Lee,J.C. Davis and G.D. Gu, Science **314**, 1914 (2006).

[20] A.V. Balatsky, I. Vekhter, and J.X. Zhu, Rev. Mod. Phys. **78**, 373 (2006).

[21] A.V. Balatsky, A. Rosengren, and B.L. Altshuler, Phys. Rev. Lett. **7**3 720 (1994).

[22] P.A. Lee, Phys. Rev. Lett. **71**, 1887 (1993)

[23] L.P. Gor'kov and P.A. Kalugin, Pis'ma Zh. ksp. Teor. Fiz. **41**, 208 (1985) [JETP Lett. **41**, 253 (1985)]

[24] A.C. Durst and P.A. Lee, Phys. Rev. B **62** 1270 (2000)

[25] M. Sutherland, S.Y. Li, D.G. Hawthorn, R.W. Hill, F. Ronning, M.A. Tanatar, J. Paglione, H. Zhang, L. Taillefer, J. DeBenedictis, R. Liang, D.A. Bonn and W.N. Hardy, Phys. Rev. Lett. **94**, 147004 (2005).

[26] D.G. Hawthorn, S.Y. Li, M. Sutherland, E. Boaknin, R.W. Hill, C. Proust, F. Ronning, M.A. Tanatar, J.P. Paglione, L. Taillefer, D. Peets, R.X. Liang, D.A. Bonn, W.N. Hardy and N.N. Kolesnikov, Phys. Rev. B **75** 104518 (2007)

[27] X.F. Sun, S. Ono, X. Zhao, Z.Q. Pang, Y. Abe and Y. Ando, Phys. Rev. B **77** 094515 (2008).

[28] N.E. Hussey, Advances in Physics, **51**, 1685 (2002).

[29] L. Taillefer, B. Lussier, R. Gagnon, K. Behnia and H. Aubin, Phys. Rev. Lett. **79**, 483 (1997).

[30] M. Chiao, R.W. Hill, C. Lupien, B. Popić, R. Gagnon and L. Taillefer, Phys. Rev. Lett. **82** 2943 (1999)

[31] M. Chiao, R.W. Hill, C. Lupien, L. Taillefer, P. Lambert, R. Gagnon and P. Fournier, Phys. Rev. B **62** 3554 (2000)

[32] S. Nakamae, K. Behnia, L. Balicas, F. Rullier-Albenque, H. Berger and T. Tamegai, Phys. Rev. B **63** 184509 (2001)

[33] C. Proust, E. Boaknin, R.W. Hill, L. Taillefer and A.P. Mackenzie, Phys. Rev. Lett. **89**, 147003 (2002).

[34] M. Sutherland, D.G. Hawthorn, R.W. Hill, F. Ronning, S. Wakimoto, H. Zhang, C. Proust, E. Boaknin, C. Lupien, L. Taillefer, R.X. Liang, D.A. Bonn, W.N. Hardy, R. Gagnon, N.E. Hussey, T. Kimura, M. Nohara and H. Tagaki, Phys. Rev. B **67** 174520 (2003)

[35] R.W. Hill, C. Lupien, M. Sutherland, E. Boaknin, D.G. Hawthorn, C. Proust, F. Ronning, L. Taillefer, R. Liang, D.A. Bonn and W.N. Hardy, Phys. Rev. Lett. **92**, 027001 (2004).

[36] X.F. Sun, K. Segawa and Y. Ando, Phys. Rev. Lett. **93**, 107001 (2004).

[37] D.G. Hawthorn, R.W. Hill, C. Proust, F. Ronning, M. Sutherland, E. Boaknin, C. Lupien, M.A. Tanatar, J. Paglione, S. Wakimoto, H. Zhang, L. Taillefer, T. Kimura, M. Nohara and N.E. Hussey, Phys. Rev. Lett. **90**, 197004 (2003).

[38] Y. Ando, S. Ono, X.F. Sun, J. Takeya, F.F. Balakirev, J.B. Betts and G.S. Boebinger, Phys. Rev. Lett. **92**, 247004 (2004).

[39] X.F. Sun, K. Segawa and Y. Ando, Phys. Rev. B **72**, 100502 (2005).

[40] X.F. Sun, S. Ono, Y. Abe, S. Komiya, K. Segawa and Y. Ando, Phys. Rev. Lett. **96**, 017008 (2006).

[41] J. Zaanen and O. Gunnarsson, Phys. Rev. B **40**, 7931 (1989).

[42] D. Poilblanc and T.M. Rice, Phys. Rev. B **39**,9749 (1989).

[43] H. Schulz, Journ. de Physique **50**, 2833 (1989).

[44] K. Machida, Physica C **158**, 192 (1989).

[45] J.M. Tranquada, B.J. Sternlieb, J.D. Axe, Y. Nakamura and S. Uchida, Nature **375**, 561 (1995).

[46] J.M. Tranquada, J.D. Axe, N. Ichikawa, Y. Nakamura, S. Uchida and B. Nachumi, Phys. Rev. B **54**, 7489 (1996).

[47] M. Vojta, arXiv.0901.3145

[48] J.E. Hoffmann, E.W. Hudson, K.M. Lang, V. Madhavan, H. Eisaki, S. Uchida, and J.C. Davis, Science **295** 466 (2002).

[49] J.E. Hoffmann, K. McElroy, D.H. Lee, K.M. Lang, H. Eisaki, S. Uchida and J.C. Davis, Science **297**, 1148 (2002).

[50] C. Howald, H. Eisaki, N. Kaneko, M. Greven and A. Kapitulnik, Phys. Rev. B **67** 014533 (2003)

[51] C. Howald, P. Fournier and A. Kapitulnik, Phys. Rev. B **64** 100505R (2001)

[52] M. Vershinin, S. Misra, S. Ono, Y. Abe, Y. Ando and A. Yazdani, Science **303**, 1995 (2004).

[53] K. McElroy, D.H. Lee, J.E. Hoffman, K.M. Lang, J. Lee, E.W. Hudson, H. Eisaki, S. Uchida, and J.C. Davis, Phys. Rev. Lett. **94**, 197005 (2005)

[54] T. Hanaguri, C. Lupien, Y. Kohsaka, D.H. Lee, M. Azuma, M. Takano, H. Takagi and J.C. Davis, Nature **430** 1001 (2004)

[55] S. Misra, M. Vershenin, P. Phillips and A. Yazdani, Phys. Rev. B **70** 220503(R) (2004).

[56] K. McElroy, D.H. Lee, J.E. Hoffman, K.M. Lang, J. Lee, E.W. Hudson, H. Eisaki, S. Uchida and J.C. Davis, Phys. Rev. Lett. **94**, 197005 (2005).

[57] Y. Kohsaka, C. Taylor, K. Fujita, A. Schmidt, C. Lupien, T. Hanaguri, M. Azuma, M. Takano, H. Eisaki, H. Takagi, S. Uchida and J.C. Davis, Science **315**, 1380 (2007).

[58] M.C. Boyer, W.D. Wise, K. Chatterjee, M. Yi, T. Kondo, T. Takeuchi, H. Ikuta and E.W. Hudson, Nature Physics **3**, 802 (2007).

[59] T. Hanguri, Y. Kohsaka, J.C. Davis, C. Lupien, I. Yamada, M. Azuma, M. Takano, K. Ohishi, M. Ono and H. Takagi, Nature Physics **3**, 865 (2007).

[60] A.N. Pasupathy, A. Pushp, K.K. Gomes, C.V. Parker, J. Wen, Z. Xu, G. Gu, S. Ono, Y. Ando and A. Yazdani, Science **320**, 196 (2008).

[61] W.D. Wise, M.C. Boyer, K. Chatterjee, T. Kondo, T. Takeuchi, H. Ikuta, Y. Wang and E.W. Hudson, Nature Physics **4**, 696 (2008).

[62] Y. Kohsaka, C. Taylor, P. Wahl, A. Schmidt, J. Lee, K. Fujita, J.W. Allredge, K. McElroy, J. Lee, H. Eisaki, S. Uchida, D.H. Lee and J.C. Davis, Nature **454**, 1072 (2008).

[63] S.A. Kivelson, I.P. Bindloss, E. Fradkin, V. Oganesyan, J.M. Tranquada, A. Kapitulnik and C. Howald, Rev. Mod. Phys. **75**, 1201 (2003)

[64] A. Fetter and D. Walecka, *Quantum Many-Particle Systems*, (Dover Publications, Mineola, 1971).

[65] Alexei Tsvelik, *Quantum Field Theory in Condensed Matter Physics*, (Cambridge University Press, London, 1995).

[66] G. Mahan, *Many-Particle Physics*, (Plenum Press, New York, 1981).

[67] E.S. Velasco, *Wave Propogation Lecture Notes*

[68] J. Rammer, *Quantum Transport Theory*, (Perseus Books, New York, 1998).

[69] K. Huang, *Statistical Mechanics*, (Wiley and Sons, New York, 1987).

[70] A.C. Durst *Solid State Physics Lecture Notes*.

[71] A.C. Durst, A. Vishwanath and P.A. Lee, Phys. Rev. Lett. **90**, 187002, (2003).

[72] W. Kim, F. Marsiglio and J. P. Carbotte, PhysRevB **68**, 174513 (2003)

[73] H. Monien, K. Scharnberg and D. Walker, Solid State Commun. **63**, 263 (1987).

[74] P.J. Hirschfeld, P. Wölffle and D. Einzel, Phys. Rev. B **37**, 83 (1988).

[75] N.W. Ashcroft and N.D. Mermin *Solid State Physics*,(Thompson Learning, London, 1976).

[76] J.M. Ziman *Principles of the Theory of Solids*, (Cambridge, Camb. Univ. Press, 1972).

[77] A. Altland, B.D. Simons and M.R. Zirnbauer, Phys. Reports **359** 283 (2002)

[78] J. Orenstein and A.J. Millis, Science **288**, 468 (2000).

[79] P.J. Hirschfeld, W.O. Putikka and D.J. Scalapino, Phys. Rev. Lett. **71**, 3705 (1993).

[80] P.J. Hirschfeld, W.O. Putikka and D.J. Scalapino, Phys. Rev. B **50**, 10250 (1994).

[81] P.J. Hirschfeld and W.O. Putikka, Phys. Rev. Lett. **77**, 3909 (1996).

[82] M.J. Graf, S-K. Yip., J.A. Sauls and D. Rainier, Phys. Rev. B **53** 15147 (1996).

[83] T. Senthil, M.P.A. Fisher, L. Balents and C. Nayak, Phys. Rev. Lett. **81**, 4704 (1998).

[84] M. Vojta, Y. Zhang and S. Sachdev, PhysṘev. B **62** 6721 (2000)

[85] D. Podolsky, E. Demler, K. Damle and B.I. Halperin, Phys. Rev. B **67** 094514 (2003)

[86] J.X. Li, C.Q. Wu and D.H. Lee, Phys. Rev. B **74** 184515 (2006)

[87] C.T. Chen, A.D. Beyer and N.C. Yeh, Solid State Communications **143** 447 (2007)

[88] K.J. Seo, H.D. Chen, and J.P. Hu, Phys. Rev. B **76** 020511 (R) (2007)

[89] E. Berg, C.C. Chen and S.A. Kivelson, Phys. Rev. Lett. **100** 027003 (2008)

[90] K. Park and S. Sachdev, PhysṘevḂ **64** 184510 (2001)

[91] A.C. Durst and S. Sachdev, http://arxiv.org/abs/0810.3914v1 (2008)

[92] P.R. Schiff and A.C. Durst, Physica C **469** 740 (2009)

[93] V.P. Gusynin and V.A. Miransky, Euro. Phys. Journal B **37**, 363 (2003).

[94] B.M. Andersen and P.J. Hirschfeld, Phys. Rev. Lett. **100** 257003 (2008).

[95] C. Nayak, Phys. Rev. B **62** 4881 (2000)

[96] J.A. Slezak, J.H. Lee, M. Wang, K. McElroy, K. Fujita, B.M. Andersen, P.J. Hirschfeld, H. Eisaki, S. Uchida and J.C. Davis, Proc. Nat. Acad. of Science, **105** 3203 (2008).

[97] C. Proust, K. Behnia, R. Bel, D. Maude and S.I. Vedeneev, Phys. Rev. B **72** 214511 (2005).

[98] O. Cyr-Choiniè, R. Daou, F. Laliberté, D. LeBoeuf, N. Doiron-Leyraud, J. Chang, J.Q. Yan, J.G. Cheng, J.S. Zhou, J.B. Goodenough, S. Pyon, T. Takayama, H. Takagi, Y. Tanaka and L. Taillefer, Nature **458**, 763 (2009).

[99] M.P.A. Fisher arXiv:cond-mat/9806164

[100] A.A. Nerseyan, A.M. Tsvelik and F. Wenger, Nucl. Phys. B **438**, 561 (1995).

[101] T. Senthil and M.P.A. Fisher, Phys. Rev. B **60** 6893 (1999).

[102] C.T. Chen and N.C. Yeh, Phys. Rev. B **6**8 220505 (2003)

[103] X. Yang and C. Nayak, Phys. Rev. B **6**5 064523 (2002)

[104] Gradshteyn and Ryzhik, *Table of Integrals, Series and Products* (Publisher, Place, Date).

Appendix A

Pairing hamiltonians in the mean field

Making the pairing approximation, the hamiltonian describing electrons and their interactions is reduced to

$$H = \sum_{k\sigma} \xi_k c^\dagger_{k\sigma} c_{k\sigma} + \sum_{kk'} V_{kk'} c^\dagger_{k\uparrow} c^\dagger_{-k\downarrow} c_{-k'\downarrow} c_{k'\uparrow}. \tag{A.1}$$

If we let

$$\begin{aligned} c_{-k'\downarrow} c_{k'\uparrow} &= b_{k'} + (c_{-k'\downarrow} c_{k'\uparrow} - b_{k'}) \\ c^\dagger_{k\uparrow} c^\dagger_{-k\downarrow} &= b^\dagger_k + (c^\dagger_{k'\uparrow} c^\dagger_{-k'\downarrow} - b^\dagger_k) \end{aligned} \tag{A.2}$$

and neglect terms which are second order in the fluctuations,

$$H = \sum_{k\sigma} \xi_k c^\dagger_{k\sigma} c_{k\sigma} - \sum_k \Big(\Delta_k c_{-k\downarrow} c_{k\uparrow} + \Delta_k c^\dagger_{k\uparrow} c^\dagger_{-k\downarrow} - b^\dagger_k \Delta_k \Big) \tag{A.3}$$

which we can diagonalize with the Bogoliubov-Valatin transformation:

$$\begin{aligned} c_{k\uparrow} &= u^*_k \alpha_k + v_k \beta^\dagger_k \qquad c_{k\uparrow}\dagger = u_k \alpha^\dagger_k + v^*_k \beta_k \\ c^\dagger_{-k\downarrow} &= -v^*_k \alpha_k + u_k \beta^\dagger_k \qquad c_{-k\downarrow} = -v_k \alpha^\dagger_k + u^*_k \beta_k, \end{aligned} \tag{A.4}$$

whereby the hamiltonian becomes

$$\begin{aligned} H = \sum_k \Big[\Big(\frac{1}{2} \xi_k (|u_k|^2 - |v_k|^2) + \Delta^*_k u^*_k v_k + \Delta_k u_k v^*_k \Big) (\alpha^\dagger_k \alpha_k + \beta^\dagger_k \beta_k) \\ + (2\xi_k u_k v_k + \Delta^*_k v^2_k - \Delta_k u^2_k) \alpha^\dagger_k \beta^\dagger_k + |v_k|^2 \xi_k - \Delta_k u_k v^*_k \Big] + \text{h.c.} - b^\dagger_k \Delta_k \end{aligned} \tag{A.5}$$

The condition that this transformation be canonical is

$$|u_k|^2 + |v_k|^2 = 1, \tag{A.6}$$

therefore, H is diagonalized by requiring

$$2\xi_k(u_k v_k + \Delta_k^* v_k^2) - \Delta_k u_k^2 = 0 \tag{A.7}$$

Multiplying by $\frac{\Delta_k^*}{u_k^2}$, we find that

$$\Delta_k^* \frac{v_k}{u_k} = -\xi_k + \sqrt{\xi_k^2 + |\Delta_k|^2}, \tag{A.8}$$

which is necessarily Real. With the definition $E_k = \sqrt{\xi_k^2 + |\Delta_k|^2}$, we find the magnitudes of the coherence factors:

$$|u_k|^2 = \frac{1}{2E_k}(E_k + \xi_k) \qquad |v_k|^2 = \frac{1}{2E_k}(E_k - \xi_k) \tag{A.9}$$

Using these in (A.5), we find that

$$H = \sum_k \Big[(\xi_k - E_k) - b_k^\dagger \Delta_k + E_k(\alpha_k^\dagger \alpha_k + \beta_k^\dagger \beta_k)\Big] \tag{A.10}$$

where the first two terms represent the normal state energy and thermodynamic condensation energy, and the final term is the energy associated with the excitations α_k and β_k, which are known as Bogoliubons.

Appendix B

Density of states

Here we will calculate the density of states in a few illustrative situations. The density of states, which is the number of quantum states per unit energy, can be computed using

$$N(\omega) = \sum_k \delta(E_k - \omega), \tag{B.1}$$

where E_k is the energy of a particle in the state k.

For example, in a three dimensional metal, where excitations are described by electrons with a renormalized (band) mass m as $E_k = \frac{\hbar^2 k^2}{2m}$, the density of states is

$$\begin{aligned} N(\omega) &= \int \frac{\mathrm{d}^3 k}{(2\pi)^3} \delta(\frac{\hbar^2 k^2}{2m^*} - \omega) \\ &= \int \frac{\mathrm{d}\Omega}{4\pi} \int \frac{k^2 \mathrm{d}k}{2\pi^2} \delta(\frac{\hbar^2 k^2}{2m^*}. \end{aligned} \tag{B.2}$$

Let $u = \frac{\hbar^2 k^2}{2m^*}$, then $\mathrm{d}u = \frac{\hbar^2 k}{m^*}\mathrm{d}k$, and

$$N(\omega) = 2\pi(\frac{m^*}{2\pi\hbar^2})^{3/2} \int \mathrm{d}u \sqrt{u} \delta(u - \omega) = 2\pi(\frac{m^*}{2\pi\hbar^2})^{3/2} \sqrt{\omega}. \tag{B.3}$$

In a two dimensional metal, the density of states is

$$\begin{aligned} N(\omega) &= \int \frac{\mathrm{d}^2k}{(2\pi)^2}\delta(\frac{\hbar^2k^2}{2m^*}-\omega) \\ &= \int \frac{\mathrm{d}\phi}{2\pi}\int \frac{k\mathrm{d}k}{2\pi}\delta(u-\omega) \\ &= \int \frac{m^*}{2\pi\hbar^2}\mathrm{d}u\delta(u-\omega), \end{aligned} \tag{B.4}$$

so that $N(\omega)=\frac{m^*}{2\pi\hbar^2}$, a constant, in two dimensions.

Meanwhile, if we consider an s-wave superconductor, which has quasiparticle spectrum $E_k=\pm\sqrt{\epsilon_k^2+\Delta^2}$, where ϵ_k is the normal state dispersion, and Δ is an isotropic gap function, we see that

$$\begin{aligned} N(\omega) &= \sum_k \delta(E_k-\omega) \\ &= \int \mathrm{d}\xi_k\delta(\sqrt{\xi_k^2+\Delta^2}-\omega), \end{aligned} \tag{B.5}$$

then, if we let $u=\sqrt{\xi_k^2+\Delta^2}$, then $\mathrm{d}u=\frac{\xi_k\mathrm{d}\xi_k}{\sqrt{\xi_k^2+\Delta^2}}$, and

$$\begin{aligned} N(\omega) &\propto \int \frac{u\mathrm{d}u}{\sqrt{u^2-\Delta^2}}\delta(u-\omega) \\ &= \frac{\omega}{\sqrt{\omega^2-\Delta^2}}\Theta(\omega-\Delta). \end{aligned} \tag{B.6}$$

On the other hand, we can consider a d-wave superconductor. For high energies, the presence of the energy gap will effect a similar trend in the density of states; a sharp increase as ω approaches the gap maximum, Δ_0, from above. At low energies, however, the density of states is not zero, however, due to the presence of quasiparticle excitations around $(\pm\pi/2,\pm\pi/2)$. These Dirac quasiparticles have electronic dispersion $\xi_k\sim v_f k_1\equiv p_1$, and gap $\Delta_k\sim v_\Delta k_2\equiv p_2$. Therefore, the low energy $\omega << \Delta_0$ density of states can be computed using

$$N(\omega)=\int \mathrm{d}p_1\int \mathrm{d}p_2\delta(E(p_1,p_2)-\omega) \tag{B.7}$$

These coordinates satisfy $p_1^2+p_2^2=p^2$, so that we can transform to an angular

integral

$$\begin{aligned} N(\omega) &\propto \int p \mathrm{d}p \delta(p-\omega) \\ &= \omega. \end{aligned} \tag{B.8}$$

Appendix C

SCBA self-energy in dSC

The retarded self-energy for the dSC quasiparticles in the self-consistent Born approximation,

$$\widetilde{\Sigma}_{\rm Ret}(\mathbf{k},\omega), \tag{C.1}$$

is realized by taking the analytic continuation of the Matsubara function,

$$\widetilde{\Sigma}(\mathbf{k},i\omega) = n_{\rm imp}\sum_{k'} V_{kk'}\widetilde{\tau}_3\widetilde{\mathcal{G}}(\mathbf{k},i\omega)V_{k'k}\widetilde{\tau}_3, \tag{C.2}$$

where $\widetilde{\tau}_3$'s arise in the Feynman rules for interactions, because the interacting term in the hamiltonian for electron-phonon and Coulomb interactions appears as $\psi_k^\dagger\widetilde{\tau}_3\psi_k$.[**?**]

The Green's function then takes the form

$$\begin{aligned}\widetilde{\mathcal{G}}(\mathbf{k},i\omega) &= \Big(\widetilde{\mathcal{G}}_0(\mathbf{k},i\omega)^{-1} - \widetilde{\Sigma}(\mathbf{k},i\omega)\Big)^{-1} \\ &= \frac{1}{D}\Big((i\omega-\Sigma_0)\widetilde{\tau}_0 + (\Delta_k+\Sigma_1)\widetilde{\tau}_1 + \Sigma_2\widetilde{\tau}_2 + (\epsilon_k+\Sigma_3)\widetilde{\tau}_3\Big),\end{aligned} \tag{C.3}$$

where $D = \Big((i\omega-\Sigma_0)^2 - (\Delta_k+\Sigma_1)^2 - (\epsilon_k+\Sigma_3)^2 - \Sigma_2^2\Big)$. The components of

the self-energy therefore obey the equations

$$\begin{aligned}
\Sigma_0(\mathbf{k}, i\omega) &= n_{\text{imp}} \sum_{k'} |V_{kk'}|^2 \frac{i\omega - \Sigma_0}{D} \\
\Sigma_1(\mathbf{k}, i\omega) &= -n_{\text{imp}} \sum_{k'} |V_{kk'}|^2 \frac{\Delta_k + \Sigma_1}{D} \\
\Sigma_2(\mathbf{k}, i\omega) &= -n_{\text{imp}} \sum_{k'} |V_{kk'}|^2 \frac{\Sigma_2}{D} \\
\Sigma_3(\mathbf{k}, i\omega) &= n_{\text{imp}} \sum_{k'} |V_{kk'}|^2 \frac{\epsilon_k + \Sigma_3}{D}.
\end{aligned} \tag{C.4}$$

Clearly, it is self-consistent to assume that $\Sigma_2 = 0$, and in the nodal parametrization

$$\sum_{k'} \to \sum_{j=1}^{4} \frac{1}{4\pi^2 v_f v_\Delta} \int_{-p_s}^{p_s} \mathrm{d}p_1 \int_{-p_s}^{p_s} \mathrm{d}p_2, \tag{C.5}$$

(where p_s represents a momentum cutoff for the "square" integration regions surrounding each node) we see that the substitutions $\epsilon_k + \Sigma_3 \to p_1$ and $\Delta_k + \Sigma_1 \to p_2$ lead to odd integrals for Σ_1 and Σ_3, so that they are also zero for the self-consistent Born approximation.

Assuming that the remaining term is of the form

$$\Sigma_0(\omega) = \Lambda(\omega) - i\Gamma(\omega), \tag{C.6}$$

and assuming that $\Lambda(\omega \to 0) = 0$, then we find that $\Sigma_0(\omega \to 0) \equiv -i\Gamma_0$.

In the nodal parametrization, we don't need all of the matrix elements of the scattering potential: the only ones which are important are one for scattering into the same node V_1, one for scattering into an adjacent node V_2, or one for scattering into the opposite node V_3. Therefore, assuming that $\mathbf{k}$ of the LHS is near the $(\pi/2, \pi/2)$ node, designated with $j = 1$, we see that the nodal sum becomes

$$\begin{aligned}
\sum_{j'=1}^{4} |V_{jj'}|^2 &= \begin{pmatrix} 1 & 0 & 0 & 0 \end{pmatrix} \begin{pmatrix} V_1 & V_2 & V_3 & V_2 \\ V_2 & V_1 & V_2 & V_3 \\ V_3 & V_2 & V_1 & V_2 \\ V_2 & V_3 & V_2 & V_1 \end{pmatrix} \begin{pmatrix} V_1 & V_2 & V_3 & V_2 \\ V_2 & V_1 & V_2 & V_3 \\ V_3 & V_2 & V_1 & V_2 \\ V_2 & V_3 & V_2 & V_1 \end{pmatrix} \begin{pmatrix} 1 \\ 0 \\ 0 \\ 0 \end{pmatrix} \\
&= V_1^2 + 2V_2^2 + V_3^2.
\end{aligned} \tag{C.7}$$

Then, defining

$$c \equiv n_{\rm imp} \frac{v_1^2 + 2V_2^2 + V_3^2}{4\pi^2 v_f v_\Delta}, \tag{C.8}$$

we find that

$$\begin{aligned} -i\Gamma_0 &= c \int \frac{\mathrm{d}^2 p}{2\pi} \frac{i\Gamma_0}{-\Gamma_0^2 - p^2} \\ &= c \int_0^{p_0} p \mathrm{d}p \frac{i\Gamma_0}{-\Gamma_0^2 - p^2}, \end{aligned} \tag{C.9}$$

so that

$$c = \frac{1}{2} \log \frac{\Gamma_0^2 + p_0^2}{\Gamma_0^2}, \tag{C.10}$$

or, since $\Gamma_0 << p_0$,

$$\Gamma_0 = p_0 \exp(-\frac{1}{2\pi c}). \tag{C.11}$$

Appendix D

Additional information for $\mathbf{Q} = (\pi, 0)$ CDW

D.1 Cutoff dependence of self-energy

Here we note that the self-consistent Born approximation, when applied to the mean-field Green's functions used in this paper, produces a self-energy which is proportional to the momentum cutoff. The physical observable, the thermal conductivity, has no such dependence. One difficulty this introduces is that the self-energy is dependent on the choice of coordinates. As the location of the nodes evolves with charge density wave order parameter ψ, computations are necessarily performed in a different local coordinate system (than one centered about a node itself). This coordinate shift in the p_1 direction introduces a constant $\widetilde{\Sigma}_{A3}$ term, even in the $\psi = 0$ instance (whereas using node-centered coordinates, the anti-symmetric integral is found to vanish). In the $\psi = 0$ case, a shift of ϵ corresponds to the integral

$$I = \int_{-p_0+\epsilon}^{p_0+\epsilon} \mathrm{d}p_1 \int_{-p_0}^{p_0} \mathrm{d}p_2 \frac{p_1}{p_1^2 + p_2^2 + \Gamma_0^2}. \tag{D.1}$$

The integration results in

$$\begin{aligned} I &= 2p_0 \Big[\sqrt{1+g^2+2m}\, \arctan\Big(\frac{1}{\sqrt{1+g^2+2m}}\Big) + \frac{1}{2} \log \frac{2+g^2+2m}{2+g^2-2m} \\ &\quad - \sqrt{1+g^2-2m}\, \arctan\Big(\frac{1}{\sqrt{1+g^2-2m}}\Big) \Big] \end{aligned} \tag{D.2}$$

where we have defined $g \equiv \Gamma_0/p_0$ and $m \equiv \epsilon/p_0$. We neglect terms of order g^2 in favor of terms of order m, since the displacement ϵ we will be considering

will be larger than $\Gamma_0 << p_0$, so

$$I = 2p_0\Big[\sqrt{1+2m}\,\arctan(\frac{1}{\sqrt{1+2m}}) - \sqrt{1-2m}\,\arctan(\frac{1}{\sqrt{1-2m}}) + \frac{1}{2}\log(\frac{1+m}{1-m})\Big], \tag{D.3}$$

so that with the series expansions

$$\begin{aligned} \arctan(\frac{1}{\sqrt{1+2x}}) &\approx \frac{\pi}{4} - \frac{x}{2} \\ \log(1+x) &\approx x - \frac{x^2}{2}, \end{aligned} \tag{D.4}$$

we find that

$$I = \pi p_0 m + \mathcal{O}(m). \tag{D.5}$$

So, shifting the coordinates adds the amount, $\pi\epsilon$, which matches the discrepancy. We therefore subtract off the $\psi = 0$ value of $\widetilde{\Sigma}_{A3}$; the results shown in Fig. 3.3 reflect this recalibration, as do the subsequent iterations of the self-consistent Born approximation.

D.2 Self-consistent Green's functions

Here are the Green's functions which fulfill the self-consistent Born approximation. The superscript $^{(3)}$ refers to the fact that 3 successive applications of our self-energy scheme were necessary for self-consistency, as is explained in

Section III.

$$
\begin{aligned}
G^{(3)}_{\rm den}(\omega) &= -(f_2^2+f_3^2)\Big((2\psi_c+\beta(p_1+p_2))^2+\frac{1}{\beta^2}(p_2-p_1)^2\Big)\\
&\quad+\left(-f_1^2+f_2^2+f_3^2+(\psi_c+\beta p_1)^2+(\frac{1}{\beta}p_2)^2\right)\\
&\quad\times\left(-f_1^2+f_2^2+f_3^2+(\psi_c+\beta p_2)^2+(\frac{1}{\beta}p_1)^2\right)\\
&\quad+4\Big(f_2^2((\psi_c+\beta p_1)(\psi_c+\beta p_2)-\frac{1}{\beta^2}p_1p_2)\\
&\quad-f_3\frac{1}{\beta}((\psi_c+\beta p_1)p_1+(\psi_c+\beta p_2)p_2)\Big)\\
\mathcal{G}^{(3)}_{A0}(\omega;p_1,p_2) &= -f_1\left(-f_1^2+(\psi_c+\beta p_2)^2+\frac{1}{\beta^2}p_1^2+f_2^2+f_3^2\right)\\
\mathcal{G}^{(3)}_{A1}(\omega;p_1,p_2) &= -\frac{1}{\beta}p_2\left(-f_1^2+(\psi_c+\beta p_2)^2+(\frac{1}{\beta}p_1)^2\right)\\
&\quad-\frac{1}{\beta}p_1(f_3^2-f_2^2)+2(\psi_c+\beta p_2)f_2f_3\\
\mathcal{G}^{(3)}_{A3}(\omega;p_1,p_2) &= -(\psi_c+\beta p_1)\left(-f_1^2+(\psi_c+\beta p_2)^2+(\frac{1}{\beta}p_1)^2\right)\\
&\quad+(\psi_c+\beta p_2)(f_3^2-f_2^2)+\frac{2}{\beta}p_1f_2f_3\\
\mathcal{G}^{(3)}_{B0}(\omega;p_1,p_2) &= f_1\left(f_3(2\psi_c+\beta(p_1+p_2))+f_2\frac{1}{\beta}(p_1+p_2)\right)\\
\mathcal{G}^{(3)}_{B1}(\omega;p_1,p_2) &= f_2\left(f_1^2-(\psi_c+\beta p_1)(\psi_c+\beta p_2)+\frac{1}{\beta^2}p_1p_2-f_2^2-f_3^2\right)\\
&\quad+f_3\Big((\psi_c+\beta p_1)p_1+(\psi_c+\beta p_2)p_2\Big)\\
\mathcal{G}^{(3)}_{B2}(\omega;p_1,p_2) &= f_1\left(f_3(\frac{1}{\beta}p_2-\frac{1}{\beta}p_1)+f_2\beta(p_2-p_1)\right)\\
\mathcal{G}^{(3)}_{B3}(\omega;p_1,p_2) &= f_3\left(f_1^2-f_2^2-f_3^2+(\psi_c+\beta p_1)(\psi_c+\beta p_2)-\frac{1}{\beta^2}p_1p_2\right)\\
&\quad+f_2\Big((\psi_c+\beta p_1)p_1+(\psi_c+\beta p_2)p_2)\Big) \qquad \text{(D.6)}
\end{aligned}
$$

$$
\begin{aligned}
\mathcal{G}^{(3)}_{C0}(\omega;p_1,p_2) &= \mathcal{G}^{(3)}_{B0}(\omega;p_1,p_2)\\
\mathcal{G}^{(3)}_{C1}(\omega;p_1,p_2) &= \mathcal{G}^{(3)}_{B1}(\omega;p_1,p_2)\\
\mathcal{G}^{(3)}_{C2}(\omega;p_1,p_2) &= -\mathcal{G}^{(3)}_{B2}(\omega;p_1,p_2)\\
\mathcal{G}^{(3)}_{C3}(\omega;p_1,p_2) &= \mathcal{G}^{(3)}_{B3}(\omega;p_1,p_2)\\
\mathcal{G}^{(3)}_{D0}(\omega;p_1,p_2) &= \mathcal{G}^{(3)}_{A0}(\omega;p_2,p_1)\\
\mathcal{G}^{(3)}_{D1}(\omega;p_1,p_2) &= \mathcal{G}^{(3)}_{C1}(\omega;p_2,p_1)\\
\mathcal{G}^{(3)}_{D3}(\omega;p_1,p_2) &= \mathcal{G}^{(3)}_{C3}(\omega;p_2,p_1)
\end{aligned}
\tag{D.7}
$$

To obtain the retarded Green's function $\mathcal{G}^R(\omega)$ from the above we set

$$
\begin{aligned}
f_1 &= \omega - \Sigma^{\rm Ret}_{A0}(\omega)\\
f_2 &= \Sigma^{\rm Ret}_{B1}(\omega)\\
f_3 &= \psi + \Sigma^{\rm Ret}_{B3}(\omega).
\end{aligned}
\tag{D.8}
$$

For the retarded Green's function $\mathcal{G}^{\rm Ret}(\omega+\Omega)$, we set $\omega \to \omega+\Omega$, and for the advanced Green's function $\mathcal{G}^{\rm Adv}(\omega)$ we set $\Sigma^{\rm Ret} \to \Sigma^{\rm Adv}$ by taking the complex conjugate *of the self-energy* , not of the entire Green's function.

D.3 Calculation of clean limit integral

For the clean limit of the thermal conductivity we need the integral

$$
I = \int \frac{{\rm d}^2q}{4\pi} \frac{A}{\Big(k_1 A + (q_2-k_2)^2 + \frac{1}{4}(q^2-k_3)^2\Big)^2},
\tag{D.9}
$$

in the limit $A \to 0$. With the substitution

$$
x_1 \equiv x\cos\theta = q_1 - 1 \qquad x_2 \equiv x\sin\theta = q_2
\tag{D.10}
$$

the quantity $Y_1 \equiv (q_2-k_2)^2 + \frac{1}{4}(q^2-k_3^2)^2$ becomes

$$
\begin{aligned}
Y_1 &= \frac{x^4}{4} + k_2^2 + \Big(\frac{1-k_3}{2}\Big)^2 + \frac{1-k_3}{2}x^2 + x^2\\
&\quad +(x^2+1-k_3)x\cos\theta - 2xk_2\sin\theta.
\end{aligned}
\tag{D.11}
$$

To simplify the angular integrand, we get rid of the $\sin\theta$ term by shifting $\theta \to \theta + \alpha$. Then, the last two terms of Eq. D.11 become

$$\frac{x^2+1-k_3}{2}\cos(\theta+\alpha) - k_2\sin(\theta+\alpha). \tag{D.12}$$

The appropriate trigonometric identities turn this into

(D.13)

We set the coefficient of the second term on the RHS of Eq. (D.13) to 0, so that the first term becomes

$$\begin{aligned} -\frac{1}{k_2}\Big((\frac{x^2+1-k_3}{2})^2 + k_2^2\Big)\sin\alpha\cos\theta = \\ \frac{-1}{r}\Big(\frac{x^4}{4} + \frac{1-k_3}{2}x^2 + (\frac{1-k_3}{2})^2 + k_2^2\Big)\cos\theta, \end{aligned} \tag{D.14}$$

where the RHS of Eq. (D.14) is obtained by setting $\sin\alpha \equiv k_2/r$, where $r = r(x)$ is an undetermined function of x. With this substitution, Eq. (D.11) becomes

$$\begin{aligned} Y_1 &= \frac{x^4}{4} + \frac{1-k_3}{2}x^2 + (\frac{1-k_3}{2})^2 + k_2^2 + x^2 \\ &\quad -\frac{2x}{r}\Big(\frac{x^4}{4} + \frac{1-k_3}{2}x^2 + (\frac{1-k_3}{2})^2 + k_2^2\Big)\cos(\theta+\alpha) \\ &\quad \Big((\frac{x^2+1-k_3}{2})^2 + k_2^2\Big)\Big(1 + \frac{x^2}{(\frac{x^2+1-k_3}{2})^2 + k_2^2} - \frac{2x}{r}\cos(\theta+\alpha)\Big) \\ &= \frac{x^2}{a^2}\Big(1 + a^2 - 2a\cos(\theta+\alpha)\Big), \end{aligned} \tag{D.15}$$

where

$$r = \sqrt{\Big(\frac{x^2+1-k_3}{2}\Big)^2 + k_2^2} \qquad \text{and} \qquad a = \frac{x}{r}. \tag{D.16}$$

Then, defining $\gamma = k_1 a^2/x^2$, the integral of Eq. (D.9) becomes

$$\begin{aligned} I &= \int \frac{\mathrm{d}^2 x}{4\pi} \frac{A}{\Big(k_1 A + \frac{x^2}{a^2}(1 + a^2 - 2a\cos(\theta + \alpha))\Big)^2} \\ &= \int_0^\infty \frac{x\mathrm{d}x}{2\pi} \frac{a^4}{x^4} \int_0^\pi \frac{A\ \mathrm{d}\theta}{\Big(A\gamma + 1 + a^2 - 2a\cos(\theta + \alpha)\Big)^2} \end{aligned} \tag{D.17}$$

after shifting $\theta \to \theta - \alpha$, and noting the evenness of the θ integral. The integral is found in standard integration tables[104], and noting that $(1 \pm a)^2 + A\gamma \geq 0$, we obtain

$$I = \int_0^\infty \frac{\mathrm{d}x}{2\pi} \frac{a^4}{x^3} \frac{A\pi(1 + a^2)}{(1 + a)^3} \Big((1 - a)^2 + A\gamma\Big)^{-3/2}. \tag{D.18}$$

Since in the limit that $A \to 0$,

$$\frac{A}{\Big((1 + a)^2 + A\gamma\Big)^{3/2}} \to \frac{2}{\gamma}\delta(1 - a), \tag{D.19}$$

we find that

$$I = \int_0^\infty \frac{\mathrm{d}x}{4k_1} \frac{x}{\Big(\frac{x^2 + 1 - k_3}{2}\Big)^2 + k_2^2}\ \delta(a - 1). \tag{D.20}$$

Making the further substitution $y = (x^2 + 1 - k_3)/2$,

$$\begin{aligned} I &= \int_{\frac{1-k_3}{2}}^\infty \frac{\mathrm{d}y}{2k_1} \frac{1}{y^2 + k_2^2}\ \delta\Big(\frac{2y - (1 - k_3)}{(y^2 + k_2^2)^2} - 1\Big) \\ &= \int_{\frac{1-k_3}{2}}^\infty \frac{\mathrm{d}y}{4k_1} \frac{y^2 + k_2^2}{\Big|k_2^2 - y^2 + y(1 - k_3)\Big|} \\ &\quad \times \Big(\delta(y - y_+) + \delta(y - y_-)\Big), \end{aligned} \tag{D.21}$$

where

$$y_\pm = 1 \pm \sqrt{k_3 - k_2^2} \tag{D.22}$$

are the intersections of the curves $y^2 + k_2^2$ and $2y - (1 - k_3)$. It is easily verified that both y_+ and y_- are in the range of integration $[\frac{\mathbf{1-k_3}}{\mathbf{2}}, \infty)$ (y_- just catching the lower bound when $\psi = 0$). Then expanding the denominator of Eq. (D.21)

using Eq. (D.22), we find

$$\left|k_2^2 - y_\pm^2 + y_\pm(1-k_3)\right| = 2\sqrt{k_3 - k_2^2}\,\left|\sqrt{k_3 - k_2^2} \pm \frac{1+k_3}{2}\right| \tag{D.23}$$

so that

$$\begin{aligned} I &= \frac{1}{2k_1}\frac{1}{2\sqrt{k_3-k_2^2}}\Big(\frac{1+k_3+2\sqrt{k_3-k_2^2}}{1+k_3+2\sqrt{k_3-k_2^2}} + \frac{1+k_3-2\sqrt{k_3-k_2^2}}{1+k_3-2\sqrt{k_3-k_2^2}}\Big) \\ &= \frac{1}{2k_1\sqrt{k_3-k_2^2}} \end{aligned} \tag{D.24}$$

Appendix E

Matsubara summations

It is much easier to calculate finite temperature properties using imaginary time (Matsubara) Green's functions than real-time Green's functions, and to then obtain the retarded Green's function through analytic continuation. Therefore, in calculating Feynman diagrams, we will frequently encounter summations over the Matsubara frequencies $i\omega_n = \frac{i\pi(2n+1)}{\beta}$ for fermions, and $i\omega_n = \frac{2\pi in}{\beta}$ for bosons.

Since we are dealing with fermionic propagators, we will explain here a trick which enables us to perform such summations over the fermionic frequencies. Noticing that the poles of the Fermi function coincide with the Matsubara frequencies, we conclude that if we wish to calculate the sum

$$S = \frac{1}{\beta}\sum_n f(i\omega_n), \tag{E.1}$$

for some analytic function f, we can instead multiply f by the Fermi function, and perform the contour integral

$$I = \lim_{R\to\infty}\oint \frac{\mathrm{d}z}{2\pi i} f(z)n_f(z), \tag{E.2}$$

where the contour is over a circle of radius R. By the residue theorem, then, we have

$$I = \sum_{z_i} \mathrm{Res}(f(z_i)n_f(z_i)) \tag{E.3}$$

where z_i are the poles of $f(z)n_f(z)$. Since f is analytic, these are simply the poles of the Fermi function, known as "thermal poles", which lie at the

Matsubara frequencies. Because

$$\mathrm{Res}(\frac{1}{e^{\beta z}+1}) = \frac{-1}{\beta}, \tag{E.4}$$

we find that

$$S = -I. \tag{E.5}$$

If there are branch cuts present in the function f, we must be careful to include the integrations along the opposing branches, which will not cancel one another.

If we use the bare-bubble approximation to evaluate a two-particle Green's function, we can make use of a spectral function to simplify a calculation. In calculating the thermal conductivity, the summation

$$S_0(i\Omega_n) \equiv \frac{1}{\beta}\sum_{i\omega_n} \frac{(i\omega_n + \frac{i\Omega_n}{2})^2}{(i\omega_n - \omega_1)(i\omega_n + i\Omega_n - \omega_2)} \tag{E.6}$$

will arise. Thus, using $S = -I$, we have

$$S_0(i\Omega_n) = -\oint \mathrm{d}z \frac{(z + i\Omega_n)^2}{(z-\omega_1)(z+i\Omega_n-\omega_2)} n_f(z), \tag{E.7}$$

which has poles at $z = \omega_1$ and $z = \omega_2 - i\Omega_n$. Thus

$$S_0(i\Omega_n) = \frac{(\omega_1 + \frac{i\Omega_n}{2})^2 n_f(\omega_1) - (\omega_2 - \frac{i\Omega_n}{2})^2 n_f(\omega_2 - i\Omega_n)}{\omega_1 - \omega_2 + i\Omega_n}. \tag{E.8}$$

Because the Matsubara frequencies for the boson are even, $i\Omega_n = \frac{2\pi i n}{\beta}$,

$$n_f(\omega_2 - i\Omega_n) = \frac{1}{\exp(\beta(\omega_2 - i\Omega_n)) + 1} = \frac{1}{\exp(\beta\omega_2) + 1} = n_f(\omega_2). \tag{E.9}$$

Analytically continuing $i\Omega_n \to \Omega + i\delta$, we find

$$S_{\mathrm{Ret}}(\Omega) = \frac{(\omega_1 + \frac{\Omega}{2})^2 n_f(\omega_1) - (\omega_2 - \frac{\Omega}{2})^2 n_f(\omega_2)}{\omega_1 - \omega_2 + \Omega + i\delta} \tag{E.10}$$

Appendix F

Current Operators

We will calculate the quasiparticle heat current in d-wave superconducting (d-SC) systems, as well as in systems with additional order parameters. The heat current is obtained by measuring energies from the Fermi level, as was noted in Chapter 2.1.2. Since the energy and spin of quasiparticles are both well-defined quantities, we can calculate the spin current, and associate the energy, rather than spin, to obtain the heat current.

We will then calculate the spin current using the Heisenberg equations of motion for the mean field hamiltonian describing the dSC+DW (d-wave superconductor + density wave) system,

$$\begin{aligned} \nabla \cdot \mathbf{j_Q} &= -\frac{\partial \rho_Q}{\partial t} \\ &= [\rho_Q, H], \end{aligned} \tag{F.1}$$

where $H = H_{d\mathrm{SC}} + \sum_{Q_i} H_{DW}^{(Q_i)}$. The density operator written in terms of the Nambu basis elements is

$$\rho_q = \sum_k (c_{k\uparrow}^\dagger c_{k+q\uparrow} + c_{-k\downarrow} c_{-k-q\downarrow}^\dagger). \tag{F.2}$$

F.1 d-wave superconductor

The mean field hamiltonian describing the d-wave superconductor has two parts;

$$H_{d\mathrm{SC}} = H_{\mathrm{TB}} + H_{\mathrm{gap}}. \tag{F.3}$$

The kinetic portion of the hamiltonian is

$$H_{\rm TB} = \sum_k (\epsilon_k c^\dagger_{k\uparrow} c_{k\uparrow} - \epsilon_k c_{-k\downarrow} c^\dagger_{-k\downarrow}), \tag{F.4}$$

where ϵ_k is obtained from a tight-binding model. Making use of the canonical [anti]-commutation relations for the fermionic operators,

$$\begin{aligned} \{c_{k\sigma}, c^\dagger_{k'\sigma'}\} &= \delta_{k,k'}\delta_{\sigma,\sigma'} \\ \{c_{k\sigma}, c_{k'\sigma'}\} &= 0 \\ \{c^\dagger_{k\sigma}, c^\dagger_{k'\sigma'}\} &= 0 \end{aligned} \tag{F.5}$$

we find that

$$\begin{aligned} [c^\dagger_{k'\uparrow} c_{k'+q\uparrow}, c^\dagger_{k\uparrow} c_{k\uparrow}] &= c_{k'\uparrow} c_{k'+q\uparrow} (\delta_{k,k'+q} - \delta_{k,k'}) \\ [c^\dagger_{k'\uparrow} c_{k'+q\uparrow}, c_{-k\downarrow} c^\dagger_{-k\downarrow}] &= 0 \\ [c_{-k'\downarrow} c^\dagger_{-k'-q\downarrow}, c^\dagger_{k\uparrow} c_{k\uparrow}] &= 0 \\ [c_{k'\uparrow} c^\dagger_{-k'-q\downarrow}, c^\dagger_{k\uparrow} [c_{k\uparrow}] &= c_{k'\uparrow} c_{k'+q\uparrow} (\delta_{k,k'+q} - \delta_{k,k'}), \end{aligned} \tag{F.6}$$

so that

$$\begin{aligned} [\rho_Q, H_{\rm TB}] &= \sum_{kk'} \Big(\epsilon_k c^\dagger_{k'\uparrow} c_{k'+q\uparrow} (\delta_{k,k'+q} - \delta_{k,k'}) - \epsilon_k c_{-k'\downarrow} c^\dagger_{-k'-q\downarrow} (\delta_{k,k'+q} - \delta_{k,k'}) \Big) \\ &= \sum_{k'} \Big((\epsilon_{k'+q} - \epsilon_{k'}) c^\dagger_{k'\uparrow} c_{k'+q\uparrow} - (\epsilon_{k'+q} - \epsilon_{k'}) c_{-k'\downarrow} c^\dagger_{-k'-q\downarrow} \Big). \end{aligned} \tag{F.7}$$

As $q \to 0$, then

$$\begin{aligned} [\rho_q, H_{\rm TB}] &= \sum_k \mathbf{q} \cdot \Big(\frac{\partial \epsilon_k}{\partial \mathbf{k}} c^\dagger_{k\uparrow} c_{k\uparrow} - \frac{\partial \epsilon_k}{\partial \mathbf{k}} c_{-k\downarrow} c^\dagger_{-k\downarrow} \Big) \\ &= \sum_k \mathbf{q} \cdot \psi^\dagger_k \begin{pmatrix} \mathbf{v}_f & 0 \\ 0 & -\mathbf{v}_f \end{pmatrix} \psi_k, \end{aligned} \tag{F.8}$$

where $\mathbf{v}_f \equiv \frac{\partial \epsilon_k}{\partial \mathbf{k}}$, and the Nambu vector is

$$\psi^\dagger_k = \begin{pmatrix} c^\dagger_{k\uparrow} & c_{-k\downarrow} \end{pmatrix}. \tag{F.9}$$

The term for the gap is (assuming $\Delta_k = \Delta_k^*$),

$$H_{\rm gap} = \sum_k \Delta_k (c^\dagger_{k\uparrow} c^\dagger_{-k\downarrow} + c_{-k\downarrow} c_{k\uparrow}). \tag{F.10}$$

For this part, we will need the relations

$$\begin{aligned}
[c^\dagger_{k'\uparrow} c_{k'+q\uparrow}, ck\uparrow^\dagger c^\dagger_{-k\downarrow}] &= c^\dagger_{k'\uparrow} c^\dagger_{-k'-q\downarrow} \delta_{k,k'+q} \\
[c^\dagger_{k'\uparrow} c_{k'+q\uparrow}, c_{-k\downarrow}, c_{k\uparrow}] &= -c_{-k'\downarrow} c_{k'\uparrow} \delta_{k,k'} \\
[c + -k'\downarrow c^\dagger_{-k'-q\downarrow}, c^\dagger_{k\uparrow} c^\dagger_{-k\downarrow}] &= -c^\dagger_{k'\uparrow} c^\dagger_{-k'-q\downarrow} \\
[c_{-k'\downarrow} c + -k' - q\downarrow^\dagger, c_{-k\downarrow} c_{k\uparrow}] &= c_{-k'\downarrow} ck' + q\uparrow \delta_{k,k'+q},
\end{aligned} \tag{F.11}$$

so that

$$\begin{aligned}
[\rho_q, H_{\rm gap}] &= \sum_{kk\prime} \Big(\Delta_k c^\dagger_{k'\uparrow} c^\dagger_{-k'\downarrow} (\delta_{k,k'+q} - \delta_{k,k'}) + \Delta_k c_{-k'\downarrow} c_{k'+q\uparrow} (\delta_{k,k'+q} - \delta_{k,k'}) \Big) \\
&= \sum_{k'} \Big((\Delta_{k'+q} - \Delta_{k'}) c^\dagger_{k'\uparrow} c^\dagger_{-k'-q\downarrow} + (\Delta_{k'+q} - \Delta_{k'}) c_{-k'\downarrow} c_{k'\downarrow} c_{k'+q\uparrow} \Big),
\end{aligned} \tag{F.12}$$

and as $q \to 0$,

$$\begin{aligned}
[\rho_q, H_{\rm gap}] &= \sum_k \mathbf{q} \cdot \Big(\frac{\partial \Delta_k}{\partial \mathbf{k}} c^\dagger_{k\uparrow} c^\dagger_{-k\downarrow} + \frac{\partial \Delta_k}{\partial \mathbf{k}} c_{-k\downarrow} c_{k\uparrow} \Big) \\
&= \sum_k \mathbf{q} \cdot \psi^\dagger_k \begin{pmatrix} 0 & \mathbf{v}_\Delta \\ \mathbf{v}_\Delta & 0 \end{pmatrix},
\end{aligned} \tag{F.13}$$

where $\mathbf{v}_\Delta \equiv \frac{\partial \Delta_k}{\partial \mathbf{k}}$.

F.2 $\mathbf{Q} = (\pi, 0)$ charge density wave

For $\mathbf{Q} = (\pi, 0)$ density waves, we add the notation $d_k \equiv c_{k+Q}$, so that the extended Nambu vector is

$$\psi^\dagger_k = \begin{pmatrix} c^\dagger_{k\uparrow} & c_{-k\downarrow} & d^\dagger_{k\uparrow} & d_{-k\downarrow} \end{pmatrix} \tag{F.14}$$

The density operator is expanded to include $d^\dagger_k d_k$ terms.

$$H^{(\pi,0)}_{\rm CDW} = \sum_k \Big(A_k d^\dagger_{k\uparrow} c_{k\uparrow} + A^*_k c^\dagger_{k\uparrow} d_{k\uparrow} - A_{-k} c_{-k\downarrow} d^\dagger_{-k\downarrow} - A^*_{-k} d_{-k\downarrow} c^\dagger_{-k\downarrow} \Big) \tag{F.15}$$

To compute $[\rho_q, H_{\rm CDW}]$, we will need the terms

$$\begin{aligned}
[c^\dagger_{k'\uparrow}c_{k'+q\uparrow}, d^\dagger_{k\uparrow}c_{k\uparrow}] &= c^\dagger_{k'\uparrow}d_{k'+q}\delta_{k+Q,k'+q} - d^\dagger_{k'\uparrow}c_{k'+q\uparrow}\delta_{k,k'} \\
[c^\dagger_{k'\uparrow}c_{k'+q\uparrow}, c^\dagger_{k\uparrow}d_{k\uparrow}] &= c^\dagger_{k'\uparrow}d_{k'+q\uparrow}\delta_{k,k'+q} - d^\dagger_{k'\uparrow}c_{k'+q\uparrow}\delta_{k+Q,k'} \\
[c^\dagger_{k'\uparrow}c_{k'+q\uparrow}, c_{-k\downarrow}d^\dagger_{-k\downarrow}] &= 0 \\
[c^\dagger_{k'\uparrow}c_{k'+q\uparrow}, d_{-k\downarrow}c^\dagger_{-k\downarrow}] &= 0 \\
[c_{-k'\downarrow}c^\dagger_{-k'-q\downarrow}, d^\dagger_{k\uparrow}c_{k\uparrow}] &= 0 \\
[c_{-k'\downarrow}c^\dagger_{-k'-q\downarrow}, c^\dagger_{k\uparrow}d_{k\uparrow}] &= 0 \\
[c_{-k'\downarrow}c^\dagger_{-k'-q\downarrow}, c_{-k\downarrow}d^\dagger_{-k\downarrow}] &= c_{-k'\downarrow}d^\dagger_{-k'-q\downarrow}\delta_{k,k'+q} - d_{-k'\downarrow}c^\dagger_{-k'-q\downarrow}\delta_{k+Q,k'} \\
[c_{-k'\downarrow}c^\dagger_{-k'-q\downarrow}, d_{-k\downarrow}c^\dagger_{-k\downarrow}] &= c_{-k'\downarrow}d^\dagger_{-k'-q\downarrow}\delta_{k+Q,k'+q} - d_{-k'\downarrow}c^\dagger_{-k'-q\downarrow}\delta_{k,k'},
\end{aligned} \tag{F.16}$$

so that

$$\begin{aligned}
[\rho_q, H^{(\pi,0)}_{\rm CDW}] &= {\sum_{kk'}}' \Big(A_k(c^\dagger_{k'\uparrow}d_{k\prime+q\uparrow}\delta_{k+Q,k'+q} - d^\dagger_{k'\uparrow}c_{k'+q\uparrow}\delta_{k,k'}) + \\
&\quad A^*_k(c^\dagger_{k'\uparrow}d_{k'+q\uparrow}\delta_{k,k'+q} - d^\dagger_{k'\uparrow}c_{k'+q\uparrow}\delta_{k+Q,k'}) \\
&\quad -A_{-k}(c_{-k'\downarrow}d^\dagger_{-k'-q\downarrow}\delta_{k,k'+q} - d_{k'\downarrow}c^\dagger_{-k'-q\downarrow}\delta_{k+Q,k'}) \\
&\quad A^*_{-k}(c_{-k'\downarrow}d^\dagger_{-k'-q\downarrow}\delta_{k+Q,k'+q} - d_{-k'\downarrow}c_{-k'-q\downarrow}\delta_{k,k'}) \Big) \\
&= {\sum_{k}}' \Big((A_{k+Q+q} - A_{k+Q})c^\dagger_{k\uparrow}d_{k+q\uparrow} + (A^*_{k+q} - A^*_k)c^\dagger_{k\uparrow}d_{k+q\uparrow} \\
&\quad -(A_{-k-q} - A_{-k})c_{-k\downarrow}d^\dagger_{-k'-q\downarrow} - (A^*_{-k'-Q-q} - A^*_{-k-Q})c_{-k'\downarrow}d^\dagger_{-k'-q\downarrow} \Big).
\end{aligned} \tag{F.17}$$

Then, as $\mathbf{q} \to 0$,

$$\begin{aligned}
[\rho_q, H^{(\pi,0)}_{\rm CDW}] &= {\sum_{k}}' \mathbf{q}\cdot\frac{\partial}{\partial\mathbf{k}}\Big(A^*_k c^\dagger_{k\uparrow}d_{k\uparrow} + A_k d^\dagger_{k\uparrow}c_{k\uparrow} - A_{-k}c_{-k\downarrow}d^\dagger_{-k\downarrow} - A^*_{-k}d^\dagger_{-k\downarrow}c_{-k\downarrow} \Big) \\
&= {\sum_{k}}' \mathbf{q}\cdot\psi^\dagger_k \begin{pmatrix} 0 & 0 & \frac{\partial A^*_k}{\partial\mathbf{k}} & 0 \\ 0 & 0 & 0 & -\frac{\partial A_{-k}}{\partial\mathbf{k}} \\ \frac{\partial A_k}{\partial\mathbf{k}} & 0 & 0 & 0 \\ 0 & -\frac{\partial A^*_{-k}}{\partial\mathbf{k}} & 0 & 0 \end{pmatrix}
\end{aligned} \tag{F.18}$$

F.3 $\mathbf{Q} = (\frac{\pi}{2}, 0)$ charge density wave

The notation is expanded to include $d_k \equiv c_{k+Q}$, $m_k \equiv c_{k+2Q}$ and $n_k \equiv c_{k+3Q}$. Thus the hamiltnonian is,

$$\begin{aligned} H_{\rm CDW}^{(\pi/2,0)} &= \sum_k{}' \Big(A_k d_{k\uparrow}^\dagger c_{k\uparrow} - A_{-k} c_{-k\downarrow} n_{-k\downarrow}^\dagger + A_k^* c_{k\uparrow}^\dagger d_{k\uparrow} - A_{-k}^* n_{-k\downarrow} c_{-k\downarrow}^\dagger \\ &\quad + A_{k+Q} m_{k\uparrow}^\dagger d_{k\uparrow} - A_{-k-Q} d_{-k\downarrow} m_{-k\downarrow}^\dagger + A_{k+Q}^* d_{k\uparrow}^\dagger m_{k\uparrow} - A_{-k-Q}^* c_{-k\downarrow} d_{-k\downarrow}^\dagger \\ &\quad + A_{k+2Q} n_{k\uparrow}^\dagger m_{k\uparrow} - A_{-k-2Q} m_{-k\downarrow} d_{-k\downarrow}^\dagger + A_{k+2Q}^* m_{k\uparrow}^\dagger n_{k\uparrow} - A_{-k-2Q}^* d_{-k\downarrow} n_{-k\downarrow}^\dagger \\ &\quad + A_{k+3Q} c_{k\uparrow}^\dagger n_{k\uparrow} - A_{-k-3Q} n_{-k\downarrow} m_{-k\downarrow}^\dagger + A_{k+3Q}^* n_{k\uparrow}^\dagger c_{k\uparrow} - A_{-k-3Q}^* m_{-k\downarrow} n_{-k\downarrow}^\dagger \Big). \end{aligned} \tag{F.19}$$

We need commutators such as

$$\begin{aligned} [c_{k'\uparrow}^\dagger c_{k'+q\uparrow}, d_{k\uparrow}^\dagger c_{k\uparrow}] &= c_{k'\uparrow}^\dagger n_{k'+q\uparrow} \delta_{k+Q,k'+q} - d_{k'\uparrow}^\dagger c_{k'+q\uparrow} \delta_{k,k'} \\ [c_{k'\uparrow}^\dagger c_{k'+q\uparrow}, c_{k\uparrow}^\dagger d_{k\uparrow}] &= c_{k'\uparrow}^\dagger d_{k'+q\uparrow} \delta_{k,k'+q} - n_{k'\uparrow}^\dagger c_{k'+q\uparrow} \delta_{k+Q,k'} \\ [c_{k'\uparrow}^\dagger c_{k'+q\uparrow}, c_{-k\downarrow} n_{-k\downarrow}^\dagger] &= 0 \\ [c_{k'\uparrow}^\dagger c_{k'+q\uparrow}, n_{-k\downarrow} c_{-k\downarrow}^\dagger] &= 0 \\ [c_{-k'\downarrow} c_{-k'-q\downarrow}^\dagger, c_{-k\downarrow} n_{-k\downarrow}^\dagger] &= c_{-k'\downarrow} n_{-k'-q\downarrow}^\dagger \delta_{k,k'+q} - d_{-k'\downarrow} c_{-k'-q\downarrow}^\dagger \delta_{k+3Q,k'} \\ [c_{-k'\downarrow} c_{-k'-q\downarrow}^\dagger, n_{-k\downarrow} c_{-k\downarrow}^\dagger] &= c_{-k'\downarrow} d_{-k'-q\downarrow} \delta_{k+3Q,k'+q} - n_{-k'\downarrow} c_{-k'-q\downarrow}^\dagger \delta_{k,k'} \\ [[c_{-k'\downarrow} c_{-k'-q\downarrow}^\dagger, d_{k\uparrow}^\dagger c_{k\uparrow}] &= 0 \\ [[c_{-k'\downarrow} c_{-k'-q\downarrow}^\dagger, c_{k\uparrow}^\dagger d_{k\uparrow}] &= 0. \end{aligned} \tag{F.20}$$

We include the computations for one "octant".

$$
\begin{aligned}
[\rho_q, H^{(\pi/2,0)}_{\rm CDW}] &= \sum_{kk'} \Big(A_k (c^\dagger_{k'\uparrow} n_{k'+q\uparrow} \delta_{k+Q,k'+q} - d^\dagger_{k'\uparrow} c_{k'+q\uparrow} \delta_{k,k'}) \\
&\quad + A +^*_k (c^\dagger_{k'\uparrow} d_{k'+q\uparrow} \delta_{k,k'+q} - n^\dagger_{k'\uparrow} c_{k'+q\uparrow} \delta_{k+Q,k'} \\
&\quad - A_{-k} (c_{-k'\downarrow} n^\dagger_{-k'-q\downarrow} \delta_{k,k'+q} - d_{-k'\downarrow} c^\dagger_{-k'+q\downarrow} \delta_{k+3Q,k'}) \\
&\quad - A^*_{-k} (c_{-k'\downarrow} d^\dagger_{-k'-q\downarrow} \delta_{k+3Q,k'+q} - n_{-k'\downarrow} c^\dagger_{-k'-q\downarrow} \delta_{k,k'}) \Big) \\
&= \sum_k \Big(A_{k+3Q} c^\dagger_{k\uparrow} n_{k+q\uparrow} - A_k d^\dagger_{k\uparrow} c_{k+q\uparrow} + A^*_{k+q} c^\dagger_{k\uparrow} d_{k+q\uparrow} \\
&\quad - A^*_{k+3Q} n^\dagger_{k\uparrow} c_{k+q\uparrow} - A_{-k-q} c_{-k\downarrow} n^\dagger_{-k-q\downarrow} + A_{-k-Q} d_{-k\downarrow} c^\dagger_{-k-q\downarrow} \\
&\quad - A^*_{-k-Q} c_{-k\downarrow} d^\dagger_{-k-q\downarrow} + A_{-k} n_{-k\downarrow} c^\dagger_{-k-q\downarrow} \Big) \\
&= {\sum_k}' \Big((A_{k+3Q+q} - A_{k+3Q}) c^\dagger_{k\uparrow} n_{k+q\uparrow} + (A^*_{k+q} - A^*_k) c^\dagger_{k\uparrow} d_{k+q\uparrow} \\
&\quad - (A_{-k-q} - A_{-k}) c_{-k\downarrow} n^\dagger_{-k-q\downarrow} - (A^*_{-k-Q-q} - A_{-k-Q}) c_{-k\downarrow} d^\dagger_{-k-q\downarrow} \Big),
\end{aligned}
\tag{F.21}
$$

so that, in the limit that $\mathbf{q} \to 0$,

$$
\begin{aligned}
[\rho_q, H^{(\pi/2,0)}_{\rm CDW}] &= {\sum_k}' \mathbf{q} \cdot \frac{\partial}{\partial \mathbf{k}} \Big(A_{k+3Q} c^\dagger_{k\uparrow} n_{k+q\uparrow} + A^*_k c^\dagger_{k\uparrow} d_{k\uparrow} \\
&\quad - A_{-k} c_{-k\downarrow} n^\dagger_{-k\downarrow} - A^*_{-k-Q} c_{-k\downarrow} d^\dagger_{-k\downarrow} \Big)
\end{aligned}
\tag{F.22}
$$